

**Electrochemical Deposition of Dye-modified ZnO
Hybrid Thin Films and Their Application to
Flexible Dye-Sensitized Solar Cells**

Von der Naturwissenschaftlichen Fakultät
der Gottfried Wilhelm Leibniz Universität Hannover
zur Erlangung des Grades

Doktorin der Naturwissenschaften

Dr. rer. nat.

genehmigte Dissertation

von

M. Sc. Juan Du

Geboren am 07.12.1981 in Hefei, China

2013

Referent: Prof. Dr. Michael Wark

Korreferent: Prof. Dr. Detlef W. Bahnemann

Tag der Promotion: 08.01.2013

ACKNOWLEDGMENTS

The presented study was carried out between February 2009 and June 2012 at the Institute of Physical Chemistry and Electrochemistry at the Faculty for Natural Sciences at the Leibniz University Hannover. It was financially supported by grants obtained from the Ministry of Education and Research (BMBF) Germany (Grant Number: 03X3519F).

First of all, I gratefully acknowledge Prof. Dr. Jürgen Caro for having given me the opportunity to perform a PhD thesis in his working group. I would like to express my gratitude to my doctoral advisor Prof. Dr. Michael Wark for the interesting subject, for his helpful discussions and for his continuous interest in my work. Special thanks are due to Dr. Torsten Oekermann. His excellent mentoring and support in all theoretical and practical questions contributed substantially to the success of this work.

I thank my research-group colleagues Dipl.-Chem. Florian Bittner, Dr. Andreas Gottschlich and Dipl.-Chem. Christian Dunkel for their discussion and technical support.

I would like to give many thanks to Yvonne Gabbey-Uebe, Kerstin Janze, and Frank Steinbach for their kind supports in the technical or the administrative aspects in the past three years. I want to express my gratitude to all the former and current members of the institute for their kindness, help, friendship and the pleasant working atmosphere. I appreciate the great job done by the mechanical and electrical workshop.

Last, I would like to express my gratitude to my family for the support they provided through my entire life and in particular, my parents, my husband and my son, without whose love, encouragement and editing assistance, I would not have finished this dissertation.

ABSTRACT

This thesis is focused on the study of dye-sensitized solar cells (DSSCs) based on electrodeposited zinc oxide films (ZnO) as electron conductor.

Finding an appropriate flexible substrate was the first issue for DSSCs based on electrodeposited ZnO films. In this work, several flexible substrates were tested, including PET-ITO, PET-CNT and metal sheets. The study demonstrated that PET-ITO was the best substrate for ZnO photoanodes, achieving the highest conversion efficiency of 3.3 %. Taking into account the relatively high resistance of the PET-CNT substrates used in this study (470 Ω /sq.) the achieved conversion efficiency of $\eta = 2.5$ % can be regarded as very promising. Because of the non-penetration of light through the metal sheets, the DSSCs based on stainless steel and titanium sheets required illumination of the dye-sensitized film through the counter electrode. They showed low efficiencies of about 1 %, which can be attributed to the absorption losses through back side illumination.

The iodine and iodide concentration in the acetonitrile-based electrolyte were optimized to 1 mol/L TPAI and 0.1 mol/L I₂. The addition of 4-tert-butylpyridine as additive in the acetonitrile-based electrolyte caused desorption of the dye D149 from ZnO films. One of the cell components limiting the long-term stability of DSSCs is the organic solvent electrolyte. The replacement of organic solvents by room temperature ionic liquids (RTIL) is very promising due to their negligible vapour pressure, which avoids evaporation problems. Mixing the most frequently used ionic liquid PMIM I with low viscosity ionic liquid EMIM TCB has a positive effect on the performance of the cells. The presence of water, acetonitrile and electrolyte additives such as NBB, DMAp and CeMim in the IL mixtures had negative influences on the photovoltaic performances of the solar cells, probably due to the undesirable desorption of the dye D149. High temperature can reduce the viscosity of the ionic liquid and affect the photovoltaic performance positively. An increase of the iodine concentration increased the short-circuit current and correspondingly the efficiency. Furthermore, it was observed that the addition of iodine to the ionic liquids decreases its viscosity, which could also contribute to the improvement. In general, it was observed that the ZnO-based solar cells with ionic liquids had much lower V_{oc} , I_{sc} , FF and efficiency values than the cells with acetonitrile-based electrolyte. But they were more stable than the cells with acetonitrile-based electrolyte in the long-term stability test.

Dyes with phosphonic acid anchoring groups were investigated and compared to dyes with carboxylic acid anchors. The conversion efficiencies of the dyes with phosphonic acid anchoring groups were much lower than dyes with carboxylic acid groups due to the lower amount of adsorbed dye molecules and consequently the lower absorbance of the sensitized ZnO films in the visible region.

Keywords: Flexible dye-sensitized solar cell, electrochemical ZnO deposition, ionic liquids

KURZZUSAMMENFASSUNG

Im Rahmen der vorliegenden Arbeit wurden elektrochemisch abgeschiedene ZnO Filme auf ihre Verwendung in farbstoffsensibilisierten Solarzellen (engl. DSSC) untersucht.

Die Suche nach einem geeigneten flexiblen leitfähigen Substrat war das erste Thema für DSSCs basierend auf elektrochemisch abgeschiedenen ZnO-Filmen. In dieser Arbeit wurden mehrere flexible Substrate getestet, einschließlich PET-ITO, PET-CNT und Metallfolien. Die Ergebnisse zeigten, dass PET-ITO das beste Substrat für die ZnO Photoanode war, hiermit wurde der höchste Wirkungsgrad von 3,3 % erreicht. Der erreichte Wirkungsgrad von $\eta = 2,5\%$ auf dem PET-CNT Substrat kann unter Berücksichtigung seines relativ hohen Widerstand ($470 \Omega/\text{sq.}$) als vielversprechend angesehen werden. Die DSSCs auf Basis von Ti- und Edelfolien zeigten trotz der guten Leitfähigkeit der Metallfolien enttäuschende Effektivitäten. Die Ursache lag darin, dass aufgrund der Undurchsichtigkeit der Metallfolien die Solarzellen nur durch die Pt-Gegenelektrode belichtet werden konnten. Dabei entstanden Verluste von Photonen aufgrund deren Absorption vor allem im Elektrolyten.

Die Konzentration von Iod und Iodid des lösungsmittelbasierten Elektrolyts wurden jeweils als 0,1 mol/L und 1 mol/L optimiert. Das von TiO_2 -basierten Zellen bekannte Additiv 4-tert-Butylpyridin ist nicht kompatibel zum Farbstoff D149. Die Zugabe von 4-tert-Butylpyridin bewirkte die Desorption des Farbstoffes D149 von ZnO Filmen. Die Anwendung von ionischen Flüssigkeiten in der Farbstoffsolarzelle kann durch den vernachlässigbaren Dampfdruck einzelne Herstellungs- und Versiegelungsschritte der DSSC erleichtern. Das Vermischen von PMIM I mit einer niedrigviskosen ionischen Flüssigkeit EMIM TCB verringert die Viskosität der Elektrolyte und verbesserte die Leistungen der Solarzellen. Die Zugaben von Wasser, Acetonitril und Elektrolytadditiven wie NBB, DMAp und CeMim in die IL Mischungen hatten negative Einflüsse auf die Leistungen der Solarzellen, was auf unerwünschte Desorption des Farbstoffes D149 zurückgeführt werden konnte. Hohe Temperaturen können die Viskosität der ionischen Flüssigkeit reduzieren und die Wirkungsgrade der Solarzellen positiv beeinflussen. Eine Erhöhung der Iod-Konzentration erhöhte die Kurzschlussströme und entsprechend die Wirkungsgrade. Zusätzlich wurde beobachtet, dass die Zugabe von Iod die Viskosität der ionischen Flüssigkeiten verringerte, was auch zur Verbesserung des Wirkungsgrads beitragen konnte. Generell wurde beobachtet, dass die Zellen mit ionischen Flüssigkeiten deutlich niedrigere Werte für V_{oc} , I_{sc} , FF und Wirkungsgrad als die Zellen mit Acetonitril basierten Elektrolyten hatten. Aber sie waren in dem Langzeitstabilitätstest deutlich stabiler als die Zellen mit Acetonitril basierten Elektrolyten.

Farbstoffe mit Phosphonsäure-Ankergruppen zeigten aufgrund der geringeren Farbstoffbeladung und folglich geringeren Absorption der sensibilisierten ZnO Filme im sichtbaren Bereich deutlich geringere Wirkungsgrade als die Farbstoffe mit Carbonsäure-Ankergruppen.

Schlagnote: Flexible farbstoffsensibilisierte Solarzelle, elektrochemische ZnO-Abscheidung, ionische Flüssigkeiten

INDEX OF CONTENTS

Acknowledgments	3
Abstract.....	5
Kurzzusammenfassung	7
Index of contents	9
Abbreviations	13
Symbols	15
1 MOTIVATION.....	17
1.1 Introduction.....	17
1.2 Objectives and structure of the present work	20
2 DYE-SENSITIZED SOLAR CELLS	21
2.1 Operating principle of DSSC	21
2.2 Basic materials of DSSC.....	24
2.2.1 Substrate	24
2.2.2 Semiconductor	25
2.2.3 Photosensitizers	28
2.2.4 Electrolyte.....	30
2.2.5 Counter electrode.....	35
2.3 Electrochemical deposition of ZnO/dye hybrid thin films	36
2.3.1 Dye desorption and re-adsorption	38
2.3.2 Fast electron transport.....	39
3 EXPERIMENTAL	41
3.1 Preparation of ZnO/Eosin Y thin film	41
3.1.1 Cleaning of the Substrate	41
3.1.2 Mounting of the substrate	41
3.1.3 Electrochemical deposition of the ZnO/Eosin Y thin film.....	42
3.2 Characterization of the ZnO thin film	45
3.2.1 Film thickness	45
3.2.2 UV-Vis spectroscopy	45
3.2.3 Dye loading in the film	46
3.2.4 Scanning Electron Microscopy (SEM)	47
3.2.5 Cyclic voltammetry (CV)	49
3.3 Fabrication of the flexible dye-sensitized solar cells.....	51
3.3.1 The process of dye re-adsorption.....	51
3.3.2 Sputtering of Pt counter electrode.....	51
3.3.3 DSSC assembly	52

3.4	Characterization of the dye-sensitized solar cells.....	53
3.4.1	Current-voltage (I-V) curves.....	53
3.4.2	Electrochemical Impedance Spectroscopy (EIS)	54
3.4.3	Intensity Modulated Photocurrent / Photovoltage Spectroscopy (IMPS/IMVS)	58
3.4.4	Long-term stability.....	59
4	SUITABLE SUBSTRATES FOR FLEXIBLE ZNO-BASED DYE-SENSITIZED SOLAR CELLS	61
4.1	PET-ITO	61
4.1.1	Scanning electron microscopy	61
4.1.2	Photovoltaic performance	62
4.1.3	Influence of light on the eosin Y desorption	63
4.2	PET-CNT	65
4.2.1	Scanning electron microscopy	65
4.2.2	Photovoltaic performance	68
4.2.3	The blocking effect of compact ZnO bottom layer	69
4.2.4	Electrochemical impedance spectroscopy.....	71
4.2.5	Intensity modulated photocurrent / photovoltage spectroscopy	75
4.3	Metal sheets.....	76
4.3.1	Scanning electron microscopy	76
4.3.2	UV-Vis spectroscopy	77
4.3.3	Photovoltaic performance	78
4.4	Other flexible Substrates	80
4.5	Summary	82
5	ELECTROLYTE FOR FLEXIBLE ZNO-BASED DYE-SENSITIZED SOLAR CELLS	83
5.1	Organic solvent electrolytes.....	83
5.1.1	Influence of the iodine concentration.....	83
5.1.1.1	<i>Photovoltaic performance</i>	<i>83</i>
5.1.1.2	<i>Electrochemical impedance spectroscopy.....</i>	<i>85</i>
5.1.1.3	<i>Intensity modulated photocurrent / photovoltage spectroscopy</i>	<i>86</i>
5.1.2	Influence of the iodide concentration.....	87
5.1.2.1	<i>Photovoltaic performance</i>	<i>87</i>
5.1.2.2	<i>Electrochemical impedance spectroscopy.....</i>	<i>88</i>
5.1.2.3	<i>Intensity modulated photocurrent / photovoltage spectroscopy</i>	<i>89</i>
5.1.3	Effect of additives	89
5.1.3.1	<i>Photovoltaic performance</i>	<i>90</i>
5.2	Ionic liquid electrolyte	93
5.2.1	Binary ionic liquid mixture PMIM I/EMIM TCB.....	93
5.2.1.1	<i>Photovoltaic performance</i>	<i>93</i>

5.2.2	Effects of water and acetonitrile addition	94
5.2.2.1	<i>Photovoltaic performance</i>	94
5.2.2.2	<i>Electrochemical impedance spectroscopy</i>	96
5.2.2.3	<i>Intensity modulated photocurrent / photovoltage spectroscopy</i>	97
5.2.3	Effect of temperature	98
5.2.3.1	<i>Photovoltaic performance</i>	98
5.2.3.2	<i>Electrochemical impedance spectroscopy</i>	99
5.2.3.3	<i>Intensity modulated photocurrent / photovoltage spectroscopy</i>	100
5.2.4	Other mixtures of ionic liquids	101
5.3	Long-term stability	105
5.3.1	Photovoltaic performance	105
5.3.2	Electrochemical impedance spectroscopy	107
5.3.3	Intensity modulated photocurrent / photovoltage spectroscopy	108
5.4	Summary.....	109
6	ZINC OXIDE SENSITIZED WITH DYES CONTAINING PHOSPHONIC ACID ANCHORING GROUPS	111
6.1	UV-Vis spectroscopy	113
6.2	Photovoltaic performances.....	114
6.3	Intensity modulated photocurrent / photovoltage spectroscopy	115
6.4	Summary.....	116
7	CONCLUSIONS AND OUTLOOK	117
8	REFERENCES	121
	Curriculum vitae	137
	Contributing work and publications.....	139
	Erklärung zur Dissertation	141

ABBREVIATIONS

AM1.5	air mass 1.5
AN	acetonitrile
BL	bottom layer
BMMIM I	1-butyl-2,3-dimethylimidazolium iodide
CB	conduction band
CdTe	cadmium telluride
CE	counter electrode
CeMim	5-chloro-1-ethyl-2-methylimidazol
CIGS	copper indium gallium diselenide
CV	cyclic voltammetry
DMAp	2-(dimethylamino)-pyridin
DSSC	dye-sensitized solar cell
EC	ethylene carbonate
e.g.	exempli gratia (for example)
EIS	electrochemical impedance spectroscopy
EMIM OTF	1-ethyl-3-methylimidazoliumtri-fluormethylsulfonat
EMIM NTF	1-ethyl-3-methylimidazolium-bis(trifluormethyl-sulfonyl) imid
EMIM TCB	1-ethyl-3-methylimidazoliumtetra-cyanoborat
EY	eosin Y
FF	fill factor
FTO	fluorine-doped tin oxide
GuaSCN	guanidiniumthiocyanat
HOMO	highest occupied molecular orbital
i.e.	id est (in other words)
IL	ionic liquid
IMPS	intensity modulated photocurrent spectroscopy
IMVS	intensity modulated photovoltage spectroscopy
ITO	indium-doped tin oxide
LUMO	lowest unoccupied molecular orbital
MPP	maximum power point
NBB	n-butylbenzimidazol
PEDOT	poly(3,4-ethylenedioxythio-phene)
PET	polyethylenterephthalat

PEN	polyethylenenaphtalate
PMIM I	3-propyl-1-methylimidazoliumiodid
PSS	polystyrenesulfonate
RDE	rotating disk electrode
RE	reference electrode
rpm	revolutions per minute
SDA	structure directing agents
SEM	scanning electrode microscopy
sq.	square
TBP	tert-butyl pyridine
TCO	transparent conducting oxide
UV-Vis	ultraviolet-visible
WE	working electrode

SYMBOLS

I_{MPP}	current at the maximum power point
I_{sc}	short-circuit current
R_{ct}	charge transfer (here: recombination) resistance
R_d	Warburg impedance of ion transport
R_{Pt}	resistance at Pt counter electrode
R_s	series resistance
R_t	electron transport resistance
S	sensitizer
S^0	ground energy state of the sensitizer
S^*	excited energy state of the sensitizer
S^+	oxidized state of the sensitizer
V_{MPP}	voltage at the maximum power point
V_{oc}	open-circuit voltage
η	power conversion efficiency
η_{cc}	charge-collection efficiency

1 Motivation

1.1 Introduction

Energy is one of the most important factors for human life in the 21st century. The ever increasing consumption of fossil fuels, causing global warming and environmental pollution, has led to a greater focus on renewable energy sources and sustainable development. Renewable energy sources such as the solar radiation, wind, hydromechanical and geothermal energy are clean, available in plentiful supply and do not introduce direct contamination of the environment. Among these, solar energy is available at any location on the earth and considered to be one of the most promising renewable energy sources for our future energy needs.

Solar cells, also called photovoltaic cells, are the smallest basic unit of solar electric devices that convert solar energy directly into electrical energy. The development of the solar cell stems from the work of the French physicist Becquerel in 1839^[1], who demonstrated that photovoltage and photocurrent are produced when a silver coated platinum electrode in an electrolyte solution is illuminated. But the modern era of photovoltaics began only in 1954 at Bell Laboratories when Chapin, Fuller and Pearson reported a solar conversion efficiency of 6 % for a single crystal silicon *p-n* semiconductor junction cell.^[2] Since that time continued research effort has led to various types of solar cells.

Today the market is dominated by crystalline silicon in its multicrystalline and monocrystalline form. It is also called the first generation solar cell with a market share of more than 80 % in 2010. For the crystalline silicon solar cell, high purity silicon is required in a form of a thin wafer and a large amount of energy is needed for purification and crystal growth. The expensive investment and purification in semiconductor-processing technologies of the silicon-based solar cells have limited their popularization in our lives.^[3]

Thin-film technologies reduce the amount of material required in creating the active material of solar cell. Thin film solar cells (second generation solar cell) are based on thin layers of various semiconductor materials such as amorphous silicon,^[4] cadmium telluride (CdTe)^[5] and copper indium gallium diselenide (CIGS).^[6] Even though the thin film solar cell requires less material, vacuum technique is required to deposit high purity films and it

is not easy to integrate low cost and large scale production line.

The emergence of the third generation photovoltaic cells based on hybrid junctions (nanocrystalline inorganic materials and organic dye) and organic photovoltaic materials (polymers and low molecular weight organic compounds) has drawn much attention because they offer a possibility of low cost fabrication (solution based printing or roll-to-roll mass production) together with other attractive features like flexibility.^[7] Despite their potential advantage, third generation solar cells still suffer from low conversion efficiencies and unproven long term stability and reliability. Among all the third generation solar cells, the dye-sensitized solar cell (DSSC), also known as Grätzel cell, appears to be most promising. A DSSC is a photoelectrochemical system in which a nanoporous metal oxide film with adsorbed dye molecules acts as the photoanode and plays a significant role in converting photons into electrical energy. TiO_2 and ZnO are wide band gap semiconductors, which have been used widely for the fabrication DSSC photoanodes. In 1991, Grätzel and O'Regan demonstrated a device based on the sensitization of mesoporous, nanocrystalline TiO_2 with a conversion efficiency of 7.1 %.^[8] This discovery opened a new field of scientific research and since then many research groups have worked on the improvement of the efficiency and the stability of this kind of solar cells. The DSSC has many advantages, such as high incident solar light-to-electricity conversion efficiency, colorful and decorative designs, and low cost of production.



Figure 1.1 The flexible DSSC module developed by Dyesol for the Australian Army camouflages itself in trees, where it provides constant voltage under a wide range of illumination.^[9]

DSSC-based photovoltaic devices are not yet generally available in the market. But there exist several companies which are already very close. The Australian company Dyesol is the current leader in industrial-scale DSSC material development and

marketing. The company has recently introduced a flexible, foldable, lightweight, and camouflaged solar panel for military applications that has been found to be superior to other photovoltaic technologies in maintaining voltage under a very wide range of light conditions.^[9] Other companies that already have automated, high throughput DSSC production are G24 Innovations, Inc. in Great Britain and Konarka, Inc. in the USA. Common to all these companies is cost-efficient roll-to-roll type manufacturing of the DSSC on flexible, plastic or metal substrates, products including for example mobile phone chargers and “electric fabric” (Figure 1.2).



Figure 1.2 Examples of flexible DSSC products.

However, several issues must be overcome before full commercial viability of the DSSC. A major technical issue of continuing using of transparent conducting oxide (TCO) based substrates is the limited availability of indium. Taking this into account, alternatives to Sn-based TCOs must be considered. Another issue concerning the industrialization of DSSC technology is the long-term stability. As will be described in Chapter 5, the substitution of organic solvent electrolyte by non-volatile ionic-liquid is a very promising approach towards reaching high stability demands.

1.2 Objectives and structure of the present work

The main objective of this study is to identify the advantages and limitations of flexible ZnO-based dye-sensitized solar cells. To achieve this general objective, this work has been divided in three main topics: (1) the search for suitable flexible conductive substrates, (2) the optimization of the organic solvent electrolyte composition to develop ZnO-based DSSC with high performance and the substitution of organic solvent electrolytes by ionic liquids to develop ZnO-based DSSC with high long-term stability and (3) the test of dyes with phosphonic acid anchoring groups in ZnO-based DSSCs.

Chapter 2 describes the principles behind the operation of DSSC and discusses the state-of-the-art in DSSC research. The key components of the DSSC and manufacturing methods are introduced.

In **Chapter 3** the methods and procedures employed for the characterization and the fabrication of DSSC in this study are described.

From **Chapter 4** to **Chapter 6** the results of the research carried out along this thesis are presented in detail.

In **Chapter 4**, alternative dye-sensitized solar cell substrate to glass, namely ITO-PET (indium-doped tin oxide coated polyethyleneterephthalate), ITO-CNT (carbon nanotubes coated polyethyleneterephthalate) and industrial metal sheets are investigated. The photovoltaic performances of dye-sensitized solar cells based on these different substrates are analyzed by several photoelectrochemical characterization methods.

In **Chapter 5**, the iodine and iodide concentration of organic solvent electrolyte are optimized in order to develop ZnO-based DSSC with high performance and several combinations of ionic liquids are tested as electrolytes for ZnO-based cells sensitized with indoline dye D149. The long-term stability of DSSCs with organic solvent electrolyte and ionic liquids are investigated.

In **Chapter 6**, a comparative study between dyes with carboxylic acid and phosphonic acid anchoring groups is carried out.

Finally in **Chapter 7**, conclusions are drawn together with an outlook on the future research of flexible ZnO-based DSSC. **Chapter 8** lists the references used in this study.

2 Dye-sensitized Solar Cells

In a conventional p-n junction photovoltaic cell the semiconductor assumes simultaneously the function of harvesting sunlight to create an electron-hole pair and the transport of charge carriers. A unique feature of DSSCs is that they separate the function of light absorption from charge carrier transport: the dye is the element responsible for light absorption and charge generation, while charge transport occurs both in the semiconductor and in the electrolyte.

The backbone of a standard dye-sensitized solar cell is a mesoporous layer of semiconductor oxide nanoparticles, which have been sintered together to allow electronic conduction. This film is deposited on a glass plate covered with a transparent conducting oxide, which allows light to enter in the cell. Attached to the surface of the oxide is a monolayer of dye molecules, which upon light absorption are promoted into an excited state. The sensitized film is surrounded by an electrolyte solution of high ionic strength, usually composed of an organic solvent containing a I^-/I_3^- redox couple (Figure 2.1).^[10]

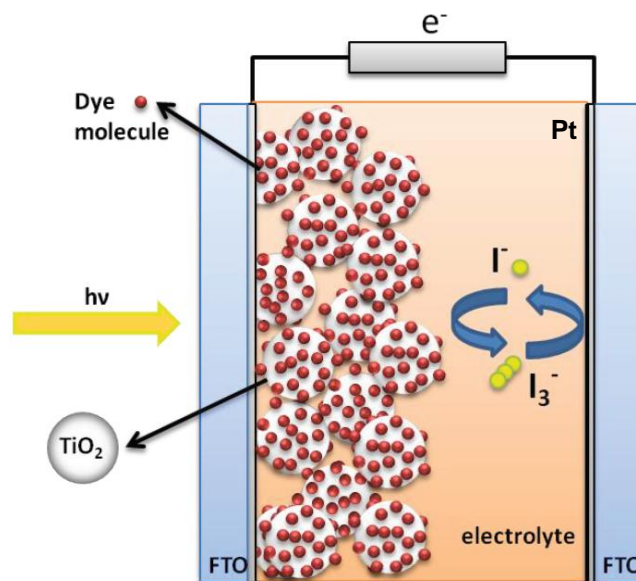


Figure 2.1 Schematic view of a dye-sensitized solar cell device.

2.1 Operating principle of DSSC

Dye-sensitized solar cells are photoelectrochemical devices where several electron transfer processes run in parallel and in competition. A scheme of the interior of a DSSC showing the principle of how the device operates is shown in Figure 2.2.

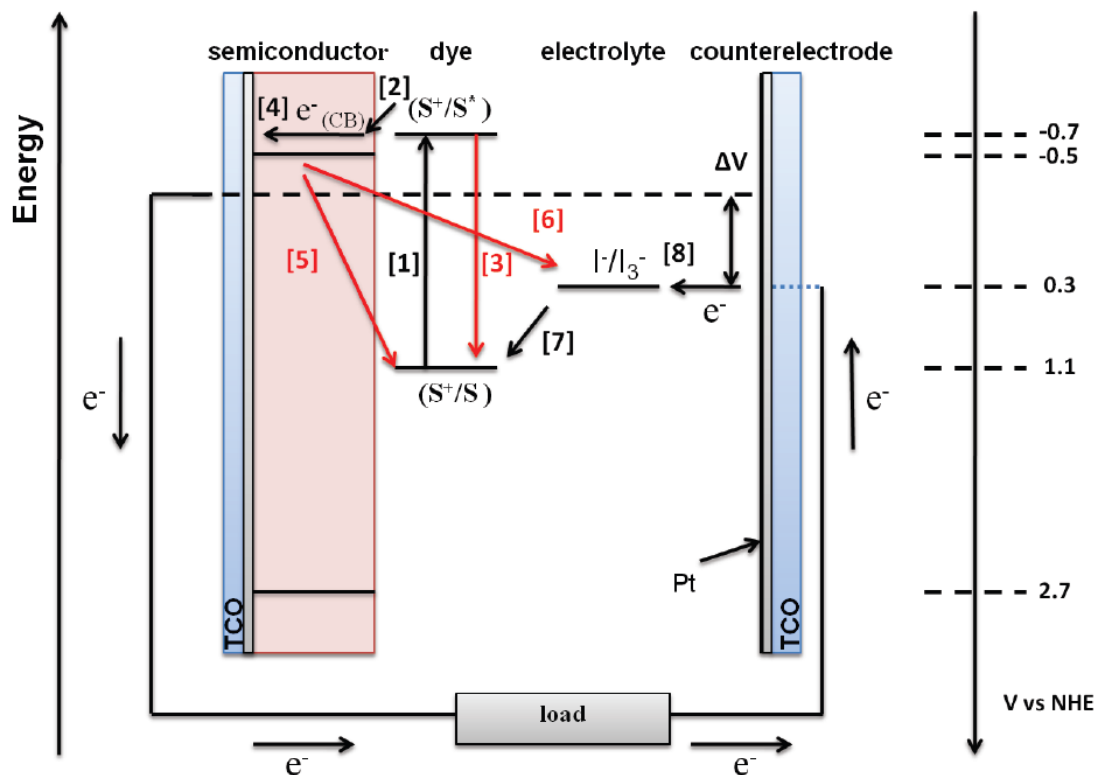


Figure 2.2 Working scheme of a typical dye sensitized solar cell.^[11] The basic electron transfer processes are indicated by numbers 1-8: the desired pathway of the electron transfer processes (processes 1, 2, 4, 7 and 8, \rightarrow) and the loss processes (processes 3, 5 and 6, \rightarrow).

Upon illumination, the incoming photon is absorbed by the dye molecule adsorbed on the surface of semiconductor oxide particle and the dye molecule is excited from a fundamental state S_0 to an excited state S^* (1). Photoexcitation of the dye results in the injection of an electron into the conduction band of the metal oxide. The electron leaves the excited dye molecule to an oxidized state S^+ (2). At the same time, relaxation of the excited dye before electron injection may occur (3) and the oxidized sensitizer can recombine with the injected electron (5). The injected electron percolates through the porous nanocrystalline structure to the transparent conducting oxide layer of the glass substrate (negative electrode, anode) and finally through an external load to the counter-electrode (positive electrode, cathode) (4). At the counter-electrode the electron reacts with triiodide in the electrolyte to yield iodide (8), and the cycle is closed by reduction of the oxidized dye by the iodide in the electrolyte (7). The major loss in this process is the recombination of the injected electrons with the oxidized redox mediator (6).

The operating cycle can be summarized in chemical reaction, as will be described below.^[11] The undesired loss processes are written in red color.

[1] Photoexcitation	$S + h\nu \rightarrow S^*$
[2] Electron injection	$S^* \rightarrow e^- + S^+$
[3] Relaxation	$S^* \rightarrow S + h\nu$
[4] Electron transport	Electron transport through porous semiconductor film
[5] Recombination with the dye	$S^+ + e^- \rightarrow S$
[6] Recombination	$2 e^- + I_3^- \rightarrow 3 I^-$
[7] Dye regeneration	$2 S^+ + 3 I^- \rightarrow 2 S + I_3^-$
[8] Reaction at the counter electrode	$I_3^- + 2 e^- \rightarrow 3 I^-$

The maximum theoretical value for the photovoltage at open circuit condition (open-circuit voltage, V_{oc}) is determined by the potential difference between the quasi-Fermi level of the semiconductor and the Nernstian potential of the redox system.^[12]

Dye-sensitized solar cells are highly complex systems. There are a lot of processes interconnected with each other and the chemical complexity of the device makes it difficult to study separately the single processes affecting the functioning of the cell. In fact, these processes must be studied in complete devices, because their characteristics are affected by the overall functioning.

2.2 Basic materials of DSSC

In the following the key components of the DSSCs will be introduced.

2.2.1 Substrate

The dye-sensitized metal oxide is always deposited on a conducting substrate. Requirements for a good conducting substrate are low sheet resistance, high transparency and ability to prevent impurities such as water from entering into the cell. The traditional approach is to build the DSSC on transparent conducting oxide (TCO) coated glass sheets. Fluorine-doped tin oxide (FTO or $\text{SnO}_2:\text{F}$) and indium-doped tin oxide (ITO or $\text{In}_2\text{O}_3:\text{Sn}$) are the most frequently used TCOs in DSSCs, whose sheet resistances are around $10 \Omega/\text{sq.}$ ^[13] While glass is obviously an effective barrier towards water and oxygen permeation into the cell, it brings restrictions related to fragility, heavy weight and shape limitations. Alternative substrate materials such as plastic foils and metal sheets overcome most of the disadvantages of glass. Replacing the glass substrate with plastic materials, like PET-ITO and PEN-ITO (indium-doped tin oxide coated polyethyleneterephthalat and polyethylenenaphtalate) makes possible the fabrication of light weight, thin, and low-cost DSSCs through roll-to-roll mass production. However, using plastics as substrate material in DSSCs causes several problems including low temperature tolerance (max. $150 - 180 \text{ }^\circ\text{C}$) and oxygen and water permeation. Compared with TCO coated polymer films, metal sheets have some advantages such as mechanical robustness, high conductivity and reflectance. High conductivity of metal sheets can reduce the internal resistance, leading to an increase in the fill factors and conversion efficiencies of the DSSCs, which plays a crucial role in cell size upscaling.^[14] For metals, the main problem is the traditionally used iodine-containing electrolyte. Triiodide ions are corrosive, and thus only stainless steel and titanium have shown sufficient chemical stability in the iodine electrolyte to be successfully employed as DSSC substrates.^[14-22] It has also been found that substrate-mediated recombination from stainless steel is equal to or less than that from TCOs.^[15] However, the main objective behind the alternative substrate research is the flexibility of both the plastic and metal substrates which enables roll-to-roll type manufacturing of the DSSC, making it possible to produce photovoltaic cells in large quantities and at high throughput, and thereby at substantially lower costs. In addition to this, flexible substrate based cells would be lighter, thinner and easier to handle and transport than

glass substrates.

2.2.2 Semiconductor

The semiconductor, typically a metal oxide, is responsible for the physical support of the sensitizer molecules and the electron transport of photogenerated electrons to the conducting substrate in a dye sensitized solar cell. The metal oxide should be chemically stable and inert towards the electrolyte species, it should have a lattice structure suitable for dye bonding and it should be available in nanostructured form to enable high enough dye loading. In addition, the position of the conduction band edge should be located slightly below the LUMO level of the dye in order to facilitate efficient electron injection. The wide band gap semiconductor TiO_2 has been by far the most widely used DSSC photoelectrode material. Other n-type metal oxide semiconductors, such as ZnO ,^[23, 24] SnO_2 ^[25] and Nb_2O_5 ^[26] can also be used in DSSCs. However, up to now, no other material has reached efficiencies comparable to TiO_2 . Nevertheless, some metal oxides present special characteristics that make them very attractive candidates as alternatives to TiO_2 . Among these potential replacements for TiO_2 , ZnO has nearly the same band gap and conduction band edge to that of anatase TiO_2 (Figure 2.3).^[27, 28] Single-crystalline ZnO presents much higher electron mobility than anatase TiO_2 , which should favour electron conduction,^[27-31] making it the best candidate for use in DSSCs beside TiO_2 .

ZnO is a direct wide band gap semiconductor with a large and diverse application potential. It crystallizes in two main forms, hexagonal wurtzite and cubic zincblende. ZnO with a wurtzite structure is naturally an n-type semiconductor due to oxygen vacancies and thermodynamically stable at ambient conditions. It can be intrinsically doped via oxygen vacancies and/or zinc interstitials.^[32, 33] Extrinsicly, ZnO can be doped both n- and p-type.^[34]

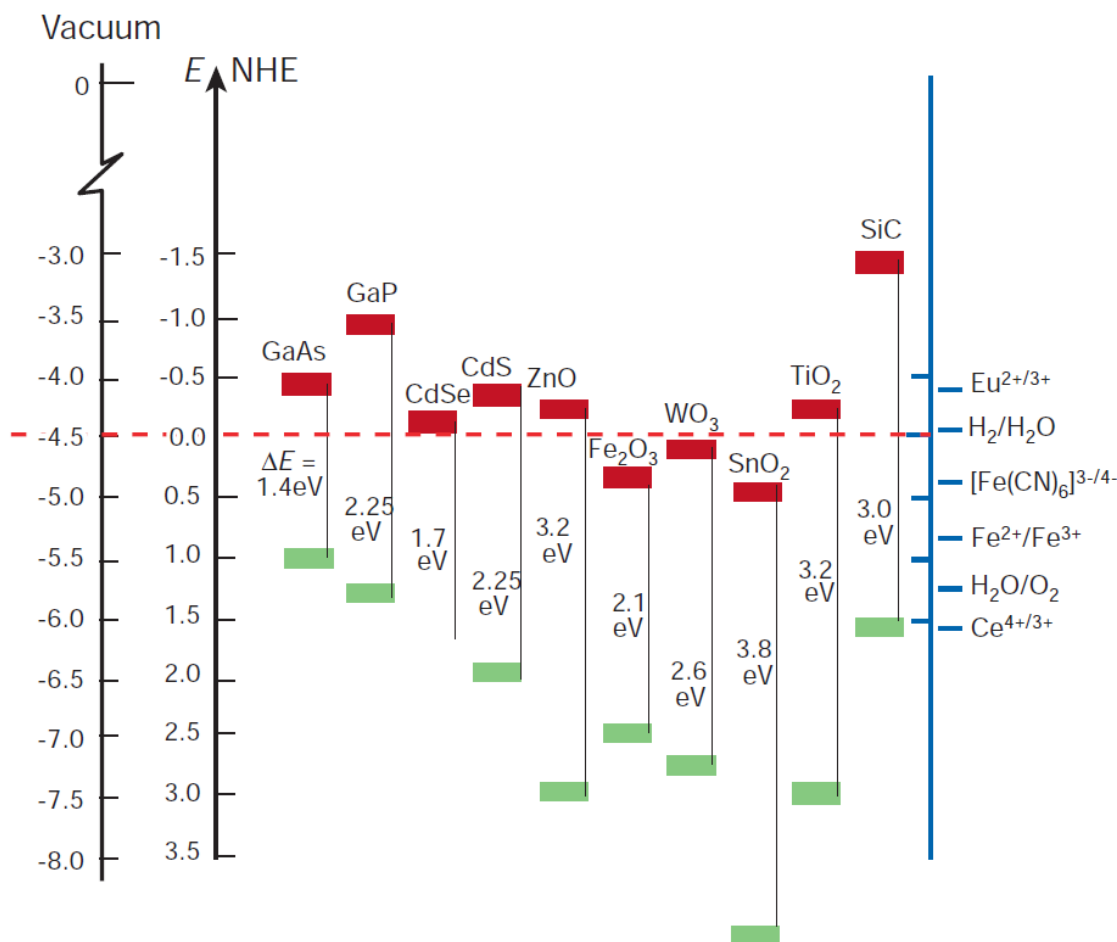


Figure 2.3 Band positions of several semiconductors in contact with aqueous electrolyte at pH 1. The lower edge of the conduction band (red color) and upper edge of the valence band (green color) are presented along with the band gap in electron volts. The energy scale is indicated in electron volts using either the normal hydrogen electrode (NHE) or the vacuum level as a reference. On the right side the standard potentials of several redox couples are presented against the standard hydrogen electrode potential.^[35]

In the last years, a great interest has been paid to this oxide in the field of DSSC and ZnO is the second most used semiconductor.^[11] Unfortunately, the efficiency of DSSC based on ZnO photoelectrodes is much lower than that based on TiO₂ photoelectrodes. Up to now the best result for a ZnO DSSC was achieved by Xu *et al.*,^[36] who obtained a 7 % overall efficiency. This is around 60 % of the maximum efficiency obtained for TiO₂ (11.5 %).^[37] In order to improve the efficiency of DSSC based on ZnO films, various methods have been used to optimize the ZnO photoelectrodes, e.g. by the shape control,^[38-40] metal and metal oxide deposition,^[41-44] element doping,^[45-47] and light-scattering layer.^[48, 49] Chen *et al.* and other groups prepared nanowire, nanosheets,^[39] nanoflowers,^[40] nanospheres, and nanorods of ZnO with good linkage to improve the electron transfer speed. Au^[41, 42], MgO^[44], and CuO^[43] were coated on the surface of

ZnO to form the core/shell composite, which provides an alternative pathway for electron to move across ZnO barrier. The aggregates formed by nano-sized ZnO crystallites are able to offer both a large specific area and desirable size comparable to the wavelength of light. The use of these aggregates in a DSSC can generate effective light scattering and thus extend the traveling distance of light within the photoelectrode film. More than 120 % increase in the conversion efficiency (from 5.6 % to 6.8 %) was achieved with photoelectrode film consisting of ZnO aggregated compared with that comprised of nanocrystallites only.^[48] Doping of the ZnO with Ga,^[45] Al,^[46] and Sn^[47] led to substantial improvements in overall conversion efficiency compared with pure ZnO.

To date, as mentioned before, the highest solar energy conversion efficiency achieved for a ZnO DSSC based on glass substrates was 7 % with multilayer ZnO nanowire arrays by Xu *et al.*^[36] Saito *et al.*^[50] reported a solar energy conversion efficiency of 6.58 % in a DSSC based on FTO glass using ZnO nanocrystalline pastes and N719 dye as sensitizer. The highest efficiency for ZnO-based DSSC prepared by a low-temperature method was reported by Yoshida *et al.*,^[51] who achieved a solar energy conversion efficiency of 5.6 % using the electrochemical deposition method for ZnO film preparation. Liu *et al.*^[52] reported a light-to-electricity conversion efficiency of 3.8 % for a flexible ZnO nanoparticle-based DSSC utilizing a PET-ITO substrate.

The TiO₂-based DSSCs exhibit excellent stability under long-term light soaking, e.g. only minor performance losses occur under light soaking for 8000 hours at 2.5 times full solar the intensity, obtaining long-term stability at temperatures of 80–85 °C had remained a major challenge for over 10 years.^[53] Only few studies have focused on the long-term stability of ZnO-based DSSCs.^[54, 55] Lin *et al.* reported the long-term stability of DSSCs based on ZnO nanowires array sensitized by N3 very poor as their photocurrents drop to zero after illuminating in the simulated sunlight for 150 hours.^[54] Tian *et al.* reported the stability of DSSCs based on aggregates of ZnO spheres sensitized by N719 was excellent. They can maintain about 90 % of their initial energy conversion efficiency after half a year running in the room or under outside ambient condition.^[55] The shorter lifetime of ZnO-based DSSCs compared to TiO₂-based DSSCs might be due to the degradation of organic materials, especially fully organic indoline dye under light irradiation and/or with increasing temperature^[56, 57]; the decrease in conductivity of ZnO upon oxygen absorption^[58] and the chemical change of the electrodes caused by acidic dyes.^[59]

2.2.3 Photosensitizers

The dye is the photoactive element of the photovoltaic device, harvesting the incident light for the photon-to-electron conversion. To be used as sensitizer for a single junction photovoltaic cell, the dye must fulfill the following requirements:^[60]

- The dye should ideally absorb all light below a threshold wavelength of about 920 nm.
- It must carry attachment groups such as carboxylate or phosphonate to graft it to the semiconductor oxide surface.
- The energy level of the excited state should be well matched to the conduction band edge of the oxide. Its redox potential should be sufficiently high that it can be regenerated via electron donation from the redox electrolyte or a solid hole conductor.
- The dye must possess long-term stability for reproducible device characterization as well as for future commercial applications.

The structural formulas of some well-known sensitizer dyes are shown in Figure 2.4. Ruthenium-complex dyes are the most used as well as the most successful sensitizers for application in DSSCs. A dye-sensitized solar cell using Ru complexes as a photosensitizer was first reported by O'Regan and Grätzel in 1991.^[8] N3 and N719, enabling DSSCs with overall power conversion efficiencies of 10.0 % and 11.2 %, respectively, harvest visible light very efficiently with their absorption threshold being at about 800 nm.^[61, 62] Based on intensive efforts to enhance spectral response in the red and near IR region, a “black dye” N749 was developed. The black dye achieves very efficient panchromatic sensitization of TiO₂ over the whole visible range extending into the near-IR region up to 920 nm.^[63] Since 1997, a large series of modifications of these early Ru(II) complexes have led to sensitizers with amphiphilic properties and/or extended conjugation, achieving power conversion efficiencies up to 11.9 %.^[37, 64-73]

Although high efficiency and stability have been achieved with ruthenium based dyes, in fact, they are not suitable for environmentally friendly photovoltaic devices because they do not meet the low cost and mass production requirements needed for potentially wide applications. Numerous metal-free organic dyes with high absorption coefficients have recently been reported to act as good sensitizers for TiO₂.^[74-77] In particular,

indoline dyes such as the D149 dye shown in Figure 2.4 have been reported to show power conversion efficiencies of over 9 % when using volatile electrolytes among organic dyes.^[78] However, organic dyes also have weaknesses such as their relatively narrow absorption bands in the visible region, leading to unsatisfactory light harvesting in the entire visible spectrum, along with questionable photostability. Another strategy to obtain a broad optical absorption extending throughout the visible and near IR region is to use a combination of two dyes which complement each other in their spectral features.^[79] The results were encouraging in as much as the optical effects of the two sensitizers were found to be additive.

Apart from seeking more efficient dyes, one can also enhance the stability and performance of DSSCs by utilizing surface coadsorbents.^[80-84] In brief, co-adsorbing the sensitizer with an amphiphilic compound on the semiconductor, apart from increasing the sensitizer's tolerance against water attack, leads to a more compact dye-amphiphile monolayer than the adsorption of the dye alone. At the same time, the formation of dye agglomerates is suppressed.

Semiconductor quantum dots are another attractive option. These are II - VI and III - V type semiconductor particles whose size is small enough to produce quantum confinement effects. By changing the particle size, different absorption spectra are obtained. Furthermore, quantum dots have a higher extinction coefficient than conventional dyes. One problem is the photo-corrosion of the quantum dots when the junction contact is a liquid redox electrolyte.^[85]

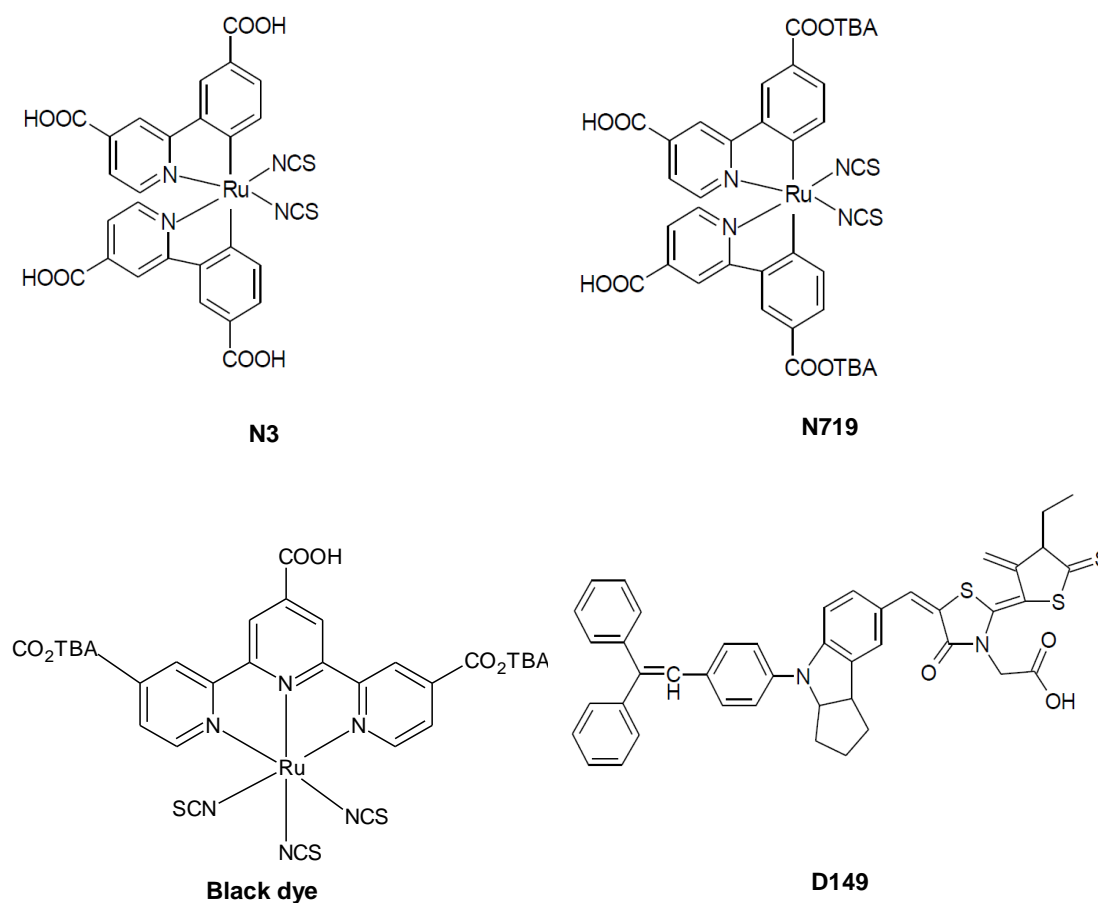


Figure 2.4. Molecular structures of sensitizing dyes N3, N719, black dye and D149.

2.2.4 Electrolyte

In DSSCs, the electrolyte regenerates the dye, following electron injection, and is responsible for charge transport between the photoanode and the counter electrode. An ideal electrolyte should display the following characteristics:^[86]

- Its redox potential should be as positive as possible but still more negative than the redox potential of the sensitizer, maximizing the cell voltage.
- The electrolyte mediator should not absorb in the visible range to prevent competition with the sensitizer.
- The redox couple must be reversible at the counter electrode and chemically inert toward all other components in the DSSC.
- The reduced and oxidized form of the redox couple should be highly stable to enable long operating life.

- The redox couple should be highly soluble in the solvent to ensure a high concentration of charge carriers in the electrolyte.
- The solvent should allow fast diffusion of the charge carriers and should not contribute to desorption of the dye from the surface of the semiconductor.

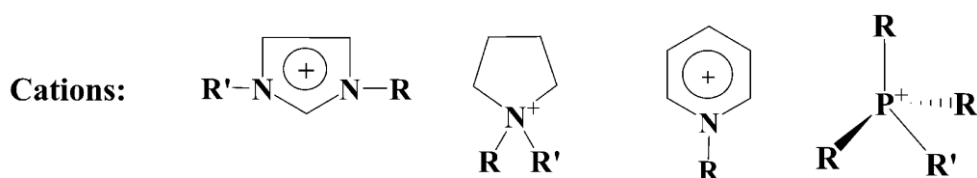
The most used liquid electrolyte in DSSCs contains a redox couple iodide/triiodide (I/I_3^-) with counter ions (e.g., Li^+ , K^+ , Na^+ , Mg^{2+} , or tetrabutylammonium TBA^+) and additives (e.g. 4-tert-butylpyridine or guanidium thiocyanate) in an organic solvent (e.g. acetonitrile, ethylene carbonate or methoxyacetonitrile). The slow recombination and fast dye regeneration rates of the I/I_3^- redox couple have resulted in relatively high power conversion efficiency.^[87] However, the iodide-based electrolytes are highly corrosive and absorb strongly in some regions of the visible spectrum.^[88] Developing alternatives to the I/I_3^- couple, including $(SeCN)_2/SeCN^-$, $(SCN)_2/SCN^-$,^[89, 90] Br_3^-/Br^- ^[91] and $Co(II)/Co(III)$ ^[92] is an active area of research. Among these the most tested and most viable alternative is the use of $Co(II)/Co(III)$ -complexes. Compared to iodide, their advantage is that they are non-volatile, non-corrosive and have the benefit of being easy for molecular modifications. However, such redox couples often yield shorter electron lifetimes when used in the DSSCs. Their faster interfacial charge recombination, when compared with I/I_3^- couple, lowers the photovoltage and reduces the efficiency of charge collection, decreasing the short circuit photocurrent density and hence the power conversion efficiency.^[92, 93] Recent evidence suggests that the introduction of long-chain alkyloxy groups in the dye structure may retard the unwanted charge recombination process.^[94] Donor- π -bridge-acceptor (D- π -A) sensitizers, endowed with such groups, recently reached V_{oc} values exceeding 0.8 V when used with $Co(II)/Co(III)$ redox electrolytes. Recently, Yella *et al.* reported mesoscopic solar cells that incorporate a $Co(II)/Co(III)$ -based redox electrolyte in conjunction with a custom synthesized donor- π -bridge-acceptor zinc porphyrin dye as sensitizer, leading to a new record power conversion efficiency of 12.3 %.^[93]

The main problem of DSSC is sealing permanently a volatile organic solvent. To avoid this problem, two alternatives have been employed in order to increase the stability in the performance of the DSSC: (i) the use of solvent free ionic liquid based electrolytes, and (ii) the application of solid electrolytes or p- type semiconductors such as copper iodide (CuI),^[95] copper thiocyanate (CuSCN)^[96] and 2,2',7,7'-tetrakis-(N,N-di-p-methoxyphenyl-amine)-9,9'-spirobifluorene (spiro-MeOTAD),^[97] but in all cases the

incident monochromatic photon-to-electron conversion efficiency remained low.^[98] The key problem is the less efficient hole transport in the solid medium as a result of the relatively low hole mobility in semiconductors.^[99]

Ionic liquids (ILs)

Attractive alternatives to volatile organic solvents are nonvolatile, room-temperature ionic liquids (RTILs). Ionic liquids possess a high chemical and thermal stability, negligible vapor pressure, non-flammability and high ionic conductivity.^[100] They are composed of aromatic or non-aromatic organic cations, such as imidazolium, pyridinium, ammonium, sulfonium and phosphonium derivatives and a wide range of anions, from simple halides to larger inorganic anions such as tetrafluoroborate and large organic anions like trifluoromethanesulfonate (Figure 2.5).



Anions: Cl^- , Br^- , I^- , PF_6^- , BF_4^- , CF_3COO^- , CF_3SO_3^- , $[\text{N}(\text{CN})_2]^-$ etc

Figure 2.5 Examples of the cationic and anionic parts of ionic liquids.^[101]

Room-temperature ionic liquids have been widely tested as alternative electrolytes for DSSCs. However, the high viscosity of ionic liquids appears to limit their use because of mass transport limitations^[102] and high recombination rates^[103]: diffusion coefficients of the redox-couple components (I_3^-) in ionic liquid electrolytes are about 1 – 2 orders of magnitude lower than those in volatile organic solvents. As a consequence, the efficiency of the reduction of oxidized dye D^+ by the reduced form of the redox couple is limited, thus decreasing the overall performance of the DSSCs.^[101]

Among the huge variety of ionic liquids available, the best results for DSSCs have been obtained with imidazolium cations. Imidazolium iodide ionic liquids have a relatively high viscosity (several hundred mPas), imposing severe mass-transfer limitations on the photocurrent in full sunlight. Additionally, the very high concentration (ca 5.8 M) of I^- present in the pure imidazolium iodide ILs entails two other disadvantages, the first being a reduction of the open circuit voltage (V_{oc}) of the cell due to the lowering of the Nernst potential of the counter-electrode^[104] and the second being that excited dye molecules can accept an electron from I^- , thus forming a reduced dye species (D^-),

which no longer injects electrons in the semiconductor, so that the short-circuit photocurrent density (I_{sc}) of the cell decreases.^[105] These problems are alleviated by using the mixtures of imidazolium iodides and a low-viscosity and low-melting IL, which functions as a so-called “solvent IL”. The nature of anions, e.g. their geometry and charge distribution, determines the strength of the cation-anion interactions and eventually the viscosity of an ionic liquid.^[106] Imidazolium salts containing non-electroactive anions such as thiocyanate,^[107] dicyanamide^[108] or tetracyanoborate^[104] have a much lower viscosity than the iodide based ionic liquids with imidazolium cations. It has been proven that the addition of imidazolium salts containing non-electroactive anions to imidazolium iodide decreases the viscosity of the electrolyte and improves the power conversion efficiencies of DSSC.^[107]

In ionic liquid electrolytes with a high iodide concentration the measured triiodide diffusion coefficient is observed to be much higher than expected on the basis of viscosity data^[109, 110] A mechanism for triiodide transport in ionic liquids has been suggested to explain this non-Stokesian behaviour. It is believed that apart from the normal physical diffusion, the triiodide transport is determined by a Grotthuss-type charge-exchange mechanism.^[109, 111, 112] The suggested charge-transfer processes for the case of triiodide is illustrated in Figure 2.6. The triiodide approaches iodide from one end, forming an encounter complex, from which triiodide is released at the other end. As a result, the triiodide is displaced by the length of one I–I bond without having to cross that distance. The Grotthuss mechanism describes charge transport rather than real mass transport. This is an apparent acceleration of the triiodide diffusion and can explain the abnormally high diffusion coefficients determined experimentally.

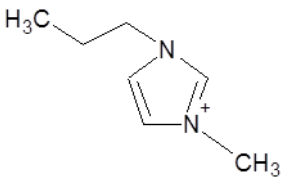
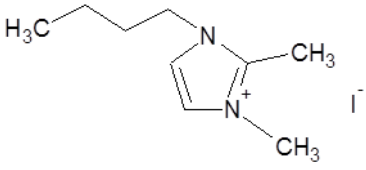
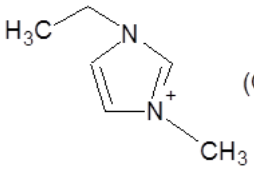
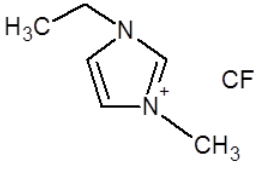
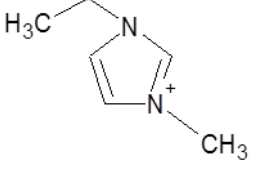


Figure 2.6 Schematic drawing of Grotthuss mechanism.^[113]

The toxicity research has demonstrated that many commonly used ionic liquids have a certain level of toxicity. The studies showed that shorter alkyl substituted chains (C_1 - C_4) demonstrate lower toxicity, whereas the toxicity of C_8 - C_{18} substituted salts worsen severely.^[114] The results also suggested that the cation type is an essential factor influencing the toxicity of ionic liquids, while the role of anion type remains uncertain, e.g. the imidazolium cation shows the highest toxicity in general, whereas the ammonium cation demonstrates the lowest toxicity.^[114]

In *Table 2.1* the molecular structure and the viscosity of the ionic liquids tested in this study is summarized.

Table 2.1 Molecular structures of the room temperature ionic liquids used in this study.

Full name	Abbreviation	Molecular structure	Viscosity (20 °C)/ mPa·s
ILs with imidazolium cations and iodide anions			
3-Propyl-1-methylimidazolium iodid	PMIM I		1132
1-Butyl-2,3-dimethylimidazolium iodid	BMMIM I		solid
Solvent ILs for adding into I⁻/I₃⁻ electrolyte			
1-Ethyl-3-methylimidazolium bis(trifluoromethylsulfonyl)imid	EMIM NTF		39.0
1-Ethyl-3-methylimidazolium trifluoromethylsulfonat	EMIM OTF		53.8
1-Ethyl-3-methylimidazolium tetracyanoborat	EMIM TCB		21.7

Additives

Different additives have been used in the electrolytes in order to enhance the photovoltaic performance of TiO₂-based DSSCs. Nitrogen heterocyclic compounds such as 4-tert-butylpyridine (TBP)^[115] and N-methylbenzimidazole (NMBI)^[116] are added to the electrolyte in order to improve the open-circuit potential (V_{oc}), while

guanidinium thiocyanate^[117] (GuNCS) was found to increase both V_{oc} and the I_{sc} . The exact role of the additives was investigated: TBP and NMBI deprotonate the TiO_2 surface by adsorption and thus shift the conduction band edge (E_c) toward negative potentials and passivate the surface active recombination sites.^[115, 116] On the contrary, guanidinium cation could suppress the surface recombination and shift the E_c to positive potentials, thus increasing the electron injection yield.^[117] Grätzel *et al.* reported that the addition of guanidinium cation to the electrolyte could control the self-assembly of the N3 dye at the TiO_2 interface and suppress the dark current, which results in a remarkable improvement of the cell voltage.^[118]

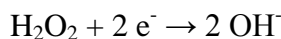
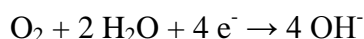
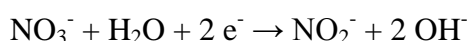
2.2.5 Counter electrode

The role of the counter electrode is to transfer electrons arriving from the external circuit back to the electrolyte at the counter electrode surface through the electrochemical reaction $I_3^- + 2e^- \rightarrow 3 I^-$.^[119] Therefore, an effective counter electrode should primarily possess an excellent catalytic activity for the reduction of triiodide ions. The most commonly used material is platinum, deposited on the conductive substrate by various methods like spin-coating, screen-printing, sputtering, etc.^[120] In order to reduce the cost of the counter electrode and prevent the corrosion of platinum by the iodide solution, other more inexpensive materials have been used, such as carbon,^[121] carbon black,^[122] graphite,^[123] carbon nanotubes^[124] and conductive polymers.^[125] Hybrid materials have been also employed, combining polymeric and carbonaceous materials such as polystyrenesulfonate doped poly(3,4-ethylenedioxythiophene) (PEDOT:PSS) with graphene^[126] and polyaniline with carbon black.^[127] Recently, a novel counter electrode was fabricated by the electrodeposition of CoS nanoparticles on flexible PEN-ITO films.^[128] Compared to the Pt deposited PEN-ITO film, the CoS deposited PEN-ITO film showed higher electrocatalytic activity for the reduction of triiodide. This was expected to have an important practical consequence on the production of flexible low-cost and lightweight thin film DSC devices based on the plastic matrix.^[128]

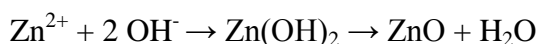
2.3 Electrochemical deposition of ZnO/dye hybrid thin films

Thin films of ZnO can be prepared by different methods such as sol-gel synthesis,^[129] hydrothermal/solvothermal growth,^[130] physical or chemical vapor deposition,^[131, 132] sputtering,^[133] spray pyrolysis^[134] or electrochemical deposition.^[135] In comparison of all these preparation methods, electrochemical deposition is the most economical due to the possibility to work at low temperature, which also allows the use of flexible conductive plastic substrates that are not stable at elevated temperatures, and without the need of vacuum conditions.

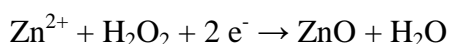
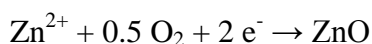
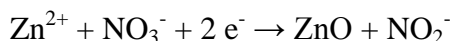
Cathodic electrodeposition of ZnO films from aqueous solution of zinc salts was first demonstrated by Izaki^[136] and Peulon^[137] in 1996, employing the reduction of the nitrate ion and dissolved oxygen, respectively. Later Pauporte demonstrated ZnO electrodeposition by reduction of hydrogen peroxide.^[138] These reactions lead to the formation of hydroxide ions as follows:



Zn²⁺ and OH⁻-ions precipitate as Zn(OH)₂, which dehydrates to ZnO at temperatures above 40 °C:

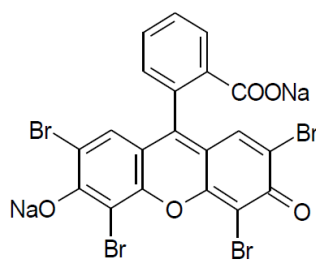


The respective overall reactions in the nitrate, oxygen, and hydrogen peroxide systems can be written as:



Among these reactions, the reduction of the nitrate ion is kinetically slow, while the other two are relatively fast. ZnO layers obtained by the latter two methods are dense and highly crystalline. The small surface area means that no appreciable amount of dye can be adsorbed, if electrodeposited ZnO films are simply soaked into solutions of photosensitizer dye. In 1998, Yoshida *et al.* reported the preparation of 2,9,16,23-tetrasulfophthalo-cyaninatozinc(II) (TSPcZn)-modified ZnO thin films by

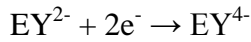
electrochemical deposition in one-step.^[139] Later the most striking example was the hybrid thin film electrodeposited in the presence of 2,9,11,23-tetrasulfophthalocyaninato-dihydroxosilicon(IV) (TSPcSi).^[140] The deposited ZnO/TSPcSi hybrid thin film has a totally different surface morphology compared to the pure ZnO thin film, as shown in SEM images, showing a lamellar structure in each single piece of ZnO crystal.^[140] It opened up the idea to utilize the dyes as structure directing agents (SDA) since the dye influences significantly the morphology and porosity. Electrodeposition of hybrid thin films was tested with various water-soluble dyes, such as eosin Y,^[141] coumarin 343^[142] and Ru(dcbpy)₂(NCS)₂.^[27] All of these dyes have carboxylic acid groups, which not only make the molecule soluble in water but also are necessary as “anchors” to stick to the ZnO surface.^[143] Among the various hybrid systems, electrodeposition of a ZnO/eosinY hybrid thin film exhibited the most interesting features.^[140, 141]



Eosin Y

Figure 2.7 Chemical structures of eosin Y.

Highly transparent and well adherent hybrid ZnO/eosinY film with high dye loading could be obtained in systems that employed reduction of O₂ and H₂O₂, while the films deposited in the nitrate system were not homogeneous and the deposition was poorly reproducible. The O₂ system turned out to be the most interesting because a hybrid thin film could be obtained over a wide potential range, even at potentials more positive than that needed for the reduction of the dye.^[143] When the dye eosin Y is added during a ZnO electrodeposition based on O₂ reduction, the dye catalyzes the reduction of O₂ and consequently the film growth. Furthermore, the dye in its reduced form is incorporated into the ZnO films via a complex formed between Zn²⁺ ions and reduced eosin Y (EY⁴⁻) ions:



Electroreduction of O_2 is a relatively fast reaction, making the process diffusion-limited. The electrodeposition of ZnO in the O_2 system receives mixed control, both by the charge transfer kinetics that is varied with the electrode potential and the mass transport that varies with the diffusion-layer thickness.^[144, 145] In order to introduce homogeneous forced convection, a rotating disk electrode is usually used during the deposition. A homogeneous thickness of the diffusion layer is achieved and thus the thin films are uniform with a high reproducibility. The eosin Y can be removed from the as-deposited ZnO/dye hybrid films by alkaline treatment, leaving a highly crystalline and porous structure. It consists of interconnected ZnO nanowires orientated perpendicular to the substrate plane. The porosity is very high, reaching a roughness factor of 400 for 3 μm thick films.^[146, 147]

2.3.1 Dye desorption and re-adsorption

Experiments have shown that eosin Y is loaded as aggregates when the hybrid film is electrodeposited. Dye molecules not bound to ZnO may absorb light but cannot inject electrons to ZnO. Additionally, eosin Y absorbs only in a very narrow range of visible light.^[143] As a consequence, the cell efficiencies are very poor when the electrodeposited ZnO/eosin Y hybrid thin films are used in DSSCs as prepared. Eosin Y can be removed following the deposition by mild alkaline solution (pH ca. 10), enabling the re-adsorption of another sensitizer with a broader absorption band on the surface of the porous ZnO (Figure 2.8). Film thickness does not change by the alkaline treatment because ZnO does not dissolve to any great extent at this pH.^[143] After these treatments, the dyes are re-adsorbed as a monolayer, so that all of the dye molecules can act as sensitizers.

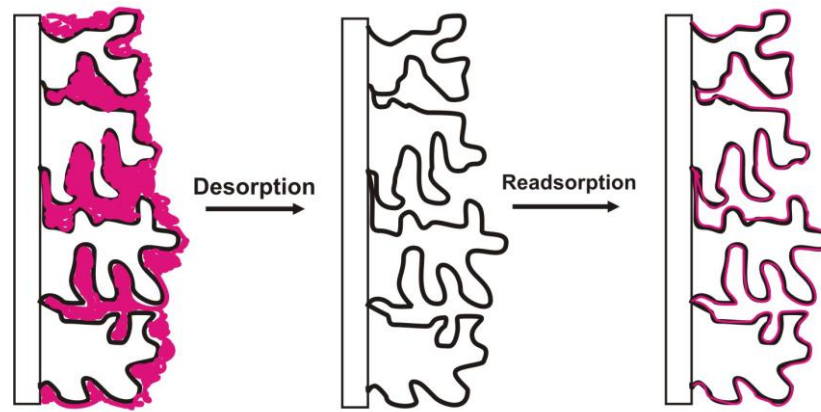


Figure 2.8 Graphical presentations of electrodeposited ZnO/EY hybrid film, dye desorption by mild alkaline treatment and re-adsorption of photosensitizer dyes.^[148]

2.3.2 Fast electron transport

A highly porous crystalline structure of ZnO is preserved after extraction of eosin Y from the electrodeposited ZnO/EY film by alkaline treatment. The electrodeposited film consists of well-grown ZnO crystals and has a large surface area because of the formation of nanopores within the grains. Oekermann *et al.* reported a very high electron collection efficiency of practically 100 % of the electrodeposited ZnO/EY films using intensity modulated photocurrent spectroscopy (IMPS) and intensity-modulated photovoltage spectroscopy (IMVS), which is caused by a remarkably fast electron transport due to the absence of grain boundaries and the high crystallinity of the electrodeposited material.^[149]

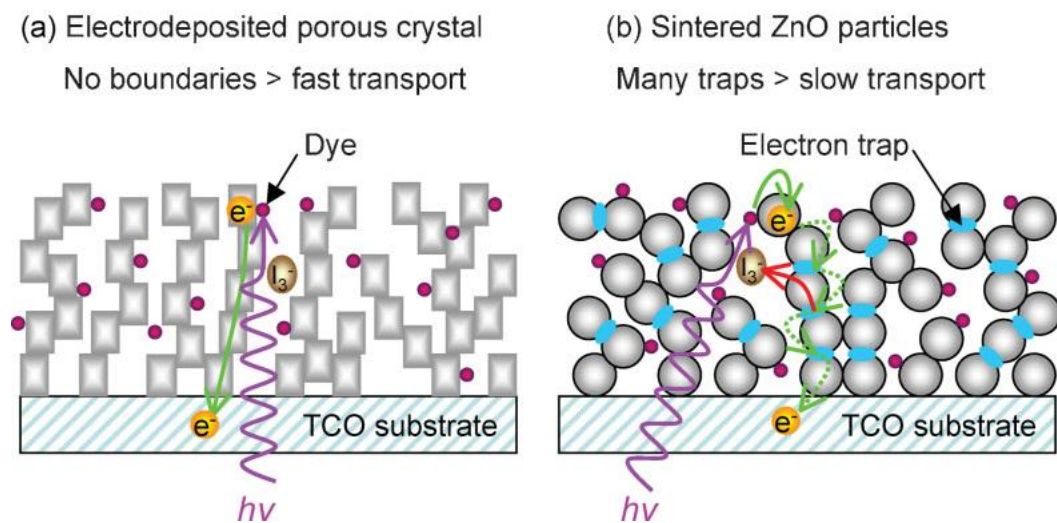


Figure 2.9 Qualitative model for the comparison of the electron transport in (a) electrodeposited ZnO/EY hybrid thin film and (b) colloid-processed ZnO film made from nanoparticles. The blue points at the grain boundaries in (b) indicate electron traps.^[143]

Figure 2.9 illustrates the reasons for the faster electron transport in electrodeposited ZnO. Electron traps, which are often located at grain boundaries and slow down the electron transport, are present in the colloidal film (Figure 2.9 b). As electrons spend some time in traps, the effective diffusion coefficient becomes smaller if the trap density becomes higher.^[149] The electrodeposited ZnO has a porous quasi-single crystalline structure, so that no or less grain boundaries can exist in the direction of electron diffusion, which leads to a higher effective diffusion coefficient (Figure 2.9 a).

3 Experimental

3.1 Preparation of ZnO/Eosin Y thin film

3.1.1 Cleaning of the Substrate

Before deposition, the substrates with a dimension of $2.5\text{ cm} \times 2.5\text{ cm}$ were ultrasonically cleaned by ultrapure water with detergent, acetone and isopropyl alcohol for 15 minutes each. Then the cleaned substrates were stored in isopropyl alcohol and dried in air before using them.

3.1.2 Mounting of the substrate

For electrodeposition, the cleaned conductive substrates were placed in a substrate holder suitable for mounting to a rotating disc electrode (RDE). The drawing of the substrate holder and the electrode preparation are illustrated in Figure 3.1. The contact between the substrate and substrate holder is established by using conductive copper tape at all 4 corners of the substrate (a-b in Figure 3.1). The deposition area of the ZnO film is defined with an insulating tape (Masking Tape N-300, Nitto Denko). A hole is made in the insulating tape by using a punch which has a diameter of 12 mm. Then, this insulating tape is attached on the substrate and substrate holder (c-d in Figure 3.1). The center of the hole in the insulating tape should be adjusted to the center of the substrate. The insulating tape is also rubbed sufficiently to make the gluing sure and to remove air bubbles which may still be enclosed by this tape. After this process, the substrate holder is screwed into the rotating disc electrode (Metrohm) and placed in the electrochemical deposition cell.

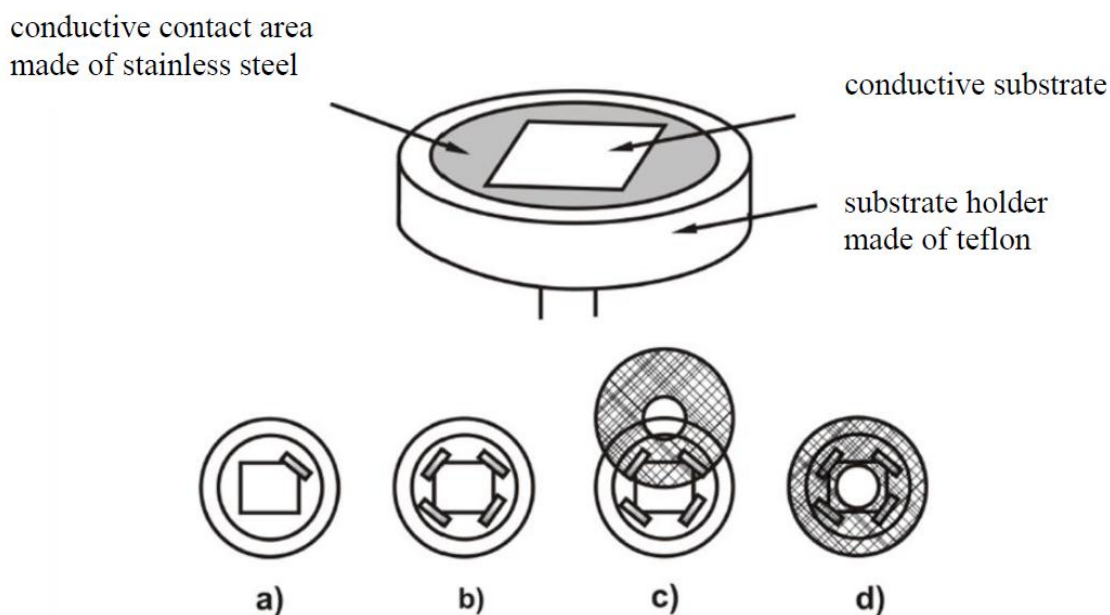


Figure 3.1 Drawing of the substrate holder and the procedure to mount the conductive substrate to the holder.

3.1.3 Electrochemical deposition of the ZnO/Eosin Y thin film

To prepare ZnO films in this study, the reduction of oxygen was utilized. An electrolyte of 180 ml ultrapure water containing 0.1 mol/L KCl (Carl Roth) is filled into the electrochemical deposition cell and maintained at 70 °C. A tube which supplies oxygen into the deposition cell is put into the electrolyte and oxygen gas is allowed to flow at a rate of 8 L/h. This condition is maintained approximately 15 minutes to achieve oxygen saturation in the electrolyte. A zinc wire is used as counter electrode. The electrodeposition was controlled with a Metrohm-Autolab PGSTAT 101 potentiostat. A potential of -0.91 V vs. Ag/AgCl reference electrode (Radiometer) is applied to the electrode and the rotational speed of RDE is set to 300 rpm. A scheme of the electrochemical deposition cell is shown in Figure 3.2.

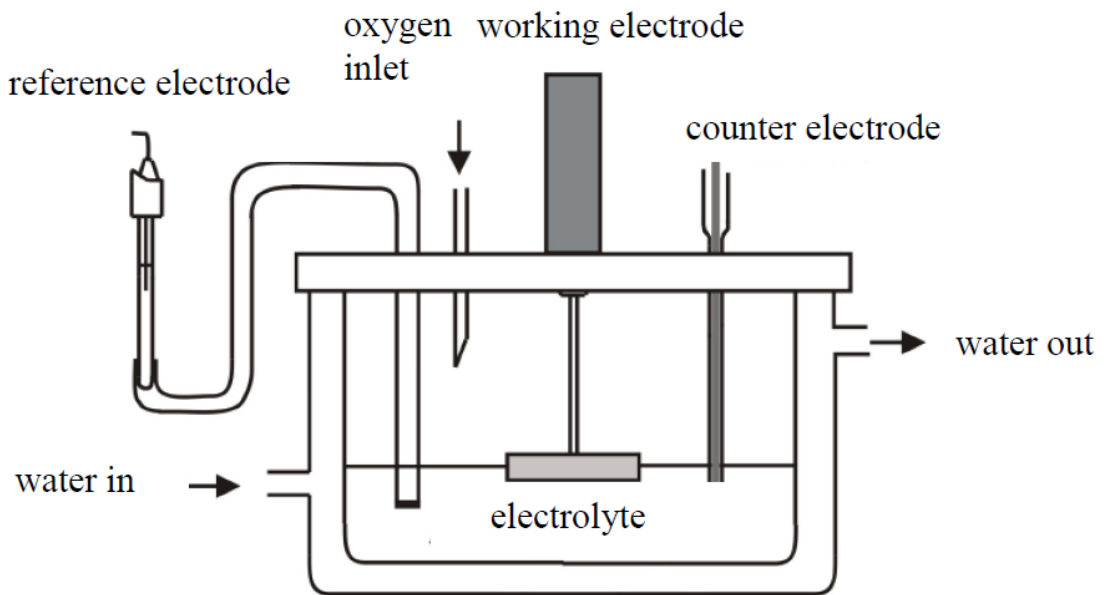


Figure 3.2 Scheme of the electrochemical deposition cell.

Before starting a deposition, the oxygen tube is taken from the electrolyte to make sure that no bubbles of oxygen reach the surface of the conductive electrode during deposition. Then a process called “pre-electrolysis” should be performed before deposition of a ZnO film (Figure 3.3, step 1). It consists of electrolysis in a solution without Zn^{2+} ions being present, so that oxygen starts to be reduced as OH^- at the electrode and makes the substrate hydrophilic, but no ZnO can precipitate. This process is necessary to activate the substrate, since it is observed that the current increases during this process.

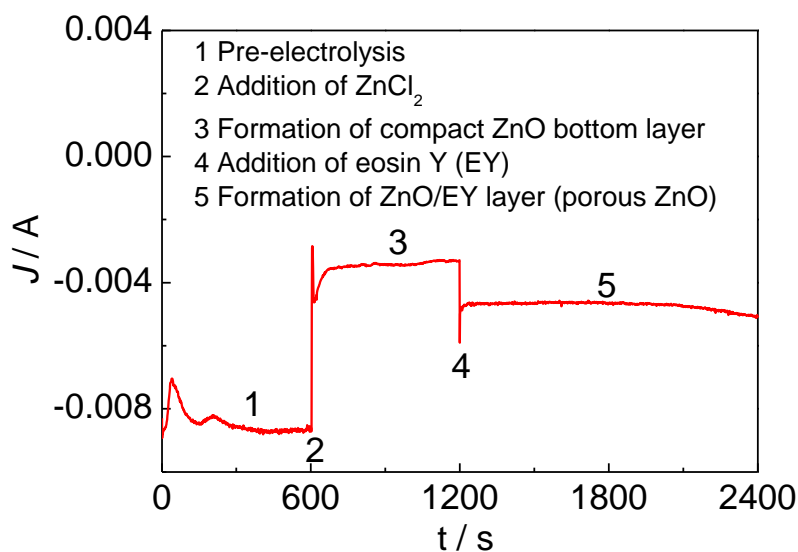


Figure 3.3 current-time curve of a one-step electrodeposition of ZnO/eosin Y hybrid thin film.

After the pre-electrolysis, 5 mmol/L ZnCl_2 (Sigma Aldrich) is added to the electrolyte to form a dense ZnO bottom layer (Figure 3.3, step 2 and 3). This ZnO bottom layer is utilized to prevent the contact between the I^-/I_3^- redox electrolyte and the conductive substrate in assembled DSSCs and thus to prevent recombination from the conducting back contact. The role of the bottom layer will be discussed in more detail in Chapter 4.2.3. Directly onto the bottom layer, a ZnO/dye layer is deposited after addition of 80 μM eosin Y dye (Figure 3.3, step 4 and 5). An increase of the current is observed upon addition of eosin Y, which may be attributed to the catalytic action of eosin Y toward oxygen reduction.^[150] The standard deposition time of the bottom layer and hybrid ZnO/dye layer is 10 minutes and 45 minutes, respectively. When the deposition is completed, the conductive substrate is removed from the substrate holder. For desorption of the dye from the hybrid layer in order to obtain a highly porous ZnO layer, the as-deposited film is soaked in a dilute aqueous KOH solution (pH 10.5) for 24 hours. After desorption of the dye the film is rinsed with water and dried under air at room temperature.

3.2 Characterization of the ZnO thin film

3.2.1 Film thickness

The film thickness of the samples was measured by a stylus method by using a DEKTAK 6M profilometer. The profilometer takes measurements electromechanically by moving a diamond-tipped stylus over the sample. The stylus is attached below a cantilever, which moved according to a user-programmed scan length, speed and stylus force. A laser beam is reflected from the top side of the cantilever to an optical detector. The stylus linearly scans the surface and the reflected beam is analyzed for determining the height difference of the structure and substrate as a function of vertical position.

3.2.2 UV-Vis spectroscopy

Ultraviolet-visible (UV-Vis) spectroscopy is used to obtain the absorbance spectra of a compound in solution or as a solid. The UV-Vis region of energy for the electromagnetic spectrum covers 1.5-6.2 eV which relates to a wavelength range of 200-800 nm. Molecules containing π -electrons or non-bonding n-electrons can absorb the energy in the form of ultraviolet or visible light to excite these electrons to higher anti-bonding molecular orbitals.^[151] The Beer-Lambert law is the principle behind absorbance spectroscopy. A simple image of this law is expressed in Figure 3.4. UV-Vis spectroscopic data can give qualitative and quantitative information of a compound or molecule.

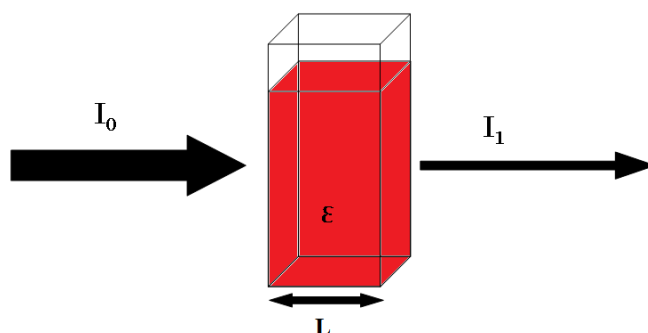


Figure 3.4 Model of Lambert-Beer absorption of a beam of light as it travels through a cell of length L .

The Lambert-Beer law is expressed by

$$A = \log_{10}\left(\frac{I_0}{I_1}\right) = \varepsilon \cdot c \cdot L \quad \text{Equation 3.1}$$

where A is the measured absorbance, I_0 is the intensity of the incident light at a given wavelength, I_1 is the transmitted intensity, ε the extinction coefficient, c the concentration of the absorbing species, and L the path length through the sample.

In this work, absorption spectra were measured by using a double beam UV-Vis-NIR Spectrometer (Cary Series 5000) at a scan speed at 600 nm/min and a slit of 1 nm. When the absorption spectrum of the ZnO film was measured, the conductive substrate was introduced as reference. For the absorption spectrum of solutions, a quartz cell with an optical path length of 1 cm was used for the measurement. An identical cell with pure solvent was introduced as reference.

Figure 3.5 shows the optical transmittance spectrum of a ZnO thin film (with 10 minutes and 45 minutes electrodeposited bottom layer and porous layer, respectively) in the wavelength range from 300 to 800 nm. The film is highly transparent in the visible range of the electromagnetic spectrum with an average transmittance of ca. 95 %.

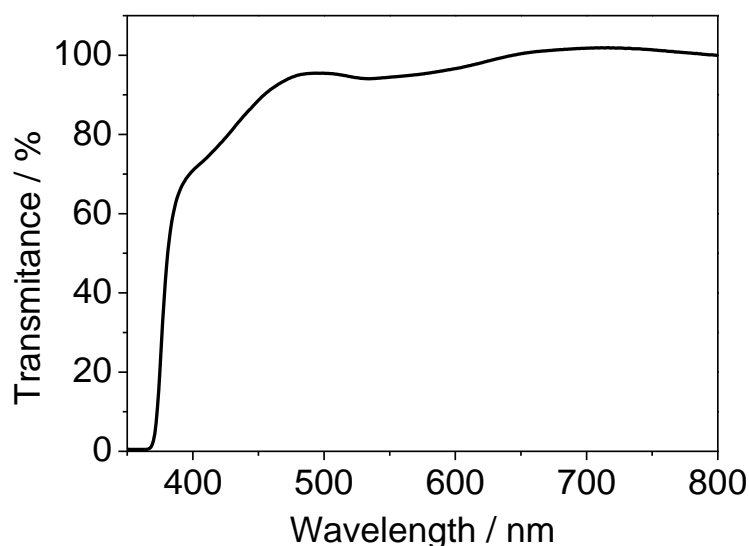


Figure 3.5 UV-Vis transmission curve of ZnO film on PET-CNT substrate.

3.2.3 Dye loading in the film

The hybrid ZnO/D149 film is put into 1 ml of dimethyl sulfoxide and dissolved completely. After the measurement of the absorption spectrum of the solution, the

amount of dye D149 loaded is calculated by using of the Lambert-Beer law and the calibration curve of D149 (Figure 3.6). The dye loading in the film was obtained by the calculation of the dye content and the film area.

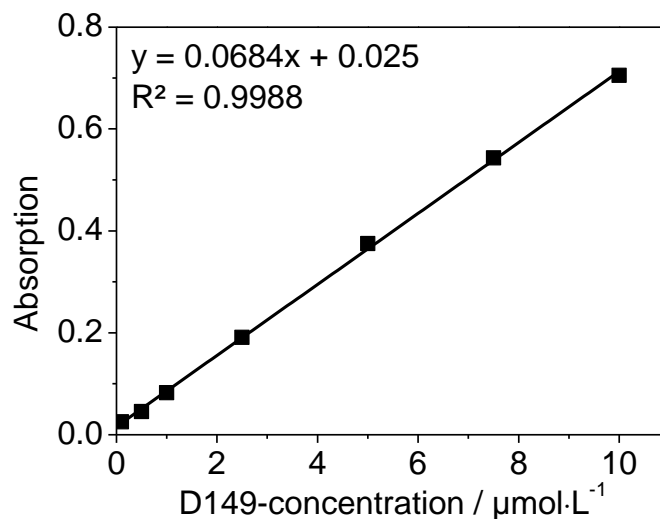


Figure 3.6 Calibration curve of D149.

3.2.4 Scanning Electron Microscopy (SEM)

A scanning electron microscope is a type of electron microscope that images a sample by scanning it with a focused beam of high-energy electrons. The electrons interact with the atoms of the sample and generate a variety of signals (Figure 3.7) that contain the morphological and topographical information of the sample surface.

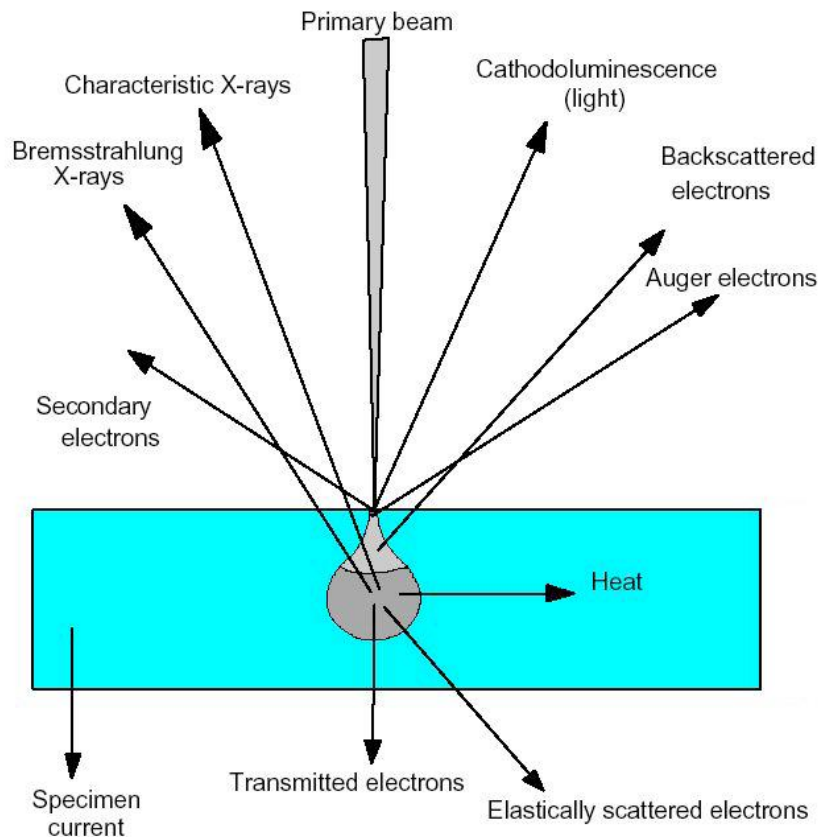


Figure 3.7 Signals resulted from electron beam-specimen interaction

An electron beam, emitted from the filament in the electron gun, is accelerated towards the sample and focused by several condenser lenses. When the focused beam hits a point on the sample, numerous collisions between the electrons from the beam and atoms in the sample will occur. Secondary electrons, backscattered electrons, and absorbed electrons are produced, flowing off as specimen current. In addition, X-rays, Auger electrons, and cathodoluminescence are produced. Secondary electrons are result of the inelastic collision and scattering of incident electrons with specimen electrons. They are generally characterized by possessing energies of less than 50 eV and used to reveal the surface structure of a material with a resolution of approximately 10 nm or better.^[152] Backscattered electrons are a result of an elastic collision and scattering event between incident electrons and specimen nuclei or electrons. They can be generated further from the surface of the material and help to resolve topographical contrast and atomic number contrast. Characteristic X-rays are emitted when the electron beam removes an inner shell electron from the sample, causing a higher-energy electron to fill the shell and release energy. They are used to identify the elemental composition in the sample through EDXS (energy dispersive x-ray spectroscopy). Cathodoluminescence is

the emission of photons of characteristic wavelengths from a material that is under high-energy electron bombardment. A compound or structure labeled with a luminescent molecule can be detected by using cathodoluminescence techniques.^[153] Auger electron production is an alternative to the characteristic X-ray emission for the relaxation of an atom after the ionization of an inner shell due to an electron-electron collision. They are exploited in Auger Electron Spectroscopy tools (AES).^[154]

Secondary electrons can easily be attracted by the detector. The detector counts the number of electrons emitted from this small area and the result is displayed as point on a computer screen. A magnified image of the sample is created by scanning the electron beam over a small area, detecting and displaying the number of electrons originating from each point. In the common detection mode “secondary electron imaging”, the SEM can produce very high-resolution images of a sample surface, revealing details less than 1 nm in size. Back scattered electrons images can provide information about the distribution of different elements in the sample, because the intensity of the back scattered electrons signals is strongly related to the atomic number of the specimen.^[155]

The morphology of the ZnO films was studied by scanning electron microscopy using a JEOL JSM-6700F field-emission instrument at a low excitation voltage of 2 kV for imaging with secondary electrons.

3.2.5 Cyclic voltammetry (CV)

Cyclic voltammetry (CV) is a very versatile electrochemical technique which allows to probe the mechanics of redox and transport properties of a system in solution. CV employs a three-electrode potentiostat with a working electrode, a reference electrode (usually saturated calomel electrode or Ag/AgCl) and an auxiliary or a counter electrode (platinum) that are immersed into an electrolyte solution. The potential is applied between the reference electrode and the working electrode and the current is measured between the working electrode and the counter electrode.^[156] In cyclic voltammetry, the electrode potential ramps linearly versus time. This ramping is known as the experiment's scan rate (V/s). The voltammogram is a display of current at the working electrode versus the applied voltage. Figure 3.8 shows the cyclic potential sweep and a typical cyclic voltammogram. As shown in Figure 3.8a, the potentiostat applies a linear potential ramp from E1 to E2 in time, and then sweeps the potential back to E1 with the same scan rate to complete a cyclic sweep. When the potentiostat applies a potential

toward a positive direction, the Fermi energy level of the working electrode decreases; then electrons in the electrolyte will cross the electrode-electrolyte interface and transfer to the working electrode. The electrolyte is oxidized in this process, and the cyclic voltammogram (Figure 3.8b) shows an oxidation peak. Afterward, the potentiostat applies potential in an opposite direction, and the free electrons in the working electrode will transfer to the electrolyte if the Fermi energy level of the working electrode is high enough. Thus a reduction peak occurs. The characteristic peaks in the cyclic voltammogram are caused by the formation of the diffusion layer near the electrode surface.^[157] The detailed shape of the cyclic voltammogram may be related to the concentration and diffusion coefficient of the electrolyte as well as the kinetics of the electron transfer and the voltage sweep rate.^[158]

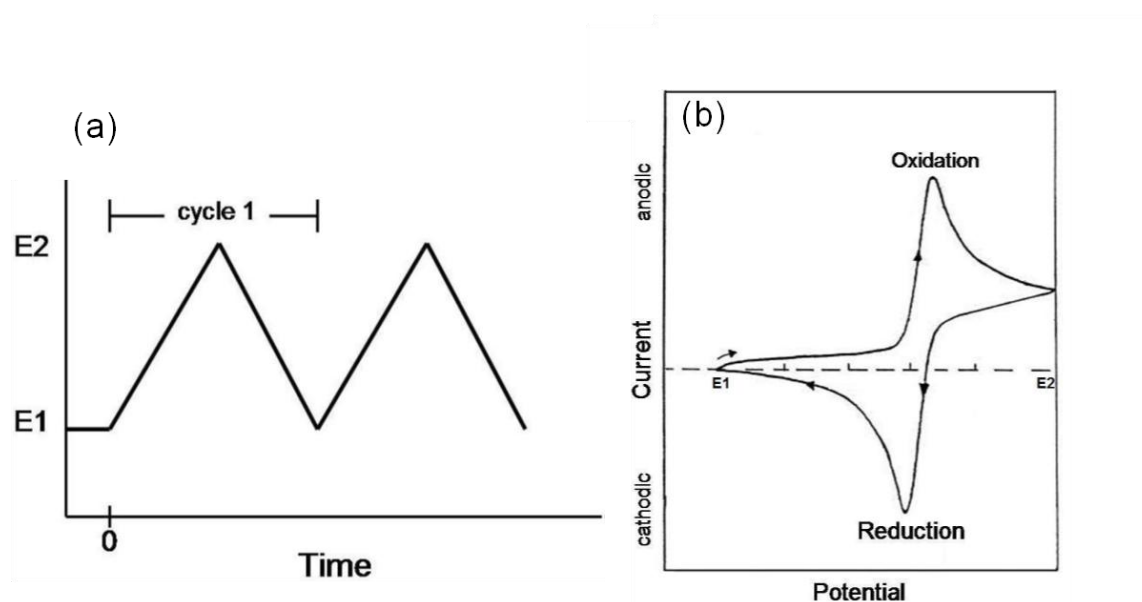


Figure 3.8 (a) Cyclic potential sweep and (b) resulting cyclic voltammogram.^[157]

In this thesis, the blocking effect of electrodeposited ZnO bottom layer was studied by using cyclic voltammetry technique. The cyclic voltammetry measurements were done in 0.1 M KCl aqueous solution containing 2.5 mM potassium ferricyanide $K_3[Fe(CN)_6]$ and 2.5 mM potassium ferrocyanide $K_4[Fe(CN)_6]$. The PET-ITO / PET-CNT substrate without or with ZnO bottom layer, a platinum wire, and a Ag/AgCl electrode were employed as working electrode, counter electrode, and reference electrode, respectively. The cyclic voltammograms were recorded with a Zahner IM6e electrochemical workstation at a scan rate of 10 mV/s in the potential interval from -0.4 V to 0.8 V.

3.3 Fabrication of the flexible dye-sensitized solar cells

3.3.1 The process of dye re-adsorption

Before re-adsorbing a sensitizer to the surface of the ZnO film, the ZnO films is dried in an oven at 120 °C in air for 1 h. The purpose of this process is to remove the water adsorbed on the surface of ZnO and to thereby activate the surface of ZnO. After this, the film is transferred into a glove box (MBRAUN MB-10-Compact) and sensitized by immersing them for 1 h into a 0.5 mmol/L indoline dye D149 solution (Mitsubishi Paper Mills Ltd.) in acetonitrile and t-butyl alcohol (v/v, 1:1), additionally containing 1 mM of cholic acid (Sigma Aldrich) to prevent the dye molecules from aggregating with each other. After the re-adsorption, the film is transferred out of the glove box and washed with little acetonitrile to remove excessive unadsorbed D149. Finally, the film is dried in air before the cell assembly.

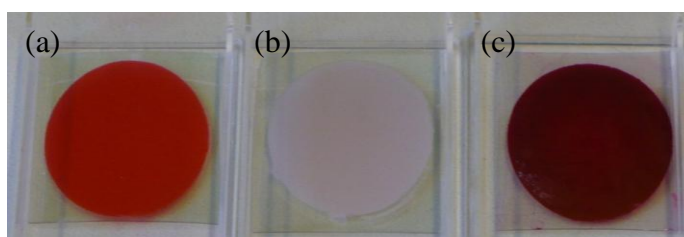


Figure 3.9 The as-deposited ZnO/EY film (a) after (b) desorption of EY and (c) re-adsorbing of indoline dye D149.

3.3.2 Sputtering of Pt counter electrode

An ITO-coated PET substrate (Pecell, 12 ohm/square) platinized by sputtering (Cressington 108 auto) is used as counter electrode. The deposition is performed at a sputtering current of 30 mA under a base Argon pressure of 0.01 torr for 120 s. The sputtered Pt counter electrode is homogeneous and highly reproducible. The thickness of the Pt layer is approximately 10 nm and the corresponding Pt loading is 0.2-0.5 $\mu\text{g}/\text{cm}^2$.

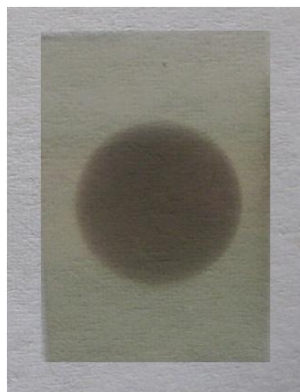


Figure 3.10 Photo of a Pt counter electrode based on PET-ITO.

3.3.3 DSSC assembly

The D149-sensitized ZnO photoanode and the Pt counter electrode were assembled to a sandwich-type cell and sealed with a polymer sealant of 25 μm thickness (tesa[®] 61562), which also served as a spacer between the electrodes (Figure 3.11). The redox electrolyte (approximately 4 μL for 1.13 cm^2 cell) is introduced drop-wise on the ZnO photoanode, allowing the electrolyte to penetrate the ZnO nanopores. Finally, silver paint is applied on the exposed areas of conductive substrates on each electrode after cell assembly to extend the contact area of the current collector.

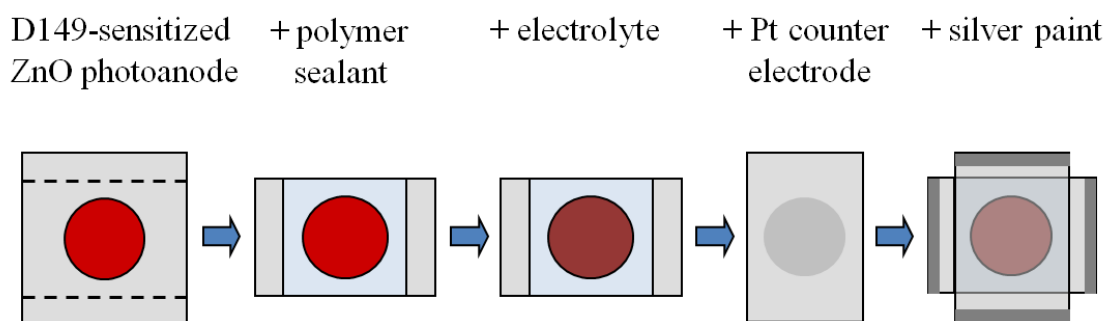


Figure 3.11 Scheme of cell assembly.

3.4 Characterization of the dye-sensitized solar cells

3.4.1 Current-voltage (I-V) curves

Current-Voltage curve measurements are the most common and important technique to characterize the photovoltaic device performance. The aim is to record the performance of the solar cell under standard illumination AM1.5, which is the spectrum of sunlight that has travelled 1.5 times the thickness of the atmosphere, corresponding to a solar zenith angle of $z=48.2^\circ$.^[159] In these measurements, the illuminated solar cell is put under a reverse bias voltage scan and the generated photocurrent is recorded (Figure 3.12). The light intensity in the standard AM1.5 condition used for testing of solar cells is 1000 W/m^2 .

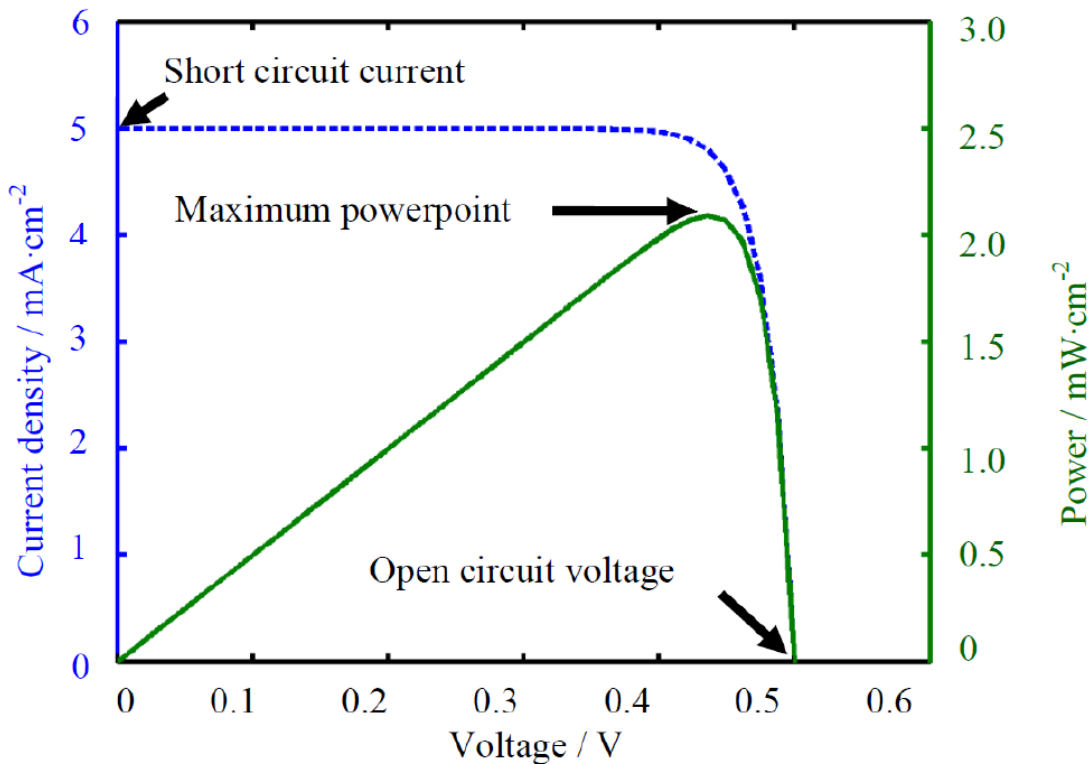


Figure 3.12 An example of an I-V curve and a power curve of a DSSC.

When the cell is short circuited under illumination, the maximum current of the cell, the short circuit current I_{sc} is generated. I_{sc} is usually correlated with the sensitizer absorption capability and electron injection efficiency.^[160] In practice, and to make the results independent of the cell size, the current density, expressed in A/cm^2 , is plotted instead of plain current.

Accordingly, when the cell is under open circuit conditions, no current flows and the

photovoltage is at its maximum, called the open circuit voltage V_{oc} . The open circuit voltage can be enhanced by (1) reducing the charge recombination in the cells; (2) increasing the electron injection efficiency (e.g. reduce dye aggregation) and (3) increasing the conduction band of semiconductor and downshifting the redox potential of the electrolyte (e.g. addition of electrolyte additives).^[160]

The maximum power is generated when the product of the current and voltage reaches its maximum, called the maximum power point (MPP).

$$P_{\max} = V_{MPP} \cdot I_{MPP} \quad \text{Equation 3.2}$$

The fill factor (FF) can assume values between 0 and 1 and is defined by the ratio of the maximum power (P_{\max}) of the solar cell divided by the open-circuit voltage and the short-circuit current.

$$FF = \frac{P_{\max}}{V_{oc} \cdot I_{sc}} \quad \text{Equation 3.3}$$

The value of the fill factor reflects the extent of electrical (Ohmic) and electrochemical (overvoltage) losses occurring during operation of the DSSC. Increasing the shunt resistance and decreasing the series resistance as well as reducing the overvoltage for diffusion and electron transfer will lead to higher fill factors, thus resulting in greater solar cell efficiency.^[161]

The solar cell efficiency is the ratio between the electrical power generated at the MPP and the power of the incident light.

$$\eta_{\max} = \frac{P_{\max}}{P_{in}} = \frac{V_{oc} \cdot I_{sc} \cdot FF}{P_{in}} \quad \text{Equation 3.4}$$

In this thesis, the cell was illuminated through the front side (i.e. the porous ZnO electrode) with a Xe arc lamp (Oriol), adjusted with optical filters to AM 1.5D conditions. The power of the simulated light was calibrated to 1000 W/m² using a bolometer. I-V curves were recorded with a Zahner IM6e electrochemical workstation.

3.4.2 Electrochemical Impedance Spectroscopy (EIS)

Electrochemical impedance spectroscopy (EIS) is a valuable tool to study the charge transfer phenomena and electrochemical processes in the cell components and interfaces. In EIS measurements the potential applied to the solar cell is perturbed by a

small amplitude sinusoidal modulation and the resulting sinusoidal current response is measured as a function of the modulation frequency.^[11] The sinusoidal voltage can be written as,

$$V_t = V_0 \sin \omega t \quad \text{Equation 3.5}$$

Where V_t is the ac potential applied to the system at time t , V_0 is the amplitude of the applied potential and ω is the angular frequency ($\omega=2\pi f$, in radians). The response in current has the same period as the voltage perturbation but will be phase-shifted by φ ,

$$I_t = I_0 \sin(\omega t + \varphi) \quad \text{Equation 3.6}$$

where I_t is the ac electrical current response signal, and I_0 the amplitude of the current signal. For further calculation, V_t and I_t can be written as complex numbers.

$$V_t = V_0 \exp[j(\omega t)] \quad \text{Equation 3.7}$$

$$I_t = I_0 \exp[j(\omega t + \varphi)] \quad \text{Equation 3.8}$$

An expression analogous to Ohm's law allows for calculation of the impedance of the system as

$$Z_t = \frac{V_t}{I_t} = \frac{V_0 \sin \omega t}{I_0 \sin(\omega t + \varphi)} = Z_0 \exp(j\varphi) \quad \text{Equation 3.9}$$

It is composed of a real ($Z'=Z_0 \cos \varphi$) and an imaginary part ($Z''=Z_0 \sin \varphi$):

$$Z_t = Z_0 (\cos \varphi + j \sin \varphi) = Z' + jZ'' \quad \text{Equation 3.10}$$

By varying the frequency of the applied signal, one can get the impedance of the system as a function of frequency. The recorded data can either be represented as magnitude and phase vs. frequency (Bode plot) or in a complex plane (Nyquist plot). The EIS spectrum can be described in terms of an equivalent circuit model consisting of elements such as resistors (R), capacitors (C) and inductors (L) connected in series or parallel.

A dye sensitized solar cell is a very complex system and its impedance response will be related to the response of the different components of the device. Generally, a transmission line model is used to describe the system, as shown in Figure 3.13. In the transmission line, there are two channels in parallel, representing electron transport through TiO_2 and redox species transport in the electrolyte in the pores, respectively.

The charge-transfer process related to the reaction of the electrons with the I_3^- ions at the semiconductor-electrolyte interface connects these two channels.^[162]

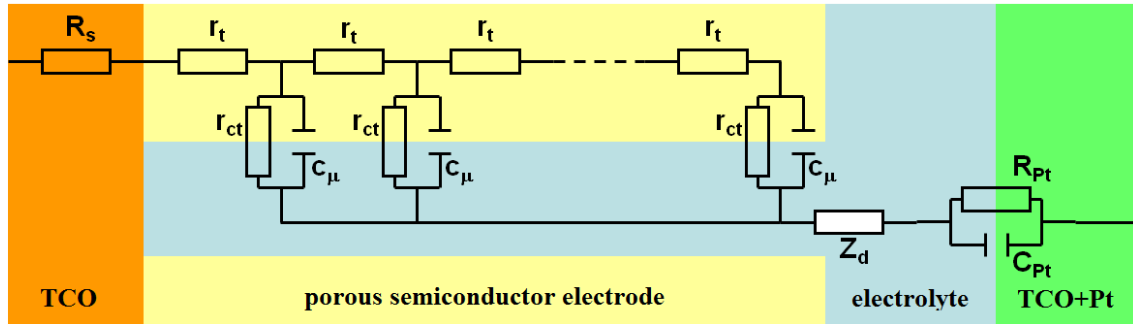


Figure 3.13 General transmission line model of a DSSC. R_s is the series resistance, including the sheet resistance of the TCO glass and the contact resistance of the cell; r_t is the transport resistance of the electrons in the semiconductor film; r_{ct} is the charge transfer resistance of the charge recombination process between electrons in the mesoscopic semiconductor film and I_3^- in the electrolyte; C_μ is the chemical capacitance of the semiconductor film; Z_d is the Warburg element showing the Nernst diffusion of I_3^- in the electrolyte; R_{Pt} and C_{Pt} are the charge-transfer resistance and double-layer capacitance at the counter electrode (platinized TCO glass), respectively. The colors orange, yellow, blue and green represent the cell components TCO, semiconductor electrode, electrolyte and Pt counter electrode, respectively.^[163]

A typical EIS spectrum for a DSSC under illumination exhibits three semicircles in the Nyquist plot and three frequency peaks in the Bode phase plot (see Figure 3.14). The impedance on the real axis at the highest frequency end indicates the series resistance (R_s) mainly imposed by the conductive substrate, while the three semicircles from high to low frequencies represent the resistance of interfacial charge transfer at the counter electrode (R_{Pt}), electron transport and charge transfer resistance in the porous ZnO ($1/3 R_t + R_{ct}$) and ion diffusion in the electrolyte (R_d) according to the model of Bisquet and co-workers.^[163] The total resistance of the cell is the sum of the resistances at different interface as

$$R_{tot} = R_s + R_{Pt} + \frac{1}{3} R_t + R_{ct} + R_d \quad \text{Equation 3.11}$$

Note that R_t is the transport resistance attributable to the whole film thickness, while $1/3 R_t$ is an average value, since most electrons are photogenerated near the back contact where the light intensity is the highest.

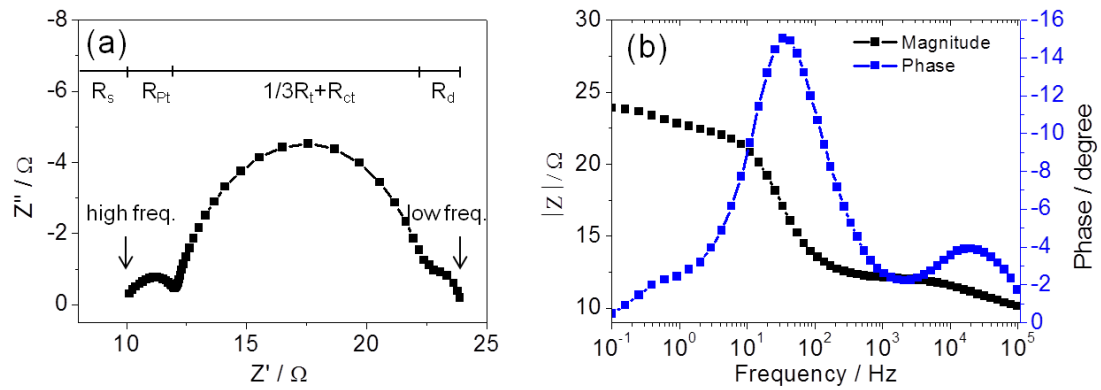


Figure 3.14 Typical (a) Bode and (b) Nyquist Plot for a flexible ZnO DSSC.

The obtained impedance spectra were measured at various forward bias voltages (from -600 mV to -300 mV) in the frequency range 100 mHz to 100 kHz with potential amplitudes of 20 mV (Zahner IM6e electrochemical workstation). Impedance characteristics were determined by fitting of impedance spectra to the above model using Z-view software (v2.8b, Scribner Associates Inc.).

3.4.3 Intensity Modulated Photocurrent / Photovoltage Spectroscopy (IMPS/IMVS)

Intensity modulated photocurrent spectroscopy (IMPS) and photovoltage spectroscopy (IMVS) are techniques that involve small amplitude modulation of the photon flux incident on the cell.^[164] In the IMPS measurement, the cell is investigated at short circuit and in the IMVS under open circuit conditions. Superimposed on a steady-state illumination level, a small sinusoidal ac modulation of the illumination intensity is applied. The magnitude of the resulting photovoltage or photocurrent and its phase-shift with respect to the illumination signal are recorded.

IMVS is typically used to characterize the recombination process in DSSC and the time constant for this process is the effective electron lifetime (τ_n).^[165] The IMPS time constant depends on both electron transport and electron recombination.^[166] Under short circuit conditions, the electron lifetime is assumed to be much larger than the electron transport time, so the measured IMPS response is nearly equal to the transport time (τ_d).^[11] The IMPS and IMVS measurements can also be operated at other potentials, such as maximum power point. The time constants were determined from the Nyquist plots of the IMPS/IMPS response, where ω_{\min} is the frequency corresponding to the minimum of the measured curve:

$$\tau_d(\text{IMPS}) = \frac{1}{\omega_{\min}} \quad \tau_n(\text{IMVS}) = \frac{1}{\omega_{\min}} \quad \text{Equation 3.12}$$

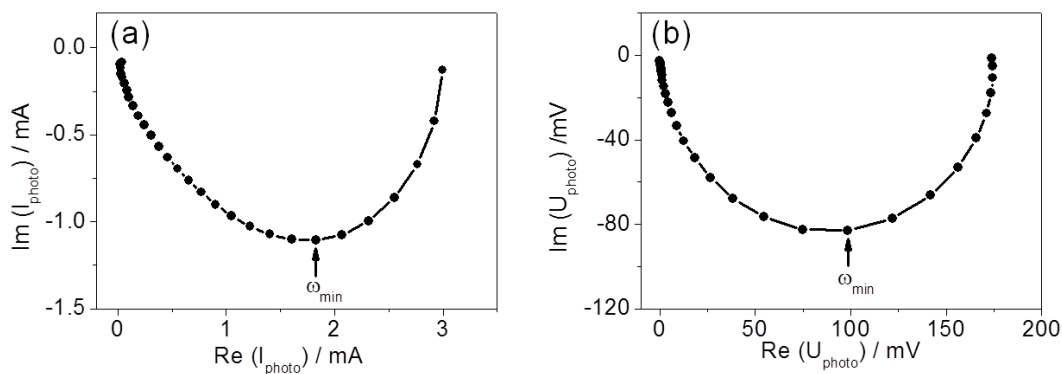


Figure 3.15 Typical (a) IMPS and (b) IMVS response in the complex plane of a DSSC.

The charge-collection efficiency (η_{cc}) is an indication of the probability that a photogenerated electron reaches the collecting substrate contact before it is lost by recombination.^[167] It can be determined by the ratio of electron transport time and life time as expressed by^[168, 169]

$$\eta_{cc} = 1 - \frac{\tau_d}{\tau_n} \quad \text{Equation 3.13}$$

Intensity modulated photocurrent and photovoltage spectroscopy (IMPS/IMVS) were performed with the Zahner IM6e electrochemical workstation connected to a Zahner PP210 potentiostat for control of the green LED ($\lambda = 530 \text{ nm}$) used for generation of the modulated light. The light intensity used in these measurements was 10 W/m^2 with a modulation amplitude of 10 %, and the cells were illuminated through the back contact of the porous ZnO electrode.

3.4.4 Long-term stability

Long-term stability is a key parameter for any type of solar cells. For commercial applications, a DSSC must be intrinsically and extrinsically stable under elevated temperature, cyclic changing temperatures, exposure to humidity and prolonged illumination.^[170] The extrinsic stability is the stability of the sealant in DSSC. The intrinsic stability is controlled by two factors, namely physical and chemical stability. Physical stability is related to the possible evaporation of the liquid electrolyte at elevated temperatures. The intrinsic chemical stability is related to irreversible (photo-) electrochemical and thermal degradation of the dye or electrolyte components, which might occur during operation of the cell.^[171] The intrinsic stability of a DSSC is usually tested in accelerated aging conditions such as 60-80 °C for 1000 h and exposure to continuous solar irradiation of $100 \text{ mW}\cdot\text{cm}^{-2}$ (one sun).^[172] This work presented focuses on the intrinsic stability of the flexible ZnO-based DSSC.

The long-term stability tests in this work including $75 \text{ mW}\cdot\text{cm}^{-2}$ (0.75 sun) light irradiation with the range from UV to IR and thermal stress (60 °C) aging of hermetically sealed cells was performed with a xenon test instrument (ATLAS suntest CPS/CPS+).

4 Suitable substrates for flexible ZnO-based dye-sensitized solar cells

4.1 PET-ITO

The most often used flexible transparent substrates in DSSCs are films of polyethylene terephthalate coated with indium doped tin oxide (PET-ITO). In this section, PET-ITO (manufactured by CPFilms Inc., resistance 15 Ω /sq. and transmittance 85 %) was studied as substrate for the photoelectrode and counter electrode.

4.1.1 Scanning electron microscopy

Figure 4.1a shows the scanning electron microscopy images of the PET-ITO substrate. The surface morphology of the PET-ITO is very smooth and homogeneous, thus creating a suitable condition for the electrodeposition of homogeneous ZnO films. The structure of electrodeposited ZnO thin films deposited on the PET-ITO substrate is illustrated in a series of SEM images shown in Figure 4.1b-d. A pure ZnO thin film electrodeposited from a dye-free electrodeposition bath consists of hexagonal columnar crystals typical for ZnO (Figure 4.1b). The surface of the crystals is smooth and each crystal appears to be dense and monolithic. Directly onto the bottom layer, a ZnO/dye hybrid layer is deposited in the presence of eosin Y dye in the electrodeposition bath. The images c and d in Figure 4.1 show the film after the deposition of this layer and the subsequent removal of the dye, leaving a layer of highly porous ZnO. Its cross section clearly shows cauliflower-like ZnO crystals with a fibrous internal nanostructure aligned in the direction of the film growth, demonstrating the significant influence of the dye on the film morphology and the crystal size due to its interaction with Zn^{2+} and incorporation into the film.

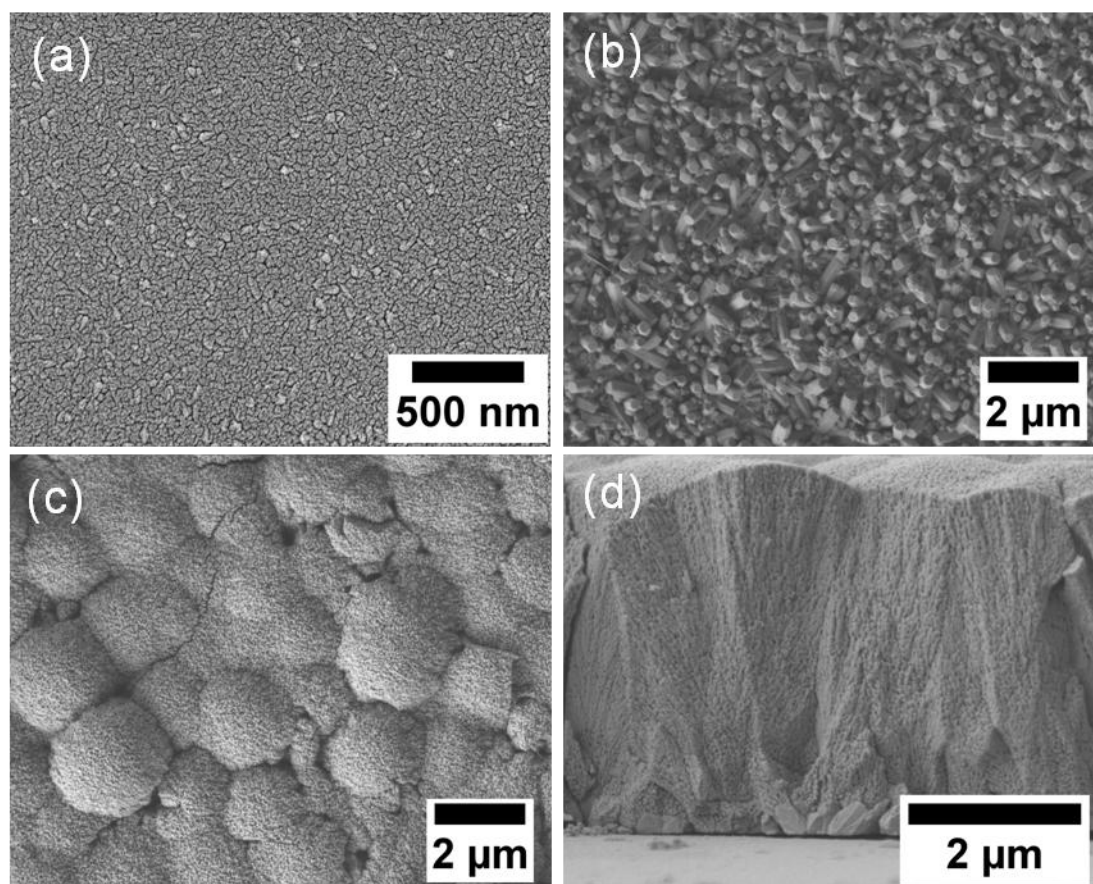


Figure 4.1 SEM images of (a) the PET-ITO substrate; (b) compact ZnO layer deposited without eosin Y; (c) top view and (d) cross section of ZnO/eosin Y hybrid films on compact ZnO films after extraction of eosin Y by soaking the film in dilute KOH aqueous solution of pH 10.5.

4.1.2 Photovoltaic performance

Figure 4.2 presents I-V curves of DSSCs electrodeposited on PET-ITO substrates with various electrodeposition times of the porous ZnO layer. The photovoltaic characteristics of the cells with re-adsorbed D149 dye are listed in Table 4.1. There is no significant difference in open-circuit voltage (V_{oc}). The short-circuit photocurrent density I_{sc} reaches a maximum of $9.5 \text{ mA}\cdot\text{cm}^{-2}$ at a deposition time of 60 minutes, which arises from the increased surface area and dye loading (the latter increasing from $1.64\cdot 10^{-8} \text{ mol}\cdot\text{cm}^{-2}$ to $3.61\cdot 10^{-8} \text{ mol}\cdot\text{cm}^{-2}$). The decrease of I_{sc} for a deposition time of 75 minutes implies that the enhancement by a further increased surface area and dye loading is more than offset by an increased back transfer of photogenerated electrons from the conduction band of ZnO to I_3^- ions in the electrolyte due to the increased surface area of the electrode.^[173] The cell with a porous ZnO layer deposited for 45 minutes has the highest fill factor, leading to a maximum conversion efficiency η of 3.3%. This value is very promising since the highest conversion efficiency for

ZnO-based DSSC on PET-ITO is 3.8%.^[52] The decrease of the fill factors for deposition times of 60 minutes and 75 minutes is also a consequence of the increased recombination in thicker films.

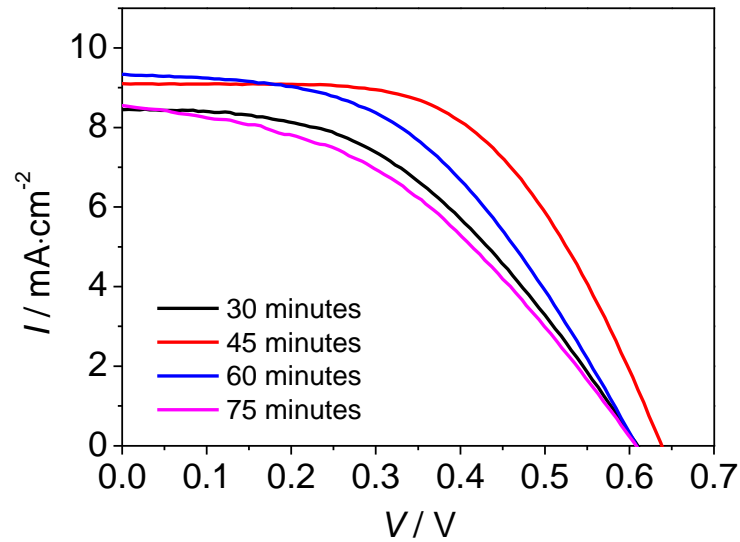


Figure 4.2 I-V characteristics of DSSCs electrodeposited on PET-ITO substrates with ZnO porous layers for 30 minutes; 45 minutes; 60 minutes and 75 minutes under AM 1.5 illumination ($100 \text{ mW}\cdot\text{cm}^{-2}$).

Table 4.1 Photovoltaic characteristics calculated from the I-V curves in Figure 4.2.

Sample	Thickness / μm	Dye loading / $\cdot 10^{-8} \text{ mol}\cdot\text{cm}^{-2}$	V_{oc} / V	I_{sc} / $\text{mA}\cdot\text{cm}^{-2}$	FF	η / %
30 min.	5 ± 0.5	1.44	-0.61	8.5	0.45	2.4
45 min.	7 ± 0.5	2.29	-0.64	9.2	0.56	3.3
60 min.	9.3 ± 0.5	3.07	-0.61	9.5	0.47	2.7
75 min.	12 ± 0.5	4.04	-0.61	8.6	0.42	2.2

4.1.3 Influence of light on the eosin Y desorption

Experiments have shown that eosin Y is loaded as aggregates when the hybrid film is electrodeposited. Desorption of the eosin Y is performed by immersing the as-deposited ZnO/EY films into an aqueous KOH solution (500 ml, pH 10.5) for 24 h. It was noted that the light could accelerate the dye desorption and lead to a more complete

desorption of EY. To confirm this observation, an as-deposited ZnO/EY film based on PET-ITO was divided into two parts. One part was desorbed under daylight (no direct sunlight shining, light intensity approximately 10 mW/cm^2), while the other part was desorbed in the dark (see Figure 4.3). Table 4.2 lists the absorption of the KOH solutions during the desorption test. It was observed that the film part 1 was colorless after 3.5 h and the absorption values of the solution reached a plateau, indicating that the EY molecules were already removed completely from the film. The desorption of EY in the dark was extremely slow, some red color of EY could still be seen in the film after the 29 h extraction process.

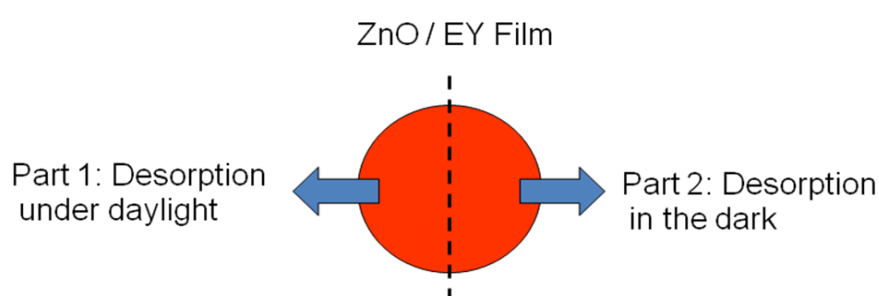


Figure 4.3 Schematic drawing of the EY desorption test.

Table 4.2 Absorption of the KOH solutions during the desorption test.

Duration of the desorption / h	Absorption of the KOH solution at 516 nm	
	Part 1	Part 2
3.5	0.064	0.014
20	0.066	0.017
24	0.063	0.033
29	0.063	0.034

These results indicate that the ester-like linkage between ZnO and EY is not stable in KOH solution because of hydrolysis. When the solution is irradiated, the linkage becomes more unstable and leads to a rapid hydrolysis of EY.

4.2 PET-CNT

A disadvantage of the usage of ITO based substrates is the limited availability and cost of indium.^[174] A possible alternative for ITO are single-walled carbon nanotube (SWCNT) films.^[175] CNTs have attracted much interest for incorporation into DSSCs because of their excellent thermal, electrical, and optical properties. Numerous studies have investigated the application of carbon nanotubes as catalyst on the counter electrode of DSSCs^[176-178] and the incorporation of carbon nanotubes into the photoanodes.^[179-182] Initial research studies demonstrate that SWCNT thin films can be used as conducting, transparent electrodes for hole collection in organic photovoltaics devices with efficiencies between 1 % and 2.5 %.^[183] However, to date only two studies have focused on the use of carbon nanotubes as conductive substrate material for the photoanode in dye-sensitized solar cells. Wei *et al.* reported a full solid-state, flexible DSSC based on ZnO nanoparticles and CNT thin film stamped on to a PET substrate, achieving an efficiency of ca. 0.2 %.^[184] On the other hand, the catalytic property of CNTs towards electron back reaction ($I_3^- + 2e^- \rightarrow 3I^-$) complicates their application as a working electrode in a liquid-type DSSC. Recently, Kyaw *et al.* demonstrated a transparent CNT film (around 400 Ω /sq.) as the working electrode in a DSSC containing porous TiO_2 and I^-/I_3^- redox couples, which gave an efficiency of 1.8 %. The recombination of electrons with I_3^- at the CNT/electrolyte interface was suppressed by covering the CNT layer with a TiO_x layer.^[185] In this section, flexible DSSCs with a liquid I^-/I_3^- electrolyte based on a transparent CNT-coated polyethyleneterephthalat (PET-CNT) substrate are investigated. To circumvent the above-mentioned problem of direct contact between the CNTs and the electrolyte, a compact ZnO bottom layer was electrodeposited onto the CNT film prior to the deposition of the porous ZnO layer. The solar energy conversion efficiency and the electrochemical impedance of the fabricated cells are determined and discussed. Because of the relatively high resistance of the PET-CNT substrates used in this preliminary study (470 Ω /sq.), the active area of DSSCs was limited to 0.0314 cm^2 .

4.2.1 Scanning electron microscopy

Figure 4.4 shows the scanning electron microscopy images of the PET-CNT substrate. It can be observed that the carbon nanotubes are randomly and inhomogeneously

distributed on the PET substrate surface. The tubes are uniform with average diameters of about 30 nm and lengths of about 1 μm .

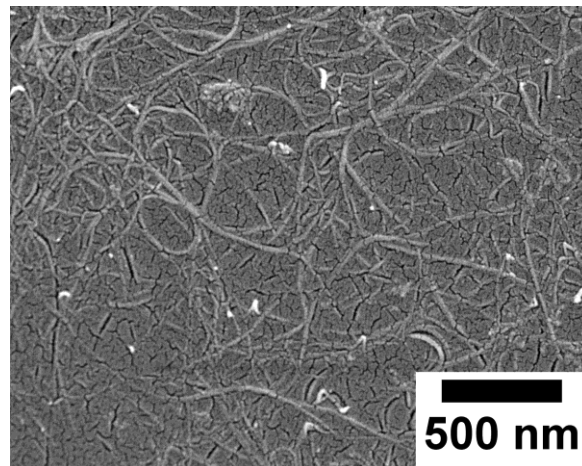


Figure 4.4 SEM images of the carbon nanotubes on PET substrate.

The structure of ZnO thin films electrodeposited on the PET-CNT substrate is similar to those on the PET-ITO substrate. The compact ZnO layer is made of hexagonal columnar particles and nanoscaled substructures are found within the porous layer (Figure 4.5a-c). The difference is that the porous layer on the PET-CNT substrate is inhomogeneous and shows a spherical top surface. Image d shows in detail the specimen near the CNT layer, clearly exhibiting the CNTs, the compact ZnO bottom layer and the lower part of the porous ZnO layer. Note that some CNTs appear partly detached from the PET surface in this image, which is probably due to the sample preparation for SEM. This is proven by the observation that all compact ZnO crystals were grown on CNTs lying flat on the PET surface, meaning that the partly detached CNTs were not present at the time of electrodeposition.

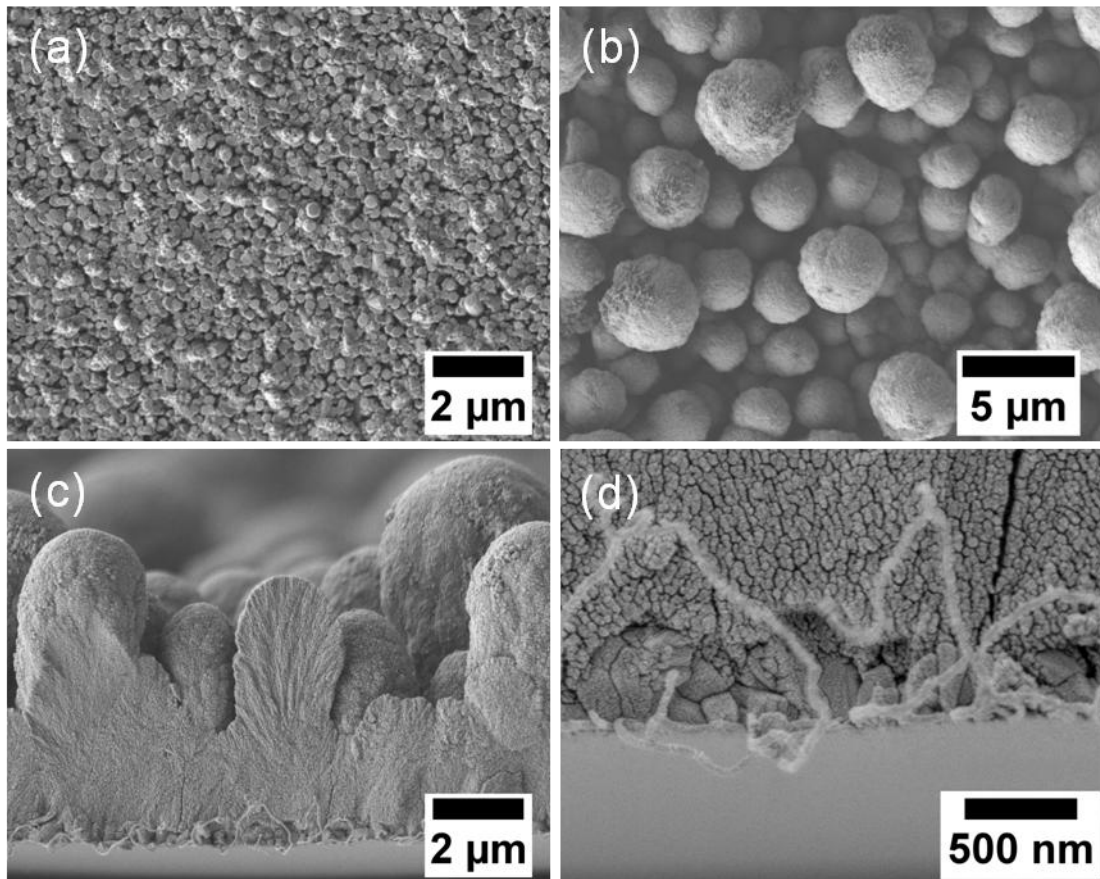


Figure 4.5 SEM images of electrodeposited ZnO thin films; (a) compact ZnO layer deposited without eosin Y; (b) top view and (c), (d) cross sections of ZnO/eosin Y hybrid films after extraction of eosin Y by soaking the film in dilute KOH aqueous solution of pH 10.5.

The cauliflower-like ZnO crystals are observed to merge in the lower part of the porous ZnO layer, however, they tend to grow separated from each other towards longer deposition times as represented in Figure 4.6a-b. If the electrodeposition time is increased from 30 minutes to 75 minutes, the length of the columns increases from approximately 4 μm to 10 μm , while the thickness of the lower merged part of the film increases only from about 2 μm to 4 μm . As shown in Figure 4.6c-d, the surface roughness of the porous ZnO film electrodeposited in 75 minutes is higher than that of the film electrodeposited in 30 minutes. Since a homogenous growth of the porous ZnO layer is usually seen in case of ITO-based conductive substrates (Figure 4.1),^[51] the film morphology observed has to be attributed to the use of the CNT-based substrate. The most probable explanation is that the conductivity of the CNT-based substrate is not as homogenous as that of typical ITO-based substrates, caused by randomly and inhomogeneously orientated CNTs. As the thickness of the ZnO layer and therefore the overall series resistance of the electrode increases during film growth, further ZnO

growth may be restricted to spots with the smallest potential drop, which are the spots with the highest conductivity of the CNT layer.

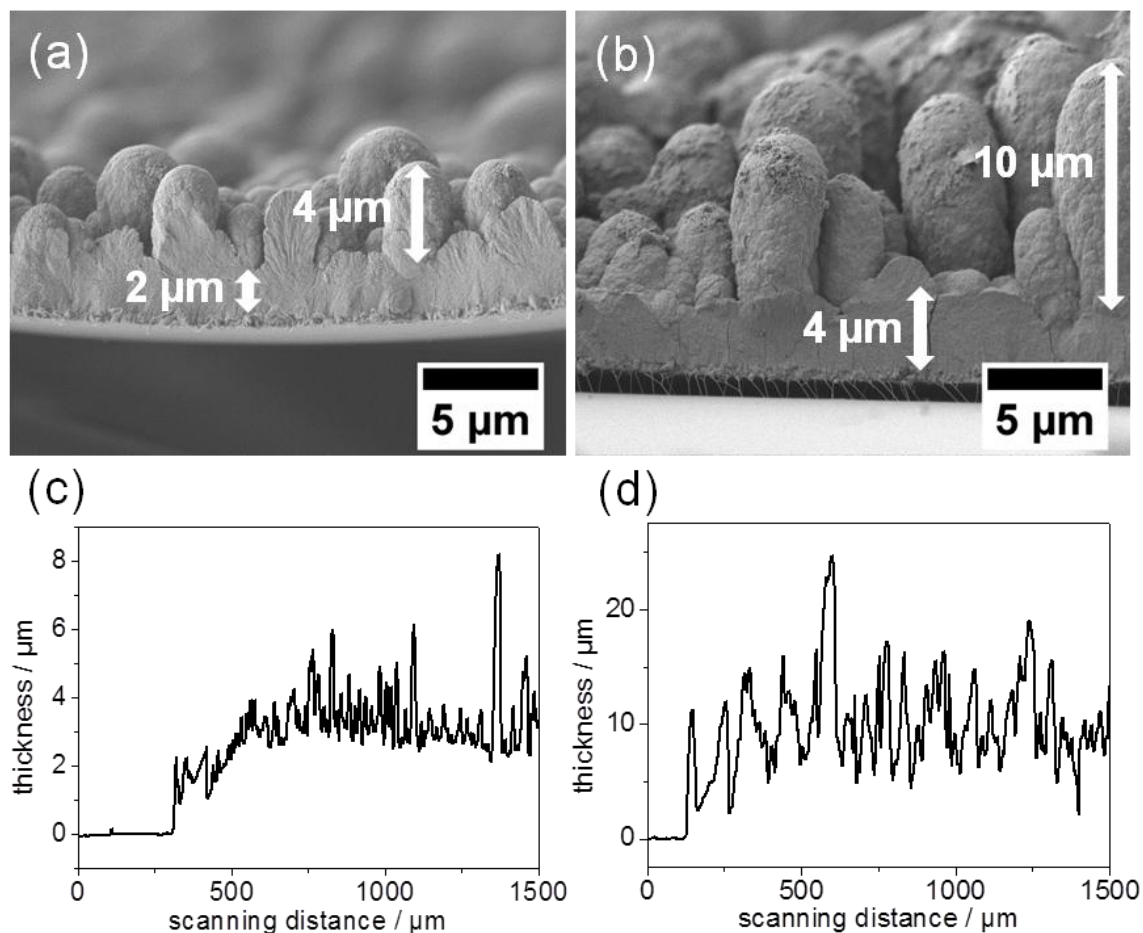


Figure 4.6 SEM cross section images and profilometer data of electrodeposited ZnO thin films; (a), (c) 30 minutes and (b), (d) 75 minutes electrodeposited porous ZnO film in the presence of $80 \mu\text{M}$ eosin Y after extraction of eosin Y.

4.2.2 Photovoltaic performance

Figure 4.7 shows I-V curves of DSSC electrodeposited on PET-CNT substrates with various electrodeposition times of the porous ZnO layer. The photovoltaic characteristics of the cells are listed in Table 4.3. While there is no change for the open-circuit voltage (V_{oc}), the short-circuit photocurrent density I_{sc} reaches a maximum of $11.9 \text{ mA}\cdot\text{cm}^{-2}$ at a deposition time of 60 minutes, leading to a maximum conversion efficiency η of 2.5 %, which is the highest reported efficiency for DSSCs with CNTs as conductive substrate material for the photoanode so far.^[184, 185] I_{sc} and η increase significantly if the deposition time is increased from 30 minutes to 60 minutes, which arises from the increased surface area and dye loading. The decrease of both values for deposition times > 60 minutes implies that although the larger film thickness further

increases the amount of adsorbed dye, it also increases the recombination of electron with triiodide on the ZnO surface. This especially applies to the added outer part of the film, since electrons photogenerated in this part of the film have the longest diffusion pathways to the conducting back contact. The fill factors of the cells decrease as the deposition time increases from 30 minutes to 75 minutes, which is also a consequence of the increased recombination in a thicker film.

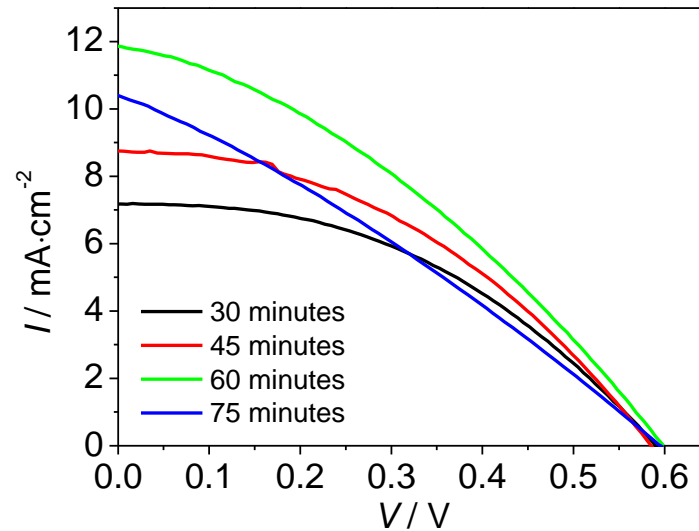


Figure 4.7 Current-voltage (*I-V*) curves of DSSCs based on D149 sensitized porous ZnO layers electrodeposited on PET-CNT substrates with non-porous ZnO bottom layers for (a) 30 minutes; (b) 45 minutes; (c) 60 minutes; (d) 75 minutes. The cells were illuminated with simulated sunlight (100 mW/cm^2 , AM 1.5D).

Table 4.3 Photovoltaic characteristics calculated from the *I-V* curves in Figure 4.7.

Sample	Dye loading $/\cdot 10^{-8} \text{ mol}\cdot\text{cm}^{-2}$	V_{oc} / V	I_{sc} $/ \text{ mA}\cdot\text{cm}^{-2}$	FF	$\eta / \%$
30 minutes	1.61	-0.59	7.2	0.44	1.9
45 minutes	2.59	-0.59	8.7	0.41	2.1
60 minutes	3.49	-0.60	11.9	0.35	2.5
75 minutes	4.55	-0.60	10.5	0.29	1.8

4.2.3 The blocking effect of compact ZnO bottom layer

A typical DSSC comprises a dye-sensitized nanocrystalline semiconductor film deposited on a transparent conducting substrate, liquid electrolyte, and a counter

electrode. The existence of small holes in the nanostructured film allows direct contact between its transparent conducting back contact and the electrolyte, which can act as short circuits in a device and cause the loss of photocurrent.^[186] To suppress this recombination, which is of great importance for achieving DSSCs with a high efficiency, a compact bottom layer (BL) can be deposited between the conducting substrate and the porous semiconductor film to prevent back electron transfer from the substrate to electrolyte. The compact bottom layer can physically avoid the contact of the electrolyte with the substrate surface, preventing occurrence of triiodine reduction by photo-injected electrons. Via electrodeposition, ZnO compact layer can be fabricated on conductive substrate at low temperature. Hu et al. reported that the resultant compact layer can block the electron transfer at the TCO/electrolyte interface, leading to an increase of open-circuit photovoltage and fill factor of the devices and, thereby, the power conversion efficiency.^[187]

The blocking effect of electrodeposited ZnO bottom layer (electrodeposited for 10 minutes, see section 3.1.3) was studied by using cyclic voltammetry (CV) technique, for which the current density presents information about the rectification ability of the ZnO bottom layer. A high current density means that more electrons can be injected from the TCO into the electrolyte, which indirectly indicates the possibility of short circuits produced in a DSSC under bias conditions.

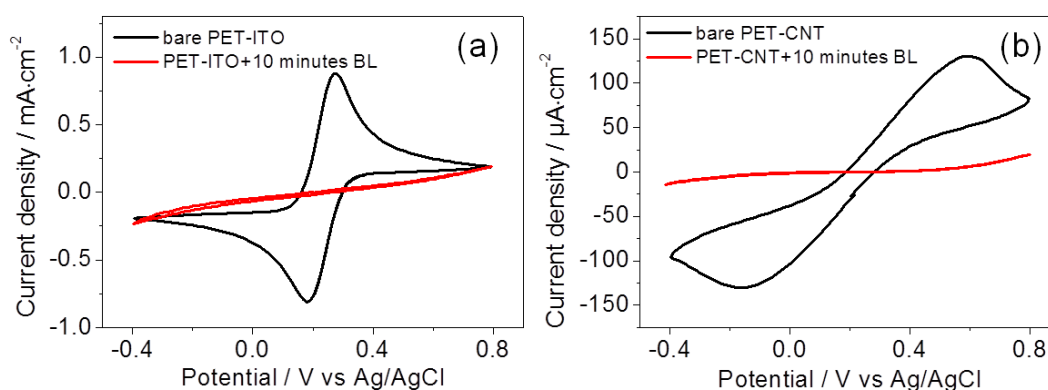


Figure 4.8 Cyclic voltammograms of (a) PET-ITO and (b) PET-CNT with and without blocking layer (BL) in 0.1 M KCl aqueous solution containing 2.5 mM $K_3[Fe(CN)_6]$ and 2.5 mM $K_4[Fe(CN)_6]$ at a scan rate of 10 mV/s.

Figure 4.8 displays the CV response showing the $Fe(CN)_6^{3-}/Fe(CN)_6^{4-}$ redox reaction at different electrodes. The bare PET-ITO and PET-CNT electrodes show quasi-reversible characteristics with cathodic and anodic peaks, suggesting that there is electron- transfer

between the bare electrodes and the redox system. In contrast, no peaks are observed in the CV response of the same substrates with bottom layers (BL), indicating that the electron transfer between the bare electrodes and the redox species is effectively suppressed.

It is also noted that the CV response of both substrates without bottom layers have different peak shape and peak position. The curve of PET-ITO shows both the oxidation and reduction rate constants are high, while the rate constants of PET-CNT are lower, which lead the peaks shift to more reductive/oxidative potentials and the peaks become more rounded.

4.2.4 Electrochemical impedance spectroscopy

The DSSCs based on PET-ITO and PET-CNT with the highest conversion efficiency (with 45 minutes and 60 minutes electrodeposited porous layer, respectively) were compared using electrochemical impedance spectroscopy.

Figure 4.9 shows Nyquist plots of EIS data measured at different cell voltages under illumination at cells based on PET-ITO and PET-CNT substrate. Both cells exhibit the three characteristic semicircles, which usually represent (from high to low frequency) the contributions of the counter electrode, electron transport and charge transfer and ion diffusion in the electrolyte (see section 3.4.2). Ion diffusion is visible only as a shoulder at the low frequency end of the middle arc. Since its contribution to the overall resistance is by far the lowest, it is neglected in the following. It is noted that the resistance represented by the first semicircle for cells on PET-CNT is considerably higher than the few Ohms usually expected for the counter electrode. As an explanation it is proposed that an additional impedance at the interface between the CNT layer and the compact ZnO layer, represented by $R_{\text{ZnO/CNT}}$ in Figure 4.10, contributed to this semicircle. The series resistance R_s of the both cells, which is the high frequency limit of the impedance spectra, does not change with the potential applied to the back contact, indicating that the ITO- and CNT-layer are behaving like ohmic conductors with no potential dependence of the conductivity.

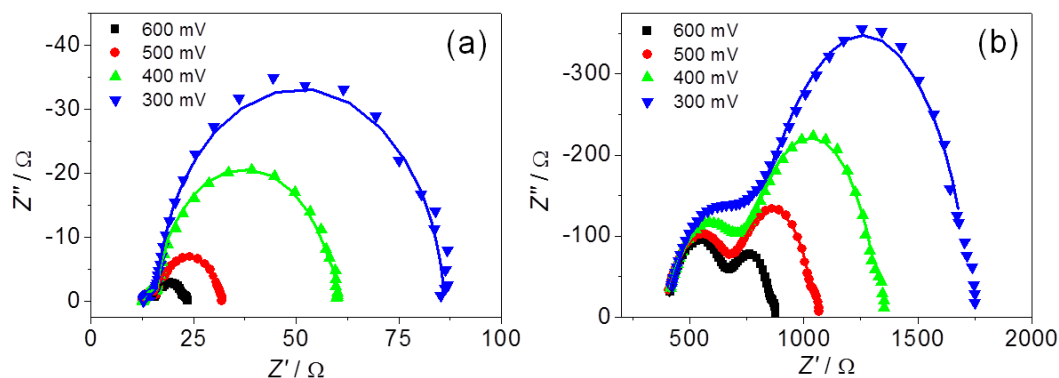


Figure 4.9 Nyquist plots of EIS data measured with 1 sun illumination at different cell voltages for DSSCs based on (a) PET-ITO and (b) PET-CNT. The ZnO photoanode consisted of a non-porous ZnO bottom layer electrodeposited for 10 minutes and a porous ZnO layer electrodeposited for 45 minutes on PET-ITO and for 60 minutes on PET-CNT, respectively. The lines show the fits according to the model illustrated in Figure 4.10. For PET-CNT-based cells ion transport is neglected by fitting the impedance spectra only down to a frequency of 2.3 Hz.

For a more detailed analysis of the impedance results, they were fitted to equivalence circuits based on the model of Bisquert and co-workers,^[163] which are shown in Figure 4.10. Here R_s is the series resistance, R_{Pt} and C_{Pt} are the resistance and capacitance of charge transfer at counter electrode, DX11 is a distributed element (transmission line model)^[188] representing the porous ZnO layer and containing R_t and R_{ct} (charge transport and recombination resistance in the ZnO film), and R_d is the Warburg resistance of ion transport in the electrolyte by diffusion. In addition to the equivalent circuit for the DSSCs electrodeposited on PET-ITO substrate, an RC element in series to the other elements is introduced in order to account for $R_{ZnO/CNT}$. Using a constant phase element ($CPE_{ZnO/CNT}$) instead of a capacitance reflects the textured, heterogeneous surface of the carbon nanotube layer. For the cells based on PET-CNT, the values of R_{Pt} and C_{Pt} were kept constant at values of 1.6Ω and $6.9 \cdot 10^{-6} F$, respectively, which were taken from separate measurements using the same kind of counter electrode in PET-ITO-based DSSCs.

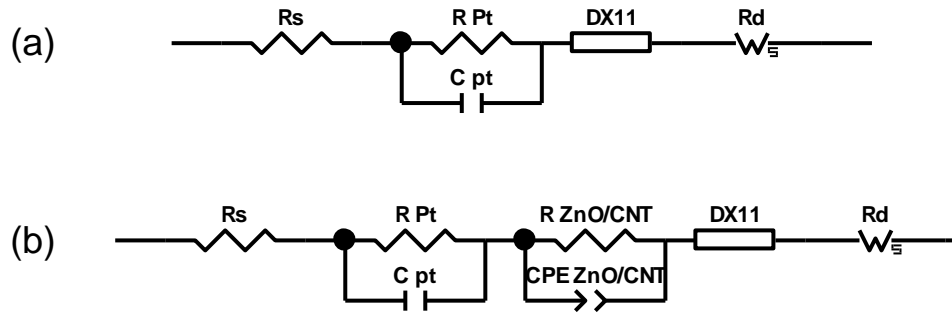


Figure 4.10 Equivalent circuits for the ZnO-based DSSCs electrodeposited on (a) PET-ITO and (b) PET-CNT substrate.

The fitting results for R_t and R_{ct} are shown in Figure 4.11. An increase of R_t and R_{ct} towards lower cell voltages is observed for both cells. Such behavior is expected for DSSCs in general since a lower cell voltage means a lower quasi-Fermi level of electrons in the ZnO and therefore a lower concentration of free electrons in the conduction band. It is noted that, the R_t and R_{ct} values of the cell on PET-CNT are about one order of magnitude higher than that of the cell on PET-ITO, which may be caused by the extremely inhomogeneous porous layer.

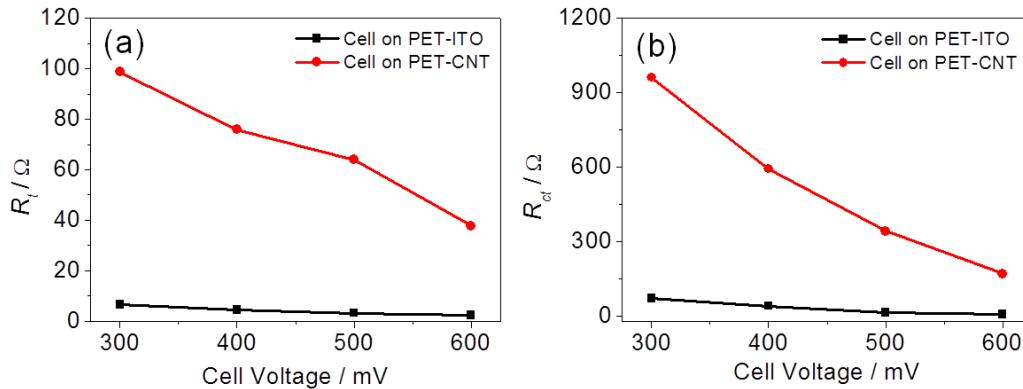


Figure 4.11 R_t (a) and R_{ct} (b) values determined by EIS measurements of D149 sensitized ZnO solar cells using PET-ITO and PET-CNT as plastic electrodes with porous ZnO films electrodeposited for 45 and 60 minutes, respectively.

The dependence of $R_{ZnO/CNT}$ on the cell voltage and film thickness is shown in Figure 4.12. It decreases with increasing deposition times up to 60 minutes and then increases again for a deposition time of 75 minutes (only for cell voltages > 300 mV). The electron concentration directly at the ZnO/CNT interface under short-circuit conditions is very well reflected by the photocurrent density I_{sc} , which shows exactly the opposite behavior (increase until 60 minutes deposition time, followed by a decrease). This means that $R_{ZnO/CNT}$ behaves inversely proportional to the electron concentration in the

ZnO film. Increasing the cell voltage also increases the electron concentration in the ZnO by injecting electrons from the CNT layer into the ZnO layer and increasing its quasi-Fermi level; in fact, the highest electron concentration in the ZnO layer will be reached under open-circuit conditions. Both observations therefore suggest that the concentration of free electrons in the conduction band of ZnO is the determining factor for $R_{\text{ZnO/CNT}}$.

In general, it can be expected that the electrical resistance at any interface depends on the charge carrier concentration in the less conducting phase (ZnO in this case) and on the area of the interface. While the first expectation has been confirmed for the CNT/ZnO interface, the second one may be an explanation for the relatively high values of $R_{\text{ZnO/CNT}}$. Significant resistances between the conducting back contact and the semiconductor layer have not been recognized so far in case of TCO-based substrates. On these substrates, the TCO usually forms rather homogenous and continuous layers, which ensure a high contact area of the TCO/semiconductor interface. In contrast, CNT layers are less homogenous and not continuous due to the molecular nature of the CNTs, as was also seen in the lower homogeneity of the porous ZnO films electrodeposited on them. It can therefore be assumed that the contact area of the CNT/ZnO interface is comparatively small, leading to the observed resistance.

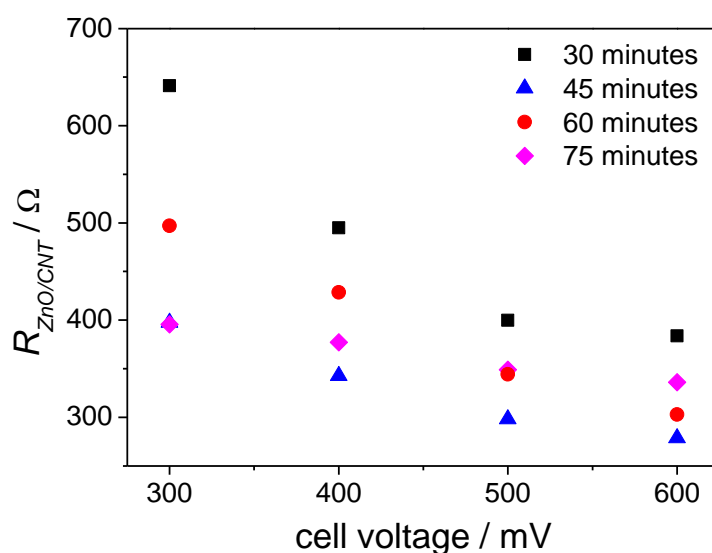


Figure 4.12 $R_{\text{ZnO/CNT}}$ values determined by EIS measurements of D149 sensitized ZnO solar cells using PET-CNT as plastic electrode with porous ZnO films electrodeposited for 30, 45, 60 and 75 minutes, respectively.

4.2.5 Intensity modulated photocurrent / photovoltage spectroscopy

The cell based on PET-ITO shows an excellent collection efficiency of over 99 %. The cell based on PET-CNT has a two order of magnitude higher electron transport time than the cell with PET-ITO, while the lifetimes of both cells are comparable, which leads to a much lower collection efficiency of 74 %. The comparable lifetimes indicate that the properties of ZnO films on both conducting substrates are similar. The extremely high electron transport time of the cell based on PET-CNT may mainly due to the high interface resistance between the CNT layer and the compact ZnO layer.

Table 4.4 Electron transport time (τ_d) and lifetime (τ_n) of D149 sensitized ZnO solar cells using PET-ITO and PET-CNT as conducting substrates with porous ZnO films electrodeposited for 45 and 60 minutes, respectively.

Sample	τ_d (IMPS) / ms	τ_n (IMVS) / ms	η_{cc} / %
Cell on PET-ITO	0.015	8.29	99.82
Cell on PET-CNT	2.88	11.20	74.28

4.3 Metal sheets

In addition to plastics, metal materials are another group of substrates that could realize both flexible and cost-efficient DSSC. In this section, the suitability of titanium ($3.5 \Omega/\text{sq.}$, Goodfellow Inc.) and stainless steel ($1 \Omega/\text{sq.}$, ABCR Inc.) for ZnO dye-sensitized solar cell substrates was investigated with respect to performance using photovoltaic characterization. The metal sheets were employed as photoelectrode substrates, while the counter electrodes were still based on PET-ITO plastic foils ($15 \Omega/\text{sq.}$) in order to allow illumination of the sensitized ZnO film. The ZnO films consisted of a non-porous ZnO bottom layer electrodeposited for 10 minutes and a porous layer electrodeposited for 45 minutes. The thickness of the whole ZnO film was about $9 \mu\text{m}$.

4.3.1 Scanning electron microscopy

The SEM images of bottom and porous ZnO layers deposited on titanium and stainless steel are shown in Figure 4.13. It is observed that the bottom layer on titanium sheet is less compact than the layer on stainless steel, which results more recombination reactions between ZnO/substrate interfaces. The porous layer on both metal sheets are similar and there is also no remarkable difference between the ZnO structure on the metal sheets and on the PET-ITO substrate demonstrated in section 4.1.

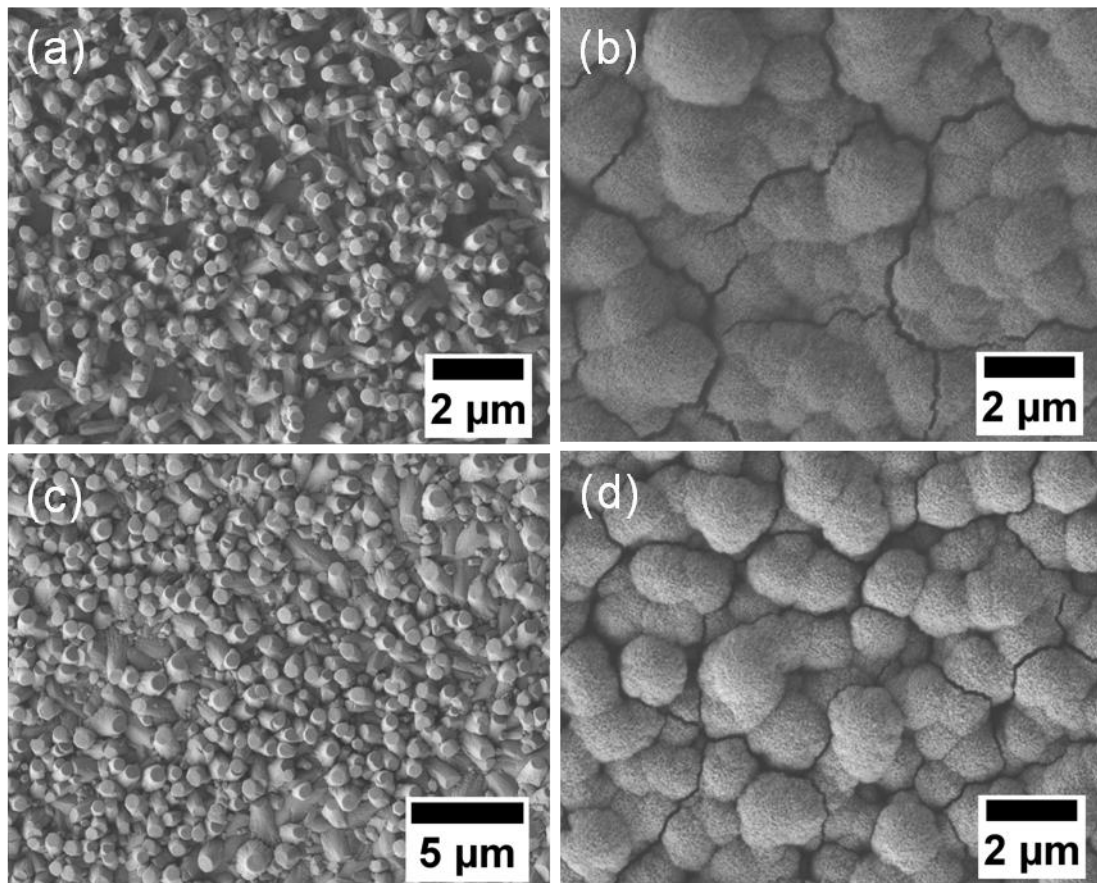


Figure 4.13 SEM images of (a) and (c) compact ZnO layer; (b) and (d) porous ZnO layer on titanium (a-b) and stainless steel (c-d).

4.3.2 UV-Vis spectroscopy

It is mentioned that the DSSCs based on metal sheets were illuminated through the counter electrode (back side), because light cannot penetrate through the metal sheets. This causes additional losses by light absorption in the electrolyte and the counter-electrode catalyst layer. Figure 4.14 illustrates that the light intensity is reduced by about 30 % between 500 nm and 600 nm and by more than 50 % between 400 nm and 500 nm.

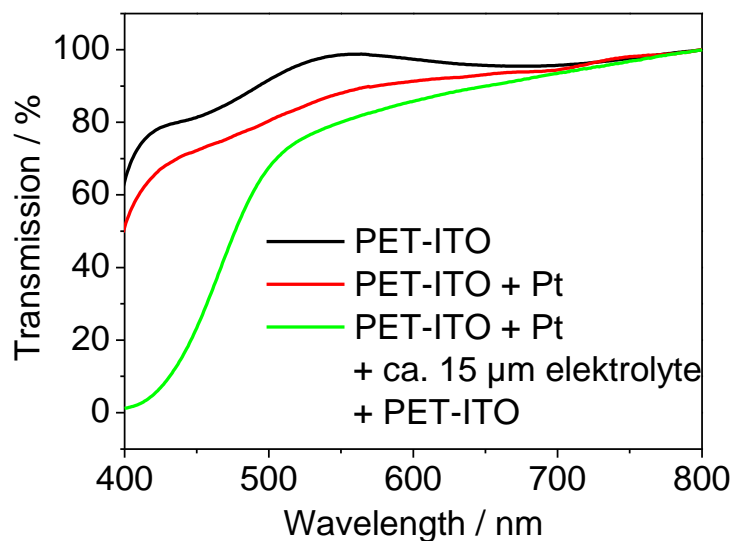


Figure 4.14 UV-Vis transmission spectra measured for PET-ITO substrate a PET-ITO based Pt counter electrode and a sandwich cell with about 15 μm liquid I/I_3^- electrolyte, enclosed between PET-ITO and a PET-ITO based Pt counter electrode. The third sample was used for analysis of the total light loss due to back side illumination.

4.3.3 Photovoltaic performance

Due to the reduced light intensity reaching the ZnO layer, the DSSCs based on stainless steel and titanium sheets show about 60 % less short-circuit currents and disappointing efficiencies compared to DSSCs based on PET-ITO substrates illuminated from front side (Figure 4.15 and Table 4.5). The fill factor of the cell based on titanium sheet is 0.2 less than the cell based on stainless steel, which may be due to the less compact bottom layer and thus more recombination reactions between the ZnO/Ti-interfaces.

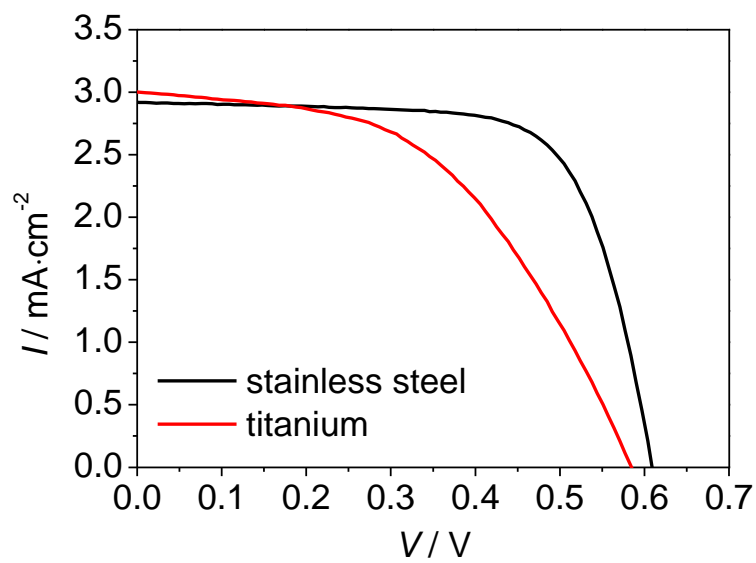


Figure 4.15 I-V curves measured at 1 sun level for DSSCs prepared with ZnO thin films on stainless steel and titanium sheet.

Table 4.5 Photovoltaic characteristics of DSSCs based on stainless steel and titanium sheet calculated from the I-V curves in Figure 4.15.

Substrate	$I_{sc} / \text{mA}\cdot\text{cm}^{-2}$	V_{oc} / V	FF	$\eta / \%$
stainless steel	2.9	-0.61	0.70	1.2
titanium	3.0	-0.58	0.50	0.9

4.4 Other flexible Substrates

In this thesis other conductive substrates based on PET have also been investigated. For this purpose, PET substrates have been coated with metals (PET-Ag, PET-Au and PET-Ti), polystyrenesulfonate doped poly(3,4-ethylenedioxythiophene), (PET-PEDOT/PSS) and a silver/poly(3,4-ethylenedioxythiophene) nanocomposite (PET-Ag/PEDOT). All these substrate materials were provided by Tesa SE.

Table 4.6 Stability of conductive polymer films in aqueous KCl solution (2. column), aqueous KCl solution at 70 °C under stirring (3. column) and in the same solution under pre-electrolysis, which is used to activate the substrate.

Substrate	0.1 M KCl(aq), 30 minutes at room temperature	0.1 M KCl(aq), 30 minutes at 70 °C, 300 rpm	Pre-electrolysis
PET-Ag	color changes at the edge of the conductive coating	conductive coating peels off partially	conductive coating peels off completely, no conductivity after pre-electrolysis
PET-Ag/PEDOT			
PET-Ti	no change	no change	conductive coating peels off partially
PET-Au			
PET-PEDOT/PSS 150 Ω/sq.	186 Ω/sq.	280 Ω/sq.	352 Ω/sq.
PET-PEDOT/PSS 350 Ω/sq.	350 Ω/sq.	320 Ω/sq.	624 Ω/sq.

All substrates show a rather disappointing thermal and chemical stability as compared to the excellent stability of PET-ITO and PET-CNT. Table 4.6 documents the stability of the substrates in aqueous KCl solution at room temperature, in the same solution at 70 °C under stirring and under pre-electrolysis, which is required for the activation of the substrates before electrodeposition of ZnO thin films. Photos of the substrates after these stability tests are shown in Figure 4.16. The metal-coated PET films were proven to be unstable during the pre-electrolysis. Although the PEDOT/PSS coating on the PET did not peel off during the pre-electrolysis, some of the conductivity was lost. Additionally, the electrodeposited ZnO films on PET-PEDOT/PSS were less porous than the films on PET-ITO and the template EY cannot be desorbed after the film

deposition. The reason may be due to a continuous degradation under elevated temperature. In view of this, PET-PEDOT/PSS is not suitable as substrate in this work.

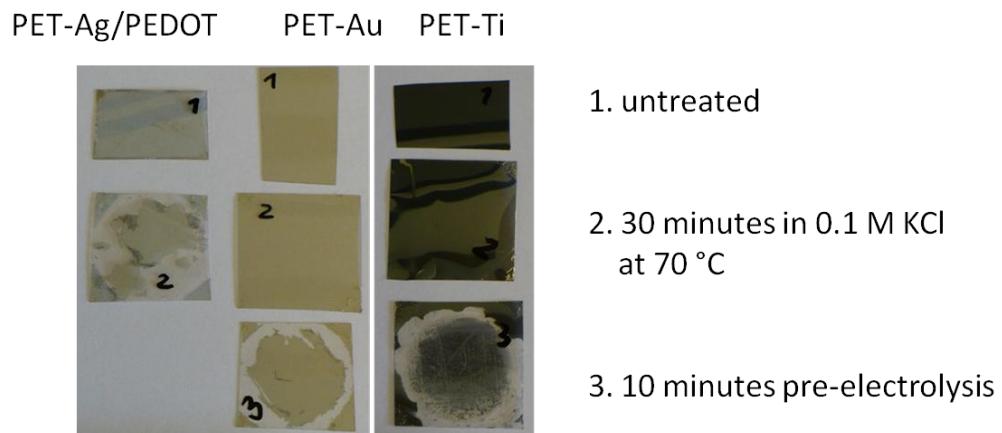


Figure 4.16 Photos of some substrates after the stability tests listed in Table 4.6.

4.5 Summary

In summary, the study demonstrated that PET-ITO is the best flexible substrate for the photoanodes of DSSCs. The surface morphology of the PET-ITO is very smooth and homogeneous, thus creating a suitable condition for the electrodeposition of homogeneous ZnO films. Using electrodeposited porous ZnO films as electron collector, a deposition time of 45 minutes has been found to give the highest photovoltaic performance with a V_{oc} of -0.64 V, a I_{sc} of $9.2 \text{ mA}\cdot\text{cm}^{-2}$, a FF of 0.56 and a conversion efficiency of 3.3 %.

SWCNT thin films can also be used as conducting, transparent substrate for the photoanode in DSSCs. Taking into account the relatively high resistance of the PET-CNT substrates used in this study ($470 \text{ }\Omega/\text{square}$ compared to typical values between $15 \text{ }\Omega/\text{square}$ for PET-ITO) the achieved conversion efficiency of $\eta = 2.5 \%$ can be regarded as very promising. Further improvements of the PET-CNT-based DSSCs can be expected after careful optimization of the CNT layer, with the goals to achieve a higher conductivity without significantly decreasing the transparency and, in case of electrodeposited porous ZnO films as electron collector, a more homogenous distribution of the CNTs in the conducting layer in order to obtain ZnO films with a more homogenous thickness.

Due to their illumination through the counter electrode, DSSCs based on metal foil substrates showed lower efficiencies than the DSSCs based on the PET-ITO substrate, despite the good conductivity of the metal sheets. Other PET-based substrates, including PET-Ag, PET-Au, PET-Ti, PET-PEDOT/PSS and PET-Ag/PEDOT, have also been investigated. These substrates have shown disappointing thermal and chemical stability, either the conductive coating on the PET peeled off during the pre-electrolysis, or some of the conductivity was lost after the electrolysis.

Daylight can accelerate the eosin Y desorption and leads to an almost complete desorption. The results of cyclic voltammetric measurements demonstrated that the electrodeposited ZnO bottom layer can efficiently suppress the electron leakage at bare substrate/electrolyte interface.

5 Electrolyte for flexible ZnO-based dye-sensitized solar cells

In this chapter, the results of the photovoltaic performances of flexible ZnO-based DSSCs with electrolyte based on organic solvent acetonitrile and ionic liquids are reported. The ZnO-based photoanode was potentiostatically deposited on PET-ITO films ($15 \Omega/\text{sq.}$). The ZnO films consisted of a non-porous ZnO bottom layer electrodeposited for 10 minutes and a porous layer electrodeposited for 45 minutes. The thickness of the whole ZnO film was about $8 \mu\text{m}$. The active area of DSSC was 1.1 cm^2 .

5.1 Organic solvent electrolytes

The optimization of the iodine and iodide concentration is one of the most important variables in the performance optimization of DSSC. As seen in the operating principle of DSSC, triiodide plays a fundamental role in the function of the dye-sensitized solar cell. Its optimization is crucial as equilibrium between fast reduction to iodide and slow recombination with the injected electrons must be achieved. In the following two sections 5.1.1 and 0, the effect of iodine and iodide concentration dependence in the acetonitrile-based electrolyte on the photovoltaic performance of DSSC was investigated. Furthermore, the effect of additives 4-tert-butylpyridine was studied. The electron transport and interfacial recombination kinetics were systematically investigated by EIS.

5.1.1 Influence of the iodine concentration

The commonly used organic solvent electrolyte for ZnO-based dye-sensitized solar cells contains $0.1 \text{ mol}\cdot\text{L}^{-1} \text{ I}_2$ and $1 \text{ mol}\cdot\text{L}^{-1}$ TPAI in an acetonitrile/ethylene carbonate solvent mixture ($v:v = 1:4$). In this study, different concentrations of iodine ($0.05, 0.1, 0.15, 0.2$ and $0.3 \text{ mol}\cdot\text{L}^{-1}$) were added to the electrolytes, while keeping the concentration of TPAI constant at $1 \text{ mol}\cdot\text{L}^{-1}$.

5.1.1.1 Photovoltaic performance

Figure 5.1 presents the I-V curves of DSSCs with the electrolyte containing different contents of iodine under illumination of $100 \text{ mW}\cdot\text{cm}^{-2}$. The photovoltaic parameters are shown in Table 5.1. It is observed that V_{oc} and I_{sc} decrease while FF increases when the concentration of iodine is increased. This leads to an optimum of the power conversion

efficiency of 3.3 % at an iodine concentration of $0.1 \text{ mol}\cdot\text{L}^{-1}$.

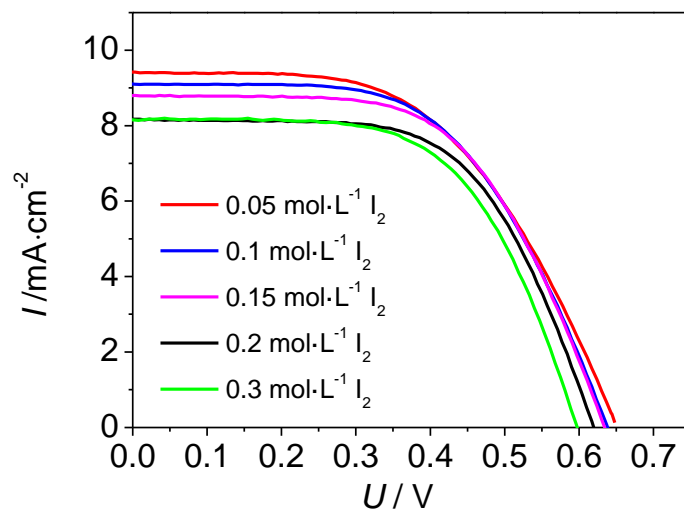
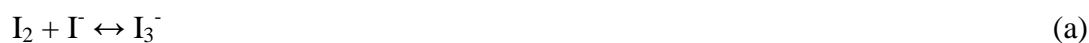


Figure 5.1 I-V characteristics of DSSCs with various iodine concentrations under AM 1.5 illumination ($100 \text{ mW}\cdot\text{cm}^{-2}$).

Table 5.1 Photovoltaic characteristics calculated from the I-V curves in Figure 5.1.

Iodine concentration / $\text{mol}\cdot\text{L}^{-1}$	V_{oc} / V	I_{sc} / $\text{mA}\cdot\text{cm}^{-2}$	FF	η / %
0.05	-0.65	9.4	0.54	3.1
0.1	-0.643	9.2	0.56	3.3
0.15	-0.637	8.8	0.59	3.2
0.2	-0.62	8.2	0.60	3.0
0.3	-0.60	8.1	0.61	2.9

The decrease in the photocurrent with increasing iodine concentration can be explained by considering the following redox reactions:



According to reaction (a), increasing the iodine concentration acts in favor of I_3^- , given

the fact that in the electrolyte the I^- concentration ($1 \text{ mol}\cdot\text{L}^{-1}$) is much higher than that of I_2 . Due to the same reason, the I^- concentration is not changed significantly. Since a critical level of I_3^- is necessary for cell functioning, reactions (b) and (c) can put in effect, further increase of I_2 and hence the I_3^- concentration, the photo-generated electrons react with the tri-iodide at the interface of ZnO with the electrolyte, the dark reaction (d) becomes dominating, decreasing the external current I_{sc} . Another reason for the decrease of I_{sc} with iodine concentration is simply increased light absorption by triiodide in the electrolyte, which interferes with the light harvesting dye molecules.

It has been reported that the relation between V_{oc} and concentration of I_3^- could be expressed as follows, ^[189, 190]

$$V_{oc} = \frac{RT}{nF} \ln\left(\frac{AI}{n_0 k_1 [I_3^-] + n_0 k_2 [D^+]}\right) \quad \text{Equation 5.1}$$

where k_1 and k_2 are kinetic constants of recombination of the injected electrons with I_3^- , and with oxidized dyes (D^+), respectively. I is the incident photon flux and n_0 is the concentration of accessible electronic states in the conduction band. When the recombination of the injected electrons with oxidized dyes can be neglected, V_{oc} should decrease with increasing iodine concentration.

However, the fill factor (FF) is slightly improved by addition of iodine to the electrolytes, reflecting a general lowering of cell resistance, which has been proven by using electrochemical impedance spectroscopy in the following section.

5.1.1.2 Electrochemical impedance spectroscopy

Figure 5.2a represents the Nyquist plots of the DSSCs with various iodine concentrations. It is noticed that with increasing the iodine concentration, the middle frequency semicircle which represents the interfacial charge recombination reaction of electrons with the I_3^- ions, shrunk markedly. This induces the reduction of the total resistance and the improvement of the fill factor. But at the same time, it also indicates increased recombination of photogenerated electrons, leading to a lower electron collection efficiency.

By fitting of the experimental data, more exact parameters to understand the underlying mechanisms for electron transport and recombination with different iodine concentration were obtained and plotted in Figure 5.2b. By varying the iodine

concentration from 0.05 to 0.3 mol·L⁻¹, the electron transport resistance R_t decreases from 1.72 to 0.77 Ω , while the charge transfer resistance R_{ct} decreases from 8.3 to 4.0 Ω . The decreased R_t value is unexpected and contradicts the theory. According to decreased photocurrent the R_t value should increase. The deviation from expectation may be due to the minor differences in the film thickness and the fitting error. The smaller R_{ct} value with higher iodine concentration also illustrates the enhanced electron recombination with triiodide ions.

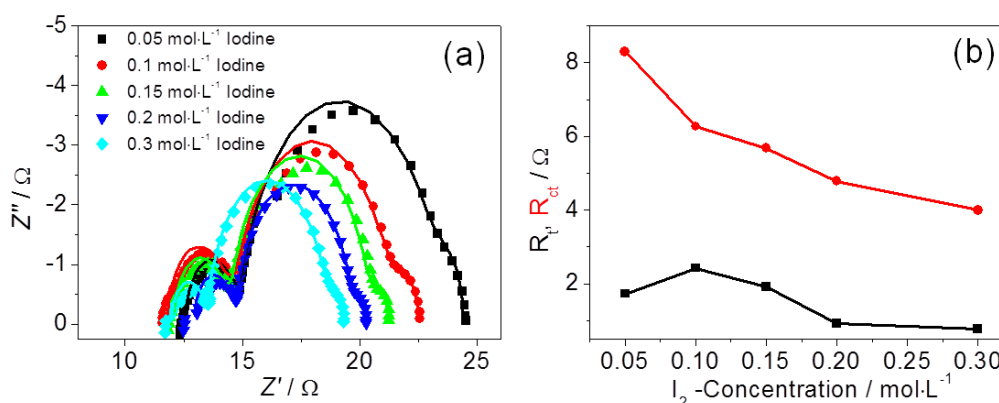


Figure 5.2 Nyquist plots (a) and characteristic parameters (b) for the corresponding DSSCs with various iodine concentrations under AM 1.5 illumination ($100 \text{ mW}\cdot\text{cm}^{-2}$) at an applied forward bias of -0.6 V . The lines in (a) show the fits according to the model illustrated in Figure 4.10a.

5.1.1.3 Intensity modulated photocurrent / photovoltage spectroscopy

As presented in Table 5.2, due to the slight changes in I_{sc} and R_t the electron transport times of DSSCs with various iodine concentrations show little differences as well. The electron lifetime decreases when the iodine concentration is increased from 0.05 to 0.15 mol·L⁻¹ and then reaches a plateau. This trend is in accordance with the decreasing R_{ct} value seen in the EIS analysis. Due to the decreasing lifetime, the collection efficiency also decreases slightly with increasing iodine concentrations. However, all cells have excellent collection efficiencies above 99 %, which indicates that light absorption by triiodide in the electrolyte at higher iodine concentration is the main reason for the decreased I_{sc} .

Table 5.2 Electron transport time (τ_d) and lifetime (τ_n) for the corresponding DSSCs with various iodine concentrations.

Iodine concentration / mol·L ⁻¹	τ_d (IMPS) / ms	τ_n (IMVS) / ms	η_{ce} / %
0.05	0.019	11.2	99.83
0.1	0.015	8.29	99.82
0.15	0.015	6.24	99.76
0.2	0.012	6.24	99.81
0.3	0.019	6.24	99.70

5.1.2 Influence of the iodide concentration

Different concentrations of TPAI (0.2, 0.5, 0.7 and 1.0 mol·L⁻¹, respectively) were added in the electrolytes. The iodine concentration was kept at 0.1 mol·L⁻¹.

5.1.2.1 Photovoltaic performance

Figure 5.3 presents the I-V curves of DSSCs with the electrolyte containing different contents of TPAI under illumination of 100 mW·cm⁻². The calculated photovoltaic parameters are shown in Table 5.3.

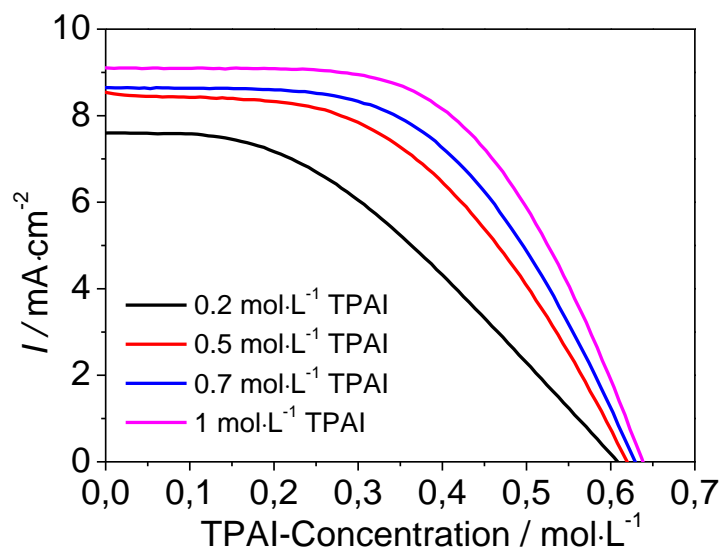


Figure 5.3 I-V characteristics of DSSCs with various TPAI concentrations under AM 1.5 illumination (100 mW·cm⁻²).

Table 5.3 Photovoltaic characteristics calculated from the I-V curves in Figure 5.3.

TPAI concentration / mol·L ⁻¹	V _{oc} / V	I _{sc} / mA·cm ⁻²	FF	η / %
0.2	-0.61	8.0	0.33	1.8
0.5	-0.62	8.5	0.49	2.7
0.7	-0.63	8.7	0.53	2.9
1	-0.64	9.2	0.56	3.3

It is observed that all parameters (V_{oc}, I_{sc}, FF and η) increase with the increasing TPAI content. The increased photovoltaic performance is attributable to a faster dye regeneration. The role of the iodide in the electrolyte is to regenerate the positively charged photoexcited dye by electron donation according to the redox reaction: 3I⁻ + 2Dye⁺ → 2Dye + I₃⁻. The lack of I⁻ leads to this reaction occurring slower, which may also lead to an incomplete dye regeneration, meaning that a part of the photooxidized dye molecules may rather recombine with a photogenerated electron from the conduction band of ZnO. Therefore, the photocurrent as well as the open-circuit voltage, FF and the conversion efficiency of DSSC will be decreased. It indicated that the dye regeneration process is incomplete when the TPAI concentration was lower than 1.0 mol·L⁻¹ in the electrolyte.

Unfortunately, the TPAI concentration could not be increased further, since it was noted that 1.0 mol·L⁻¹ is already the saturation concentration of TPAI in the acetonitrile/ethylene carbonate solvent mixture.

5.1.2.2 Electrochemical impedance spectroscopy

Figure 5.4a represents the Nyquist plots of the DSSCs with various TPAI concentrations. The fitted parameters of electron transport and recombination resistance are shown in Figure 5.4b. It is noticed that with increasing TPAI concentration the total resistance is reduced, resulting in the improvement of the fill factor. The decreased total resistance is due to a decrease of both the electron transport resistance R_t and the charge transfer resistance R_{ct}. The decrease in both values is caused by the increased electron concentration in the ZnO (as indicated by the increased photocurrent) due to the more efficient photogeneration of electrons.

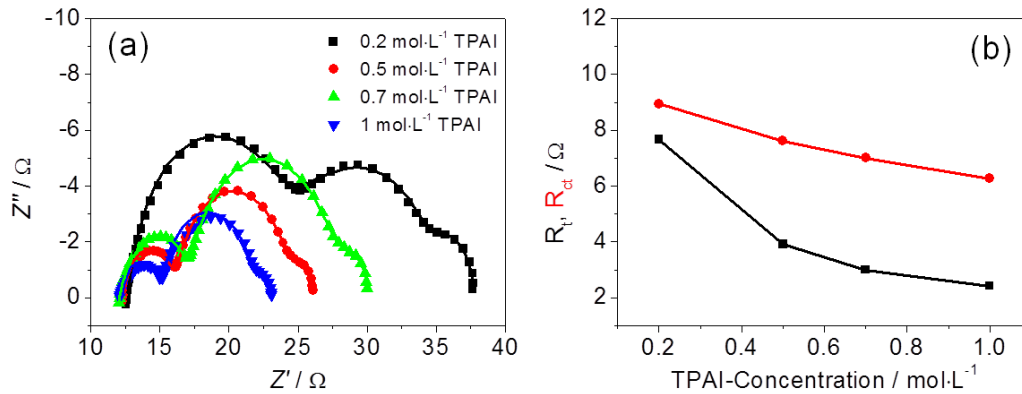


Figure 5.4 Nyquist plots (a) and characteristic parameters (b) for the corresponding DSSCs with various TPAI concentrations under AM 1.5 illumination ($100 \text{ mW}\cdot\text{cm}^{-2}$) at an applied forward bias of -0.6 V . The lines in (a) show the fits according to the model illustrated in Figure 4.10a.

5.1.2.3 Intensity modulated photocurrent / photovoltage spectroscopy

As presented in Table 5.4, both the electron transport time and lifetime decrease with increasing TPAI concentration. The decrease is also caused by the increased electron concentration in the ZnO films and this trend correlates well with the decreasing R_t and R_{ct} values seen in the EIS analysis. The collection efficiency is slightly enhanced with increasing TPAI concentration and leads to better photovoltaic performance.

Table 5.4 Electron transport time (τ_d) and lifetime (τ_n) for the corresponding DSSCs with various TPAI concentrations.

TPAI concentration / mol·L ⁻¹	τ_d (IMPS) / ms	τ_n (IMVS) / ms	η_{cc} / %
0.2	0.045	11.2	99.60
0.5	0.03	8.28	99.64
0.7	0.01	8.28	99.88
1.0	0.015	8.28	99.82

5.1.3 Effect of additives

It is well known that the presence of some additives in the electrolyte can lead to a significant improvement of the photovoltaic performance of TiO₂-based DSSCs. One of the most used additives for organic liquid electrolytes is 4-tert-butylpyridine (TBP) in a

concentration of about $0.5 \text{ mol}\cdot\text{L}^{-1}$. Detailed IMVS studies revealed that the positive effect of TBP on the V_{oc} is due to a positive band edge movement and that charge recombination is only slightly effected.^[168] Thus upon adsorption on the TiO_2 -surface the pyridine ring induces electron density into the TiO_2 creating a surface dipole. The band edge movement reduces the driving force for electron injection and thus the I_{sc} is a little bit lower than in untreated cells. After studying the effect of the iodine and iodide concentrations in the organic liquid electrolyte, the influence of the addition of TBP on the performance of the ZnO-based DSSC was analyzed.

5.1.3.1 Photovoltaic performance

In Figure 5.5 the photovoltaic performance of a reference cell without additive and cells with TBP added at various concentrations can be found.

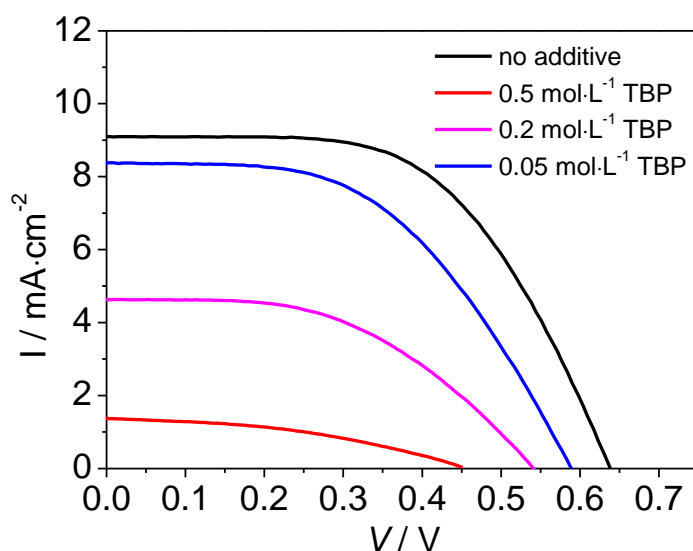


Figure 5.5 I-V characteristics of DSSCs with various TBP concentrations under AM 1.5 illumination ($100 \text{ mW}\cdot\text{cm}^{-2}$).

Table 5.5 Photovoltaic characteristics calculated from the I-V curves in Figure 5.5.

TBP concentration / mol·L⁻¹	V_{oc} / V	I_{sc} / mA·cm⁻²	FF	η / %
0	-0.64	9.2	0.56	3.3
0.05	-0.59	8.4	0.51	2.5
0.2	-0.54	5.0	0.46	1.2
0.5	-0.45	1.4	0.40	0.3

As can be observed in Table 5.5, TBP has a significantly negative effect on all cell parameters (V_{oc}, I_{sc}, FF and overall efficiency). A possible reason for the decreased photovoltaic performance could be the desorption of the dye D149 on ZnO films by addition of TBP. To prove this hypothesis, a ZnO/D149 film was divided into two parts. One part was immersed in acetonitrile, another in a TBP/acetonitrile mixture. Just after waiting for an hour, it was observed that the TBP added acetonitrile solution was clearly colored by the dye, while the solution without TBP was still colorless. The two samples were immersed in the solutions overnight (Figure 5.6 and Figure 5.7).

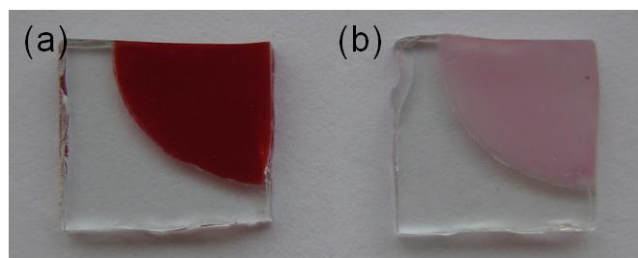
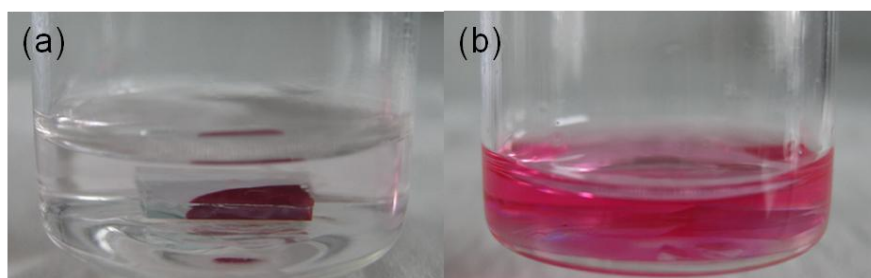
*Figure 5.6 ZnO/D149 films after immersion in the acetonitrile solutions without (a) and with TBP overnight (b).**Figure 5.7 Acetonitrile solutions without (a) and with TBP (b) after immersion with ZnO/D149 films overnight.*

Figure 5.6 and Figure 5.7 show that the ZnO/D149 film retained its color in acetonitrile solution, while the same ZnO film in TBP bleached. This indicates that TBP caused the desorption of the dye D149 from porous ZnO film.

5.2 Ionic liquid electrolyte

5.2.1 Binary ionic liquid mixture PMIM I/EMIM TCB

As mentioned in chapter 2, the photovoltaic performance of the cells can be strongly improved by mixing PMIM I with less viscous ionic liquids. For this purpose PMIM I was mixed with 1-Ethyl-3-methylimidazoliumtetra-cyanoborat (EMIM TCB, Figure 2.5) in the present section. The iodine concentration was constant at $0.2 \text{ mol}\cdot\text{L}^{-1}$. The tested ionic liquid mixtures were provided by Merck KGaA.

5.2.1.1 Photovoltaic performance

A summary of the photovoltaic parameters as a function of the PMIM I/EMIM TCB mixing ratio is shown in Table 5.6.

Table 5.6 Photovoltaic parameters as a function of PMIM I/EMIM TCB mixing ratio.

Sample	PMIM I / mol-%	Viscosity / mPa·s (20 °C)	V_{oc} / V	I_{sc} / mA·cm ⁻²	FF	η / %
M166	20	33.4	-0.51	5.9	0.39	1.2
M170	40	58.9	-0.48	6.6	0.45	1.4
M173	50	89.2	-0.50	6.8	0.46	1.5
M175	60	137.8	-0.50	6.9	0.53	1.7
M223	70	236.1	-0.52	7.2	0.51	1.9
M224	80	420.2	-0.51	5.9	0.56	1.6
M225	100	1132	-0.51	3.8	0.65	1.3

With respect to the overall power efficiency, an optimum mixing ratio of 70 mol-% PMIM I and 30 mol-% EMIM TCB is found. The photovoltaic parameters I_{sc} , FF and η of the cells are clearly affected by PMIM I/EMIM TCB mixing ratio. The first factor to explain the behavior of cells with different electrolyte composition is the viscosity. It can be seen that reducing the PMIM I content from 100 mol-% to 80 mol-% by mixing this ionic liquid with EMIM TCB results in a decrease in the viscosity of about 60%. Therefore, larger triiodide diffusion coefficients are expected for the binary ionic liquid

mixture compared to the pure PMIM I electrolyte. It is observed that the reduction of PMIM I from 100 mol-% to 70 mol-% induces a significant improvement of the photocurrent from $3.8 \text{ mA}\cdot\text{cm}^{-2}$ to $7.2 \text{ mA}\cdot\text{cm}^{-2}$.

However, it is observed that the photocurrent decreases again when the EMIM TCB content is further increased, i.e. at low PMIM I concentrations. In terms of charge transport via the Grotthuss mechanism (see section 2.2.4) in ionic liquids, a high iodide concentration would promote exchange transport of triiodide. Therefore, lowering the PMIM I/EMIM TCB mixing ratio not only would induce an increase of physical diffusion as a consequence of viscosity decrease, but also a slow-down of the exchange reaction due to the diminution of iodide concentration.

The conversion efficiency η reflects the same trend observed in the photocurrent. An improvement of the photovoltage is expected with a reduction of the PMIM I content in the electrolyte due to the displacement of the equilibrium redox potential of the I/I_3^- couple. If the Fermi level in the semiconductor is fixed, as expected for constant illumination intensity, this displacement will lead to a higher photovoltage. However, no significant trend of the photovoltage was observed in this study. The fill factor is increased by more than 0.2 when the PMIM I content is increased from 20 mol-% to 100 mol-%. An improvement of the fill factor may be due to the more complete dye regeneration at high PMIM I concentrations.

5.2.2 Effects of water and acetonitrile addition

The ionic liquids have generally higher viscosities, which limit iodide transport speed and decrease cell efficiencies. The presence of water and organic solvents in ILs is expected to decrease the viscosity, which should affect DSSC efficiency. In this section, the effects of water and acetonitrile (AN) addition on photovoltaic performances for DSSCs with IL M175 are discussed.

5.2.2.1 Photovoltaic performance

Figure 5.8 and Table 5.7 show the photovoltaic performances of the cells when the amount of water and acetonitrile was varied. Large decreases in I_{sc} are observed as the amount of water and acetonitrile increased. V_{oc} remains constant with an increase in water content, while it decreases slightly with an increase in acetonitrile content. The decrease in V_{oc} may be due to the downshift of the ZnO conduction band. FF and η

decrease significantly when water and acetonitrile were added.

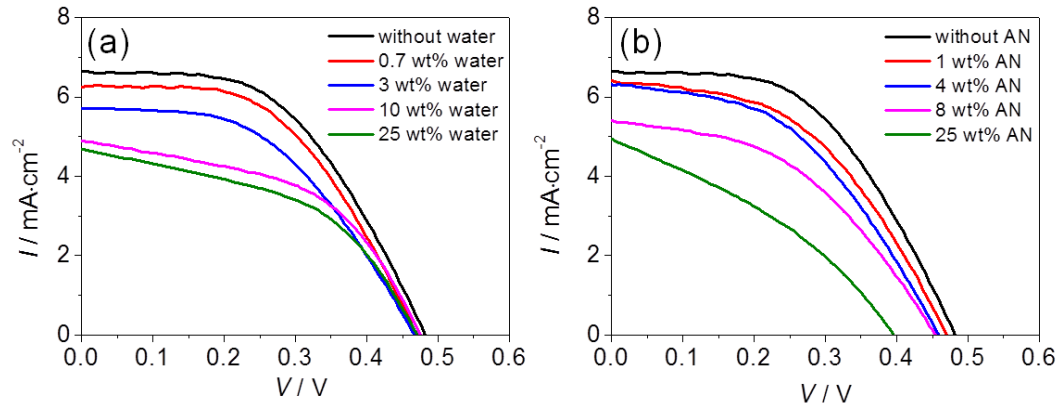


Figure 5.8 I-V characteristics of DSSCs with various water and AN concentrations under AM 1.5 illumination ($100 \text{ mW}\cdot\text{cm}^{-2}$).

Table 5.7 Photovoltaic characteristics calculated from the I-V curves in Figure 5.8.

Water / wt%	V_{oc} / V	I_{sc} / $\text{mA}\cdot\text{cm}^{-2}$	FF	η / %	AN / wt%	V_{oc} / V	I_{sc} / $\text{mA}\cdot\text{cm}^{-2}$	FF	η / %
0	-0.48	6.6	0.52	1.6	0	-0.48	6.6	0.52	1.6
0.7	-0.47	6.3	0.51	1.5	1	-0.47	6.4	0.47	1.4
3	-0.47	5.8	0.49	1.3	4	-0.46	6.3	0.46	1.3
10	-0.47	4.9	0.48	1.2	8	-0.45	5.4	0.44	1.1
25	-0.47	4.7	0.47	1.0	25	-0.40	4.9	0.34	0.7

The decrease of the photocurrent with the increase of the water and acetonitrile content in the ILs may be due to the decreased triiodide concentration in the electrolytes and the deteriorating effect of free water and acetonitrile on the dye-conjugated ZnO. Free water and acetonitrile molecules can strongly adsorb onto the ZnO surface and block the reaction of triiodide with the electron of the conduction band. The more water and acetonitrile in the electrolyte solution, the more water and acetonitrile molecules are adsorbed at the ZnO surface and the stronger the blocking effect. It was also reported that water and acetonitrile exhibit interactions with the ionic liquid, the former by strong directional hydrogen bond, the latter with the methyl group pointing towards the anion and acts as a hydrogen bond acceptor with regard to the interaction with the cation. The addition of water and acetonitrile can cause the ions to rearrange into aggregates and

finally lead to a disruption of the ionic network.^[191] In the case of water, the dye adsorbed on the ZnO surface may dissolve into the water-containing electrolyte solution or that the interaction of the dye with ZnO may be weakened by free water molecules. Additionally, a change of the link of the dye to the ZnO surface may also decrease the sensitization efficiency, thus decreasing the photocurrent.

5.2.2.2 Electrochemical impedance spectroscopy

Figure 5.9 and Table 5.8 show the Nyquist plots and fitted parameters of the DSSCs with various water and acetonitrile concentrations. It is noticed that with increasing the water and acetonitrile concentration, the semicircles in the low frequency range decrease, indicating a reduction of the electrolyte viscosity and the diffusion of triiodide becomes easier. Despite of the significantly decreased photocurrent, there is no clear trend for the electron transport resistance R_t . The charge transfer resistance R_{ct} increases slightly with increasing the water and acetonitrile concentration, revealing that the rate of the electron recombination is a little suppressed, which may also be caused by the above-mentioned blocking effect.

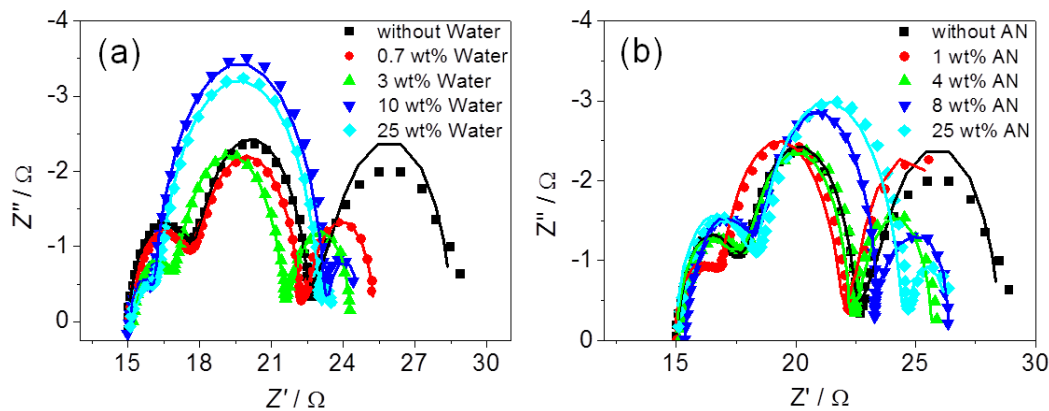


Figure 5.9 Nyquist plots for the corresponding DSSCs with various water and AN concentrations under AM 1.5 illumination ($100 \text{ mW}\cdot\text{cm}^{-2}$) at an applied forward bias of -0.5 V . The lines show the fits according to the model illustrated in Figure 4.10a.

Table 5.8 Characteristic fitted parameters of the DSSCs with various water and AN concentrations.

Water / wt%	R_t / Ω	R_{ct} / Ω	R_d / Ω	AN / wt%	R_t / Ω	R_{ct} / Ω	R_d / Ω
0	2.33	4.39	6.23	0	2.33	4.39	6.23
0.7	2.17	4.15	3.25	1	2.30	4.98	4.83
3	1.97	4.38	2.89	4	3.42	4.22	3.44
10	1.00	7.09	1.48	8	3.13	5.69	2.74
25	2.16	6.66	0.77	25	3.01	6.00	2.02

5.2.2.3 Intensity modulated photocurrent / photovoltage spectroscopy

The electron transport time and lifetime of the DSSCs with various water and acetonitrile concentrations are shown in Table 5.9. There is no clear trend for the electron transport time and collection efficiency with increasing water and acetonitrile concentrations, the values vary between 0.038-0.060 ms and 96-98 %, respectively. The lifetime increases above the water and acetonitrile of 10 wt% and 8 wt%, which correlates well with the increased R_{ct} . Because of the limited ion transport in high viscose ILs the collection efficiencies are generally lower than cells based on organic solvent electrolyte (>99.5 %).

Table 5.9 Electron transport time (τ_d) and lifetime (τ_n) of the DSSCs with various water and AN concentrations.

Water / wt%	τ_d (IMPS) / ms	τ_n (IMVS) / ms	$\eta_{cc} / \%$	AN / wt%	τ_d (IMPS) / ms	τ_n (IMVS) / ms	$\eta_{cc} / \%$
0	0.048	1.44	96.67	0	0.048	1.44	96.67
0.7	0.038	1.15	96.69	1	0.048	1.44	96.67
3	0.048	1.44	96.67	4	0.060	1.44	95.83
10	0.038	1.82	97.91	8	0.060	1.82	96.70
25	0.038	1.82	97.91	25	0.060	1.82	96.70

5.2.3 Effect of temperature

As mentioned above, the high viscosity of ionic liquids renders physical transport processes significantly slower than in common organic solvent based electrolytes and therefore limits the application of these electrolytes. To decrease viscosity, the addition of low viscous ILs as well as solvents such as water and acetonitrile were tested for application in ZnO-based DSSCs, and improved performances were obtained with low viscous ILs. Since the problem seems also to be that the ionic liquids cannot enter into the nanopores of the ZnO, another possibility may be the elevated temperature, which is expected to be helpful to reduce the high electrolyte viscosity and to improve the penetration of ILs into the pores. The binary IL mixture M321 (PMIM I:EMIM OTF=50:50, $I_2=0.2 \text{ mol}\cdot\text{L}^{-1}$) was maintained at elevated temperatures (60 °C and 80 °C) for 30 minutes before it was introduced on the ZnO photoanode. After the cell assembly, the whole cells were placed at high temperatures again for 15 minutes to ensure a homogeneous penetration of the IL into the pores of ZnO. Photoelectrochemical measurements were taken after the cells cooled to room temperature. A cell filled with IL at room temperature (around 20 °C) was used as a reference.

5.2.3.1 Photovoltaic performance

Figure 5.10 and Table 5.10 show the photovoltaic performances of cells filled with IL at various temperatures. The increase in I_{sc} and η with increasing temperature may be mainly due to the decrease in the viscosity of the electrolyte and resulting improved penetration of the electrolyte into the nanopores of ZnO. The temperature effect on the V_{oc} and FF can be neglected in the investigated domain.

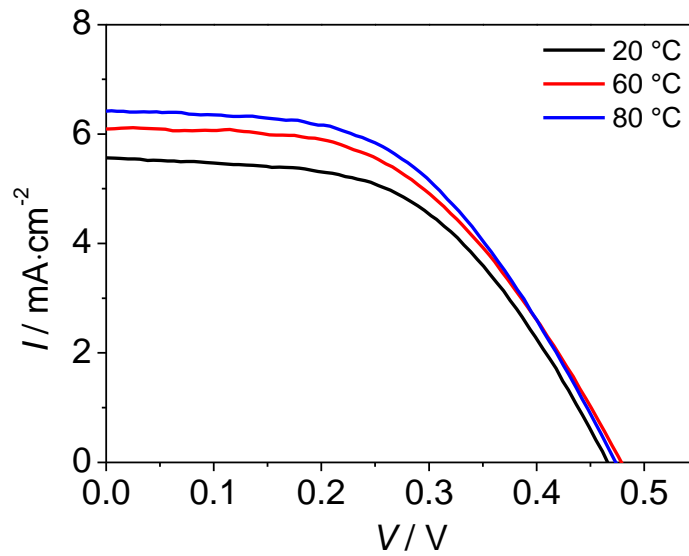


Figure 5.10 I-V characteristics of DSSCs with ILs at various temperatures under AM 1.5 illumination ($100 \text{ mW}\cdot\text{cm}^{-2}$).

Table 5.10 Photovoltaic characteristics calculated from the I-V curves in Figure 5.10.

Temperature	V_{oc} / V	$I_{sc} / \text{mA}\cdot\text{cm}^{-2}$	FF	$\eta / \%$
20 °C	-0.47	5.6	0.52	1.3
60 °C	-0.48	6.1	0.51	1.5
80 °C	-0.47	6.4	0.51	1.6

5.2.3.2 Electrochemical impedance spectroscopy

Figure 5.11 and Table 5.11 show the Nyquist plots and the fitted parameters of the cells with ILs at various temperatures. As a consequence of the increased photocurrent in the cell, the electron transport resistance R_t decreases with increasing temperature, while the charge transfer resistance R_{ct} remains almost constant. It is observed that the ion diffusion resistance R_d decreases also slightly with the increasing temperature, indicating that high temperature enables the movement of triiodide to be facilitated through the ZnO network.

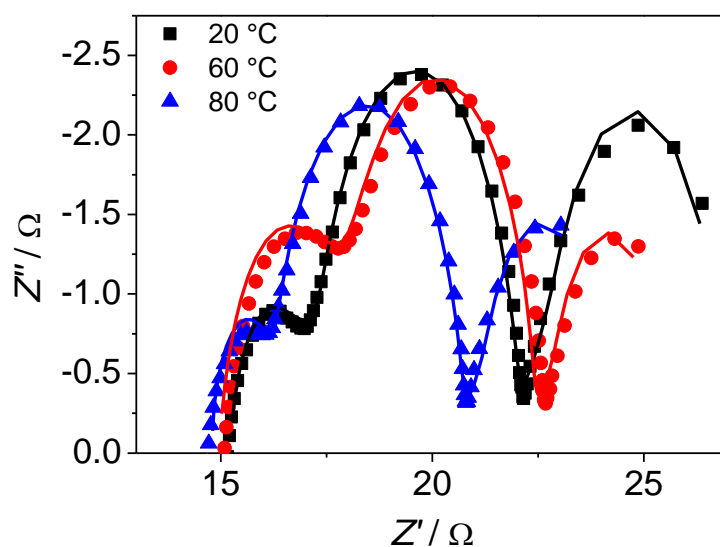


Figure 5.11 Nyquist plots for the corresponding DSSCs with ILs at various temperatures under AM 1.5 illumination ($100 \text{ mW}\cdot\text{cm}^{-2}$) at an applied forward bias of -0.5 V . The lines show the fits according to the model illustrated in Figure 4.10a.

Table 5.11 Characteristic fitted parameters of the DSSCs with ILs at various temperatures.

Temperature	R_t / Ω	R_{ct} / Ω	R_d / Ω
20 °C	4.03	4.58	4.98
60 °C	3.14	4.30	4.38
80 °C	2.73	4.38	4.29

5.2.3.3 Intensity modulated photocurrent / photovoltage spectroscopy

As shown in Table 5.12, the electron transport time decreases with increasing temperature and the lifetime is independent on the temperature, which agree well with the trends of R_t and R_{ct} in the EIS measurements. The rise in the collection efficiency can also be ascribed to the improved penetration of the electrolyte into the pores of ZnO.

Table 5.12 Electron transport time (τ_d) and lifetime (τ_n) of the DSSCs with ILs at various temperatures.

Temperature	τ_d (IMPS) / ms	τ_n (IMVS) / ms	η_{cc} / %
20 °C	0.060	1.45	95.86
60 °C	0.048	1.45	96.69
80 °C	0.038	1.45	97.38

5.2.4 Other mixtures of ionic liquids

To study the performance of ZnO-solvent free solar cells, other imidazolium-based ionic liquid mixtures in various compositions and mixing ratios have been tested in combination with PMIM I and BMMIM I (Table 5.13). The solvent ionic liquids were EMIM OTF, EMIM NTF and EMIM TCB, all three with a much lower viscosity than PMIM I and BMMIM I (Figure 2.5). The photovoltaic performances for the tested cells are shown in Table 5.14.

The mixtures M238 and M233 as well as M239 and M234 have the same compositions with different iodine concentrations (0.1 and 0.2 mol·L⁻¹). Both pairs show that an increase in the I₂ concentration increases the short-circuit current and correspondingly the overall efficiency, which could be a consequence of diffusion limitation in the electrolyte associated to the low I₃⁻ concentration. Furthermore, it is observed that the addition of iodine to the ionic liquids decreases its viscosity. This could also contribute to the improvement.

The mixtures M208, M240 and M266 contain the same components with increasing N-butylbenzimidazole (NBB) concentrations in steps of 0.2 mol·L⁻¹. In TiO₂-based solar cells with Ru-complexes as sensitizer, additives including TBP and NBB give generally a significant improvement of open-circuit photovoltage, a higher fill factor and therefore a solar energy conversion efficiency, while the short-circuit current is not much affected or slightly decreased. The additives probably decrease the rate constants of triiodine reduction, thereby suppressing the dark current at the TiO₂/electrolyte interfaces and increasing the electron lifetime. They also cause the TiO₂ conduction band to move up, resulting in an increase of V_{oc} at a fixed photoinduced charge density.^[192] Unlike TiO₂-based solar cells, the photovoltaic performance of the ZnO-

based solar cells with M208, M240 and M266 indicate that the additive NBB has a negative influence on the properties of the solar cells. The photovoltaic parameters V_{oc} , I_{sc} and η decrease significantly with increasing concentration of NBB. This may be a consequence of dye desorption in the presence of NBB, which could be explained by a stronger interaction between the pyridyl group of the NBB and the carboxyl group of D149 than the interaction between carboxyl group and ZnO surface.

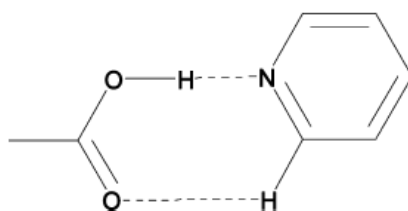


Figure 5.12 Intermolecular hydrogen bond of a carboxyl group and a pyridyl group.

The photovoltaic performance of the cells with IL M275 and M276, which contain the additives DMAP and CeMim, also show that the N-containing heterocyclic additives deteriorate the properties of D149-sensitized ZnO solar cells.

In general, it was observed that the ZnO-based solar cells with ionic liquids had much lower V_{oc} , I_{sc} , FF and efficiencies than the cells with acetonitrile-based electrolyte. The cell with the same deposition parameter and active area, which filled with acetonitrile-based electrolyte, had a V_{oc} of 0.64 V, a I_{sc} of 9.2 mA cm⁻², a FF of 0.56 and an efficiency of 3.3% (see section 4.1).

Table 5.13 Other imidazolium-based ionic liquids mixtures.

Sample	Viscosity 40°C / mPa·s	I ₂ / mol·L ⁻¹	PMIM I / mmol	BMMIM I / mmol	EMIM / mmol			Additive / mol·L ⁻¹				
					OTF	NTF	TCB	MgI ₂	NBB	GuaSCN	DMAp	CeMim
M238	26.81	0.1	-	25	-	-	75	0.05	0.4	0.1	-	-
M233	24.11	0.2	-	25	-	-	75	0.05	0.4	0.1	-	-
M239	40.64	0.1	35	-	16	21.67	21.67	0.05	0.4	0.1	-	-
M234	36.87	0.2	35	-	16	21.67	21.67	0.05	0.4	0.1	-	-
M208	20.73	0.1	-	26.5	-	-	87	-	0.4	0.1	-	-
M240	20.74	0.1	-	26.5	-	-	87	-	0.6	0.1	-	-
M266	21.54	0.1	-	26.5	-	-	87	-	0.8	0.1	-	-
M275	23.72	0.1	-	26.5	-	-	87	0.05	0.4	0.1	0.5	-
M276	22.18	0.1	-	26.5	-	-	87	0.05	0.4	0.1	0.5	0.5

PMIM I:	3-Propyl-1-methylimidazoliumiodid
BMMIM I:	1-Butyl-2,3-dimethylimidazoliumiodid
EMIM OTF:	1-Ethyl-3-methylimidazoliumtrifluormethylsulfonat
EMIM NTF:	1-Ethyl-3-methylimidazolium-bis(trifluormethylsulfonyl)imid
EMIM TCB:	1-Ethyl-3-methylimidazoliumtetracyanoborat
NBB:	N-Butylbenzimidazole
GuaSCN:	Guanidiniumthiocyanat
DMAp:	2-(Dimethylamino)-pyridin
CeMim:	5-Chloro-1-ethyl-2-methylimidazol

Table 5.14 Photovoltaic parameters of ionic liquid mixtures shown in Table 5.13.

Sample	$I_{sc} / \text{mA}\cdot\text{cm}^{-2}$	V_{oc} / V	FF	$\eta / \%$
M238	2.4	0.49	0.27	0.3
M233	5.6	0.46	0.35	0.8
M239	3.5	0.43	0.27	0.4
M234	5.7	0.43	0.37	0.9
M208	3.7	0.53	0.48	0.9
M240	2.4	0.54	0.29	0.4
M266	0.04	0.45	0.76	0.01
M275	0.07	0.40	0.83	0.02
M276	0.08	0.55	0.62	0.03

5.3 Long-term stability

The long-term stability of DSSCs with electrolyte based on organic solvent acetonitrile and ionic liquids was investigated. After the assembly the ZnO-based DSSCs were stored under various conditions (see Table 5.15). The aging of cells was accelerated by elevated temperature (60 °C) or humidity (desiccator with saturated KCl solution). Photoelectrochemical measurements were taken after the cells cooled to room temperature.

Table 5.15 Samples for the long-term stability tests.

Number	Electrolyte	Conditions
1		24 h/d in the dark at room temperature
2		24 h/d on the windowsill at room temperature
3		24 h/d during light soaking (0.75 sun) at 60 °C
4	Acetonitrile-based liquid electrolyte	24 h/d in the dark at 60 °C
5		12 h/d during light soaking (0.75 sun) at 60 °C+12 h/d in the dark at room temperature
6		12 h/d during light soaking (0.75 sun) at 60 °C+12 h/d in the dark at room temperature and under high humidity
7	IL M175	24 h/d during light soaking (0.75 sun) at 60 °C
8		24 h/d in the dark at 60 °C

5.3.1 Photovoltaic performance

The results for the tested cells are shown in Figure 5.13. It is noted that the parameter V_{oc} , J_{sc} , and η decrease with time. The continuous light irradiation and elevated temperature have accelerated the decrease. The fill factors of the cells with acetonitrile-based liquid electrolyte decrease with time, while the fill factors of the cells with ionic liquids increase slightly with time, which may be due to improvement in electrolyte penetration into the porous ZnO film at high temperature.

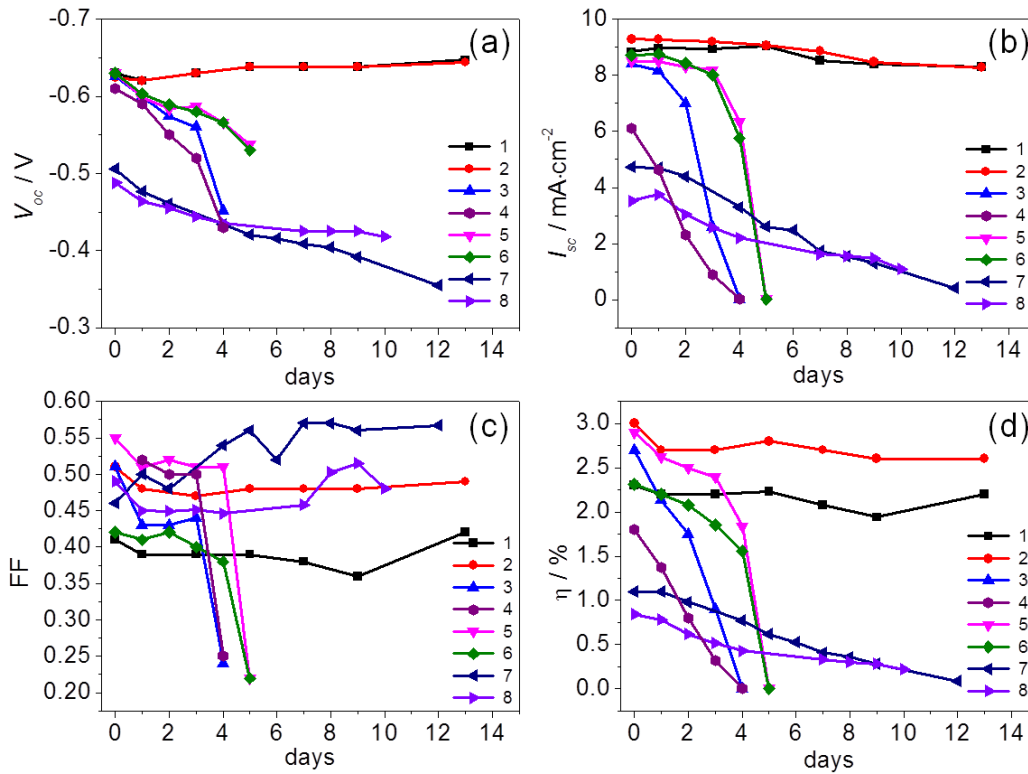


Figure 5.13 Photovoltaic parameters V_{oc} (a), I_{sc} (b), FF (c), and η (d) of DSSCs during long-term stability test.

Among these cells, the cells 1 and 2 showed the highest stability. Even after 100 days, they still showed efficiencies of 1.6 % and 1.8 %, respectively (not shown in Figure 5.13). The cells 3 and 4 had the lowest stability; they were completely inactive after 4 days. The decrease rates of the photovoltaic parameters between cells 1 and 2 and between cells 5 and 6 differed only slightly from each other, suggesting that window glass filtered daylight, and increased humidity did not affect the cells significantly in the investigated time period. The cells 7 and 8, in which an IL was used, showed better long-term stabilities than the cells 4 and 5 with acetonitrile-based electrolyte, although they were aged under the same conditions. The difference is, it was noted for cells 4 and 5 that the solvent acetonitrile evaporated during the test, leaving air bubbles in the cells. The elevated temperature has accelerated the rate of evaporation. Comparisons between cells 3 and 4 and between cells 7 and 8 showed that the decrease of the photovoltaic parameters mainly caused by the elevated temperature.

As mentioned in chapter 2, DSSCs with IL-based electrolytes are interesting because they do not present evaporation losses and, as a consequence, they are considered good candidates for fabricating stable devices. In this long-term stability test, the instability

of the DSSCs with IL observed in Figure 5.13 could be a consequence of dye desorption in the presence of ionic liquid and sublimation of iodine during the test.

Photos of the ZnO/D149 films after the long-term stability test are shown in Figure 5.14. The ZnO/D149 films of cells 7 and 8 were slightly bleached, which revealed that small amounts of dye get detached from the ZnO surface in the presence of ionic liquid. Dye desorption is expected to be stronger under illumination.^[193] Cell degradation due to dye desorption has been reported before for indoline dyes.^[194] Kubo et al. observed desorption of the dye from the surface of TiO₂ during stability tests with ionic liquid electrolytes containing 1-alkyl-3-methylimidazolium iodides (C₃-C₉).^[195] In addition, it has been reported that a high iodide concentration is detrimental to stability. In line with this, Zhang et al. found poor stability with electrolytes containing a high PMIMI concentration.^[196] Bahers et al. also reported on dye desorption for D149-sensitized ZnO cells in organic solvent such as dimethylformamide.^[197]

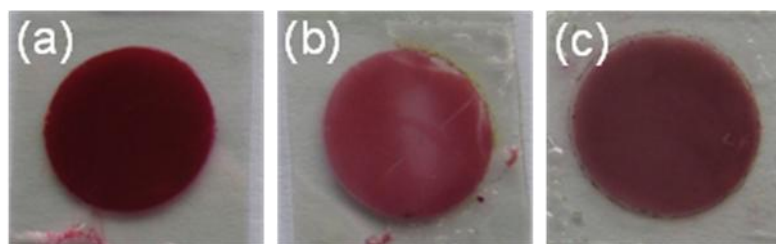


Figure 5.14 ZnO/D149 films of (a) cell 3, (b) cell 7 and (c) cell 8 after the long-term stability test.

5.3.2 Electrochemical impedance spectroscopy

Figure 5.15 shows the electrochemical impedance spectra as the Nyquist plots of the cells 3 and 7 before (both 0th day) and after (3rd day and 11th day, respectively) the long-term stability test. Table 5.16 lists the parameters determined by fitting the EIS experimental data. Firstly, the semicircles in the low frequency of both cells become larger after the long-term stability test, indicating an increase of Nernst diffusion impedance of triiodide (R_d), resulting from the change of the ingredients of the electrolyte.^[198] The reason why the concentration of triiodide decreased and the ingredients of the electrolyte changed may be due to the evaporation of acetonitrile (in the case of cell 3) and the sublimation of iodine during the test. A more reliable sealing and encapsulation of the cell will be necessary to obtain a longer lifetime of the cell. Secondly, the electron transport resistance (R_t) of cell 7 increases, which is caused by the dye desorption in the presence of ionic liquid. Thirdly, the recombination resistance

(R_{ct}) at the ZnO/electrolyte interface of the cell 7 increases. This indicates that the back electron transfer from the ZnO conduction band to triiodide was suppressed by the decrease of the triiodide concentration. Fourthly, the series resistances R_s of the both cells increases high with time, which may be due to a continuous increase in PET-ITO sheet resistance under prolonged exposure to elevated temperatures.

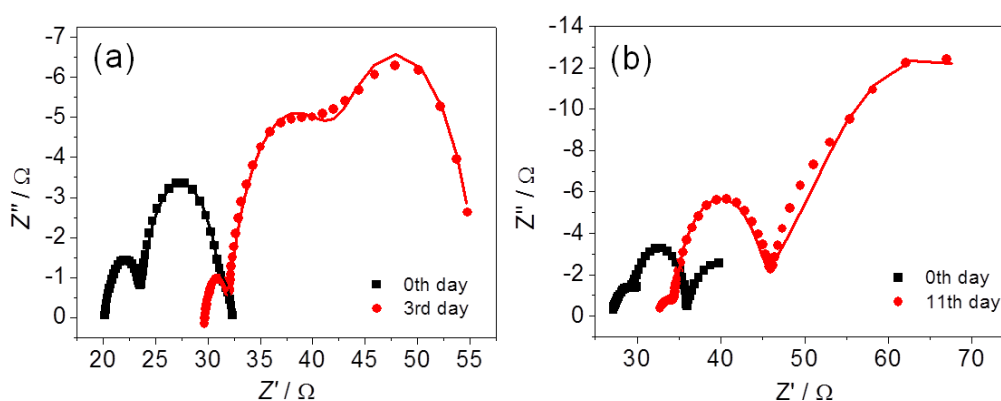


Figure 5.15 Nyquist plots of the cell 3 (a) and cell 7 (b) before/after the light soaking tests at 60 °C under AM 1.5 illumination ($100 \text{ mW}\cdot\text{cm}^{-2}$) at an applied forward bias of -0.6 V for cell 3 and -0.5 V for cell 7. The lines show the fits according to the model illustrated in Figure 4.10a.

Table 5.16 Characteristic fitted parameters of the cell 3 (a) and cell 7 (b) before/after the light soaking tests at 60 °C.

	Cell 3				Cell 7			
	R_s / Ω	R_t / Ω	R_{ct} / Ω	R_d / Ω	R_s / Ω	R_t / Ω	R_{ct} / Ω	R_d / Ω
Before	20.30	1.92	7.34	1.44	27.1	3.04	5.93	7.07
After	29.80	2.0	7.42	16.71	33.0	4.82	8.92	38.8

5.3.3 Intensity modulated photocurrent / photovoltage spectroscopy

As shown in Table 5.17, the electron transport time and lifetime of the both cells increase after the long-term stability test, while the collection efficiencies decrease. The increased transport time is due to the decrease of photocurrent, while the increased lifetime is caused by the suppressed recombination reaction through the decreased triiodide concentration.

Table 5.17 Electron transport time (τ_d) and lifetime (τ_n) of the cell 3 and cell 7 before/after the light soaking tests at 60 °C.

	Cell 3			Cell 7		
	τ_d (IMPS) / ms	τ_n (IMVS) / ms	η_{cc} / %	τ_d (IMPS) / ms	τ_n (IMVS) / ms	η_{cc} / %
Before	0.06	6.24	99.03	0.12	1.44	91.67
After	0.47	8.56	94.51	0.30	1.82	83.51

5.4 Summary

The iodine and iodide concentration in the acetonitrile-based electrolyte have been optimized (1 mol/L TPAI and 0.1 mol/L I₂). The well known additive 4-tert-butylpyridine was not compatible with the D149 dye. The addition of TBP caused desorption of the dye D149 from ZnO films.

The performance of ZnO solvent free solar cells has been analyzed. Binary mixtures of the most frequently used ionic liquid PMIM I with the low viscosity ionic liquid EMIM TCB have proven to have a positive effect on the performance of the cells. An optimum mixing ratio of 70 mol-% PMIM I and 30 mol-% EMIM TCB was found. The presence of water and the organic solvent acetonitrile in this binary IL mixture could reduce the viscosity but caused desorption of indoline dye D149, which affected the efficiency negatively. With an increasing electrolyte temperature, the cells show enhanced photovoltaic parameters I_{sc} and η as a result of the improved penetration of ILs into the nanoporous ZnO. The addition of iodine to the ionic liquids decreased its viscosity and increased the short-circuit current, which contributed to the improvement of the efficiency. The photovoltaic performances of ZnO solvent free solar cells with additives such as NBB, DMAp and CeMim indicated that the additives have a negative influence on the properties of the solar cells. The photovoltaic parameters V_{oc} , I_{sc} and η decrease significantly with increasing concentration of additives. This might be a consequence of dye desorption in the presence of additives, which could be explained by a stronger interaction between the pyridyl group of the additives and the carboxyl group of D149 than the interaction between carboxyl group and ZnO surface.

Because of volatility of the solvent-based electrolyte and assembly problems, the cells

with acetonitrile-based electrolyte have shown short lifetimes under continuous light irradiation and elevated temperature. Window glass filtered daylight and increased humidity did not affect the long-term stability of the cells significantly. The cells with IL-based electrolytes were more stable than the cells with acetonitrile-based electrolyte. However, it was observed that small amounts of dye D149 got detached from the ZnO surface in the presence of ionic liquid and the dye desorption was stronger under illumination.

6 Zinc oxide sensitized with dyes containing phosphonic acid anchoring groups

Most of the dyes employed in DSSCs have carboxylic acid groups to anchor on the semiconductor surface. The binding is reversible with high binding equilibrium constants ($K \approx 10^5 \text{ M}^{-1}$).^[199] In basic conditions (usually $\text{pH} \geq 9$) the equilibrium is typically shifted to the reactant side and the dye molecules desorb.^[200] This somewhat fragile linkage triggered the development of dyes with different anchoring groups. In general the binding strength to a metal oxide surface decreases in the order phosphonic acid > carboxylic acid > ester > acid chloride > carboxylate salts > amides,^[200] so most of the research is focused on phosphonic acids. Experimental studies have proven that it tends to bind more strongly to metal oxide surfaces, thus displaying better long-term stability compared to carboxylic acid anchors.^[201, 202] However, the phosphonic acid groups are not in conjugation with the polypyridyl plane due to their non-planar structures, which is a disadvantage for the injection of electrons.^[203] Wang et al.^[204] reported a Ru-complex with a phosphonic acid anchoring group (Z955), which gives a conversion efficiency of 8 % under AM1.5 accompanied by a good stability under prolonged light soaking (1000 h at AM1.5 and 55°C). This is the highest efficiency for a dye with a phosphonic anchoring group so far.

In this section, a study of ruthenium dyes with phosphonic acid anchoring groups is described, making a comparison of their performance with a ruthenium dye with carboxylic acid groups and the fully organic dye D149. Figure 6.1 shows the chemical structures of the ruthenium dyes used in this section, which were synthesized by Iolitec GmbH.

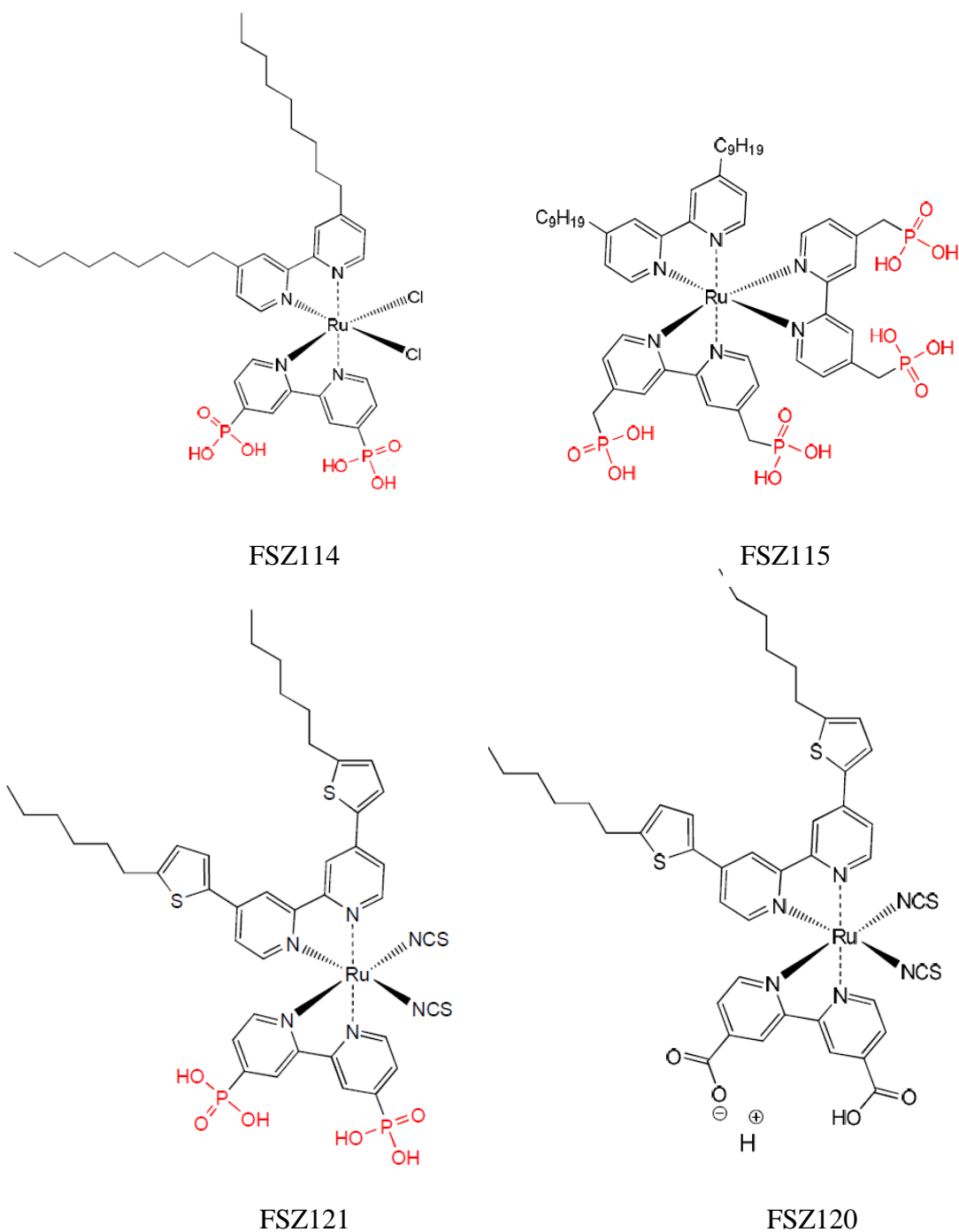


Figure 6.1 Chemical structures of ruthenium dyes with phosphonic acid groups FSZ114, FSZ115, FSZ121 and a ruthenium dye with carboxylic acid groups FSZ120.

The above-mentioned sensitizers were dissolved in methanol and stirred at room temperature for 1 h. The concentration of the sensitizer was kept at 0.5 mmol/L. Figure 6.2 shows photos of all dyes in methanol solutions at concentrations of 0.5 mmol/L and the ZnO films sensitized with these dyes. It is clearly observed that the solutions of the sensitizer with phosphonic acid anchoring groups and the respective films appear less

colored compared to the dyes with carboxylic acid groups.

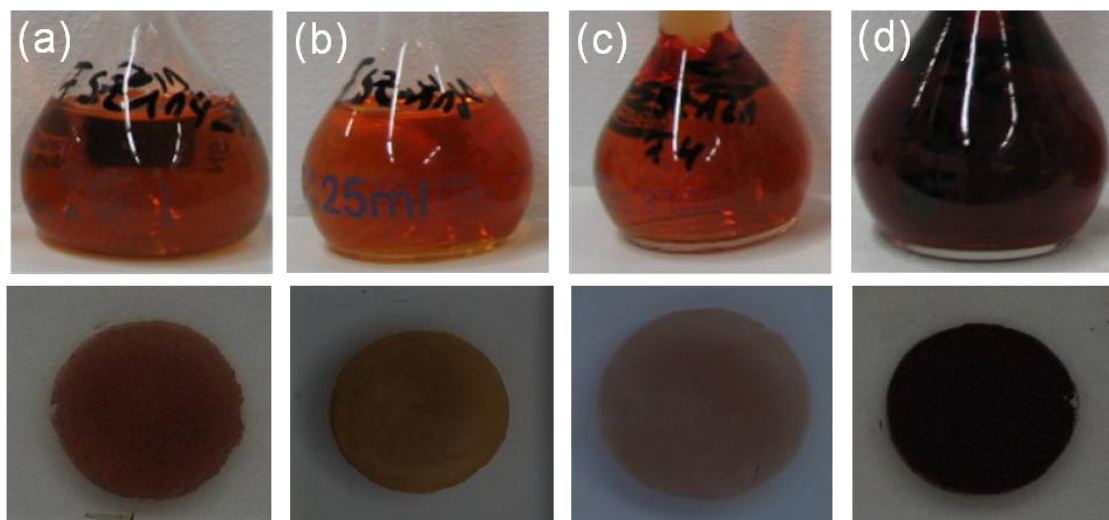


Figure 6.2 Photos of the dye solutions and ZnO films sensitized with the dyes (a) FSZ114, (b) FSZ115, (c) FSZ121 and (d) FSZ120

6.1 UV-Vis spectroscopy

UV-Vis extinction spectra of the dye solutions are shown in Figure 6.3a. In the spectra, the dye solutions exhibit two major prominent bands, appearing at 300-400 nm and at 400-600 nm, respectively. The former is ascribed to a localized aromatic π - π^* transition and the latter is of charge-transfer character. The absorption maxima for FSZ114, FSZ115, FSZ120 and FSZ 121 are at $\lambda = 467$ nm, 462 nm, 526 nm and 472 nm, respectively.

Figure 6.3b shows the absorption spectra of the dyes on ZnO films after 24 hours adsorption. As shown in Figure 6.3, the maxima absorption peaks for FSZ114, FSZ115, FSZ120 and FSZ 121 on the ZnO films are at $\lambda = 523$ nm, 470 nm, 535 nm and 490 nm and their absorption bands are red-shifted by 56 nm, 8 nm, 9 nm and 18 nm compared with the solution spectrum, respectively. The red shifts of the absorption spectra on ZnO could be ascribed to the aggregation of the dyes on the ZnO surface, which can occur readily because of the presence of phosphonic acid or carboxylic acid groups in the molecules. The interaction between the functional groups and the surface Zn^{2+} ions may lead to increased delocalization of the π^* orbital of the conjugated framework. The energy of the π^* level is decreased by this delocalization, which explains the red shift for the absorption spectra. Additionally, after the sensitization, the absorption of the ZnO films with dye FSZ114, FSZ115 and FSZ121 are relatively weak due to the low

amount of the adsorbed dye, indicating that they harvest little light in the visible region and would therefore perform less efficiently in DSSCs. In contrast, broad absorption band of the ZnO film sensitized with FSZ120 reveals that the dye with the carboxylic acid anchoring group adsorbed better on ZnO film.

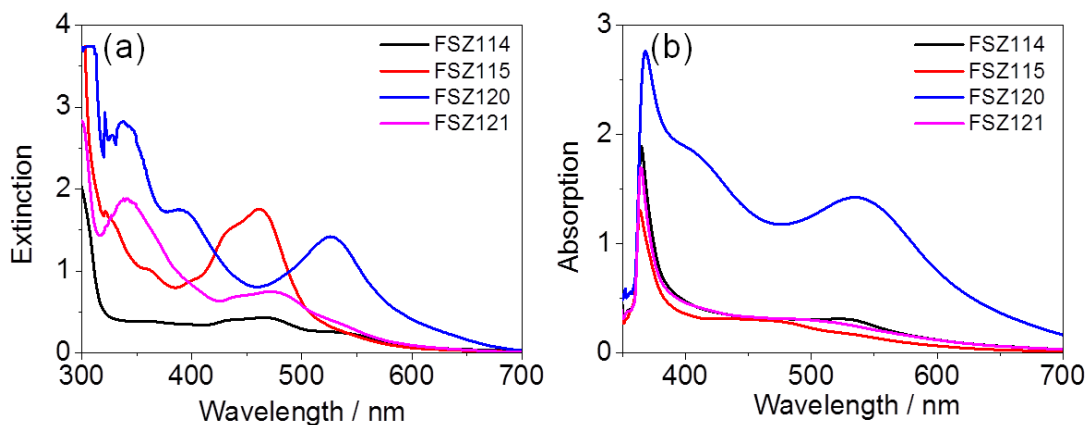


Figure 6.3 UV-Vis spectra of (a) the dye solutions and (b) the ZnO films sensitized with the dyes FSZ114, FSZ115, FSZ120 and FSZ121.

6.2 Photovoltaic performances

Cells employing the different dyes were fabricated and characterized. In Figure 6.4 and Table 6.1 the photovoltaic performances for the tested cells are summarized.

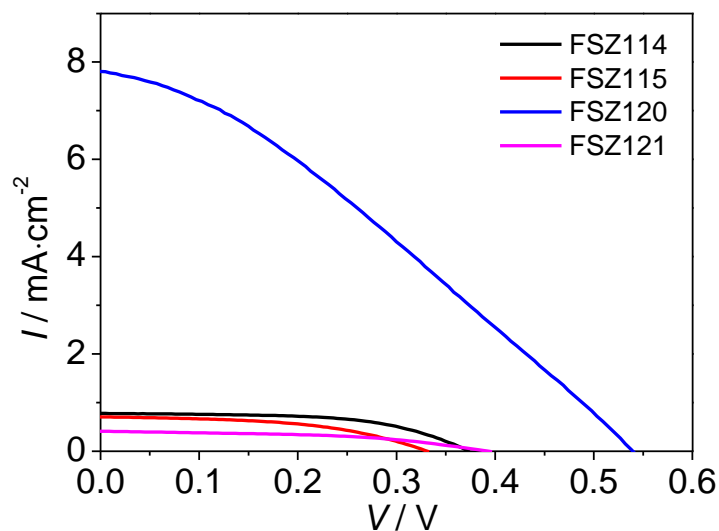


Figure 6.4 I-V characteristics of DSSCs sensitized with the dyes FSZ114, FSZ115, FSZ120 and FSZ121 under AM 1.5 illumination ($100 \text{ mW}\cdot\text{cm}^{-2}$).

Table 6.1 Photovoltaic characteristics calculated from the I-V curves in Figure 6.4.

Sensitizer	V_{oc} / V	$I_{sc} / mA \cdot cm^{-2}$	FF	$\eta / \%$
FSZ114	-0.37	0.78	0.57	0.17
FSZ115	-0.33	0.70	0.49	0.11
FSZ121	-0.39	0.41	0.48	0.08
FSZ120	-0.54	7.81	0.31	1.31
D149	-0.64	9.20	0.56	3.30

As expected, the photovoltaic performances of the dyes with phosphonic acid anchoring groups are much lower than that with carboxylic acid groups due to the lower amount of the adsorbed dye and accordingly the lower absorbance of the ZnO films in the visible region. Since the characteristics of the cells sensitized with FSZ114, FSZ115 and FSZ121 are very similar and their performance is rather poor, an influence of the different alkyl chains in the dyes on the photovoltaic performance is not clearly visible.

6.3 Intensity modulated photocurrent / photovoltage spectroscopy

The electron transport time and lifetime of the DSSCs sensitized with various dyes are compared in Table 6.2. It is found that the DSSCs sensitized with the dyes FSZ114, FSZ115 and FSZ121 exhibit much longer transport times and shorter lifetimes than the DSSCs sensitized with dyes FSZ120 and D149, resulting significantly lower charge-collection efficiencies. The slow electron transport can be attributed to the low electron concentration in the ZnO film (as indicated by the low photocurrent) and probably the low injection efficiency, which is determined by the electronic structures of the dye molecule and needs further investigation. The short lifetime may be related to the low surface coverage of the dye in the ZnO film. The presence of the unloaded film surface enhances the interfacial charge transfer recombination reactions and leading to a decrease in electron lifetime. It is also noted that the collection efficiencies of the dyes FSZ114, FSZ115 and FSZ121 differ greatly and the trend is in good agreement with the photovoltaic performances of these dyes. The extreme low collection efficiency of FSZ121 is probably caused by inserting thiophene between hydrophobic alkyl chain and the pyridine ring. The long alkyl chains of dyes FSZ114 and FSZ115 can reduce the

back electron transfer reactions between the photogenerated electrons and the oxidized species in the electrolyte. Moreover, ruthenium complexes have been shown to display improved efficiencies with increasing alkyl chain length.^[205] They found that the addition of alkyl chains to the sensitizer dye results in an electrically insulating barrier, thereby reducing interfacial charge recombination losses in the DSSCs. However, the design and examination of new complexes would allow us to develop a better understanding of how the molecular structure affects the photovoltaic performance of ZnO-based DSSCs.

Table 6.2 Electron transport time (τ_d) and lifetime (τ_n) for the corresponding DSSCs sensitized with various dyes.

Sensitizer	τ_d (IMPS) / ms	τ_n (IMVS) / ms	η_{cc} / %
FSZ114	0.67	6.34	89.43
FSZ115	1.29	4.00	67.75
FSZ121	2.53	3.18	20.44
FSZ120	0.18	10.07	98.21
D149	0.015	8.29	99.82

6.4 Summary

In this chapter, the performance of ZnO-based DSSCs sensitized with dyes containing phosphonic acid and carboxylic acid anchoring groups has been compared. The dyes with phosphonic acid anchoring groups have shown disappointing photovoltaic performances compared to the dye with carboxylic acid groups. It was found that the main factor that limits the efficiencies of the dyes with phosphonic acid anchoring groups is the low amount of the adsorbed dye and accordingly the low absorbance of the sensitized ZnO films in the visible region.

7 Conclusions and Outlook

In this thesis the flexible dye-sensitized solar cells based on electrodeposited porous ZnO films were investigated towards their optimization and the use of new components to lower their costs and increase their stability.

Firstly for a flexible dye-sensitized solar cell is the search for a suitable flexible, light weight substrate for ZnO photoanode, which enables high throughput roll-to-roll type manufacturing of the cells and widens the variety of applications this cell type could be used in. Several flexible substrates have been explored, including PET-ITO, PET-CNT and metal sheets. Among these, PET-ITO was proved as the best substrate for the ZnO photoanode, achieving the highest conversion efficiency of 3.3 %. The PET-CNT substrates used in this thesis had a relatively high resistance (470 Ω /sq.) and randomly and inhomogeneously distributed carbon nanotubes. In this respect, preliminary tests with a conversion efficiency of $\eta = 2.5$ % can be regarded as very promising. Further improvements of the PET-CNT-based DSSCs can be expected after careful optimization of the CNT layer, with the goals to achieve a higher conductivity and a more homogenous distribution of the CNTs without significantly decreasing the transparency. In addition, PET coated with graphene and multi-walled carbon nanotubes can also be considered to reduce the material costs. The DSSCs using metal substrates for the ZnO layer required illumination of the dye-sensitized film through the counter electrode. As a consequence, the metal sheet-based DSSCs showed low efficiencies of about 1 %, which attributed to the decreasing light intensity through back illumination. To enhance the light-harvesting capability of the photoelectrode film so as to improve DSSC performance, a light scattering layer (layer with submicrometer-sized ZnO particles) could be introduced on the top of the nanocrystalline ZnO layer. This bi-layer structure is expected to improve photocurrent density because of the improved light scattering effect.^[78, 206] Some PET-metal based substrates, such as PET-Ag, PET-Au, PET-Ti and PET-Ag/PEDOT, have also been investigated. These substrates have shown disappointing thermal and chemical stability and they were not suitable as substrates for the electrodeposition of ZnO thin films.

Daylight accelerates the eosin Y desorption and leads to almost colorless ZnO films. For further shortening of desorption time, a higher pH value of the KOH solution and a higher light intensity will be considered. The incorporation of an electrodeposited ZnO

bottom layer can efficiently suppress the electron leakage at bare substrate/electrolyte interface.

The iodine and iodide concentration in the acetonitrile-based electrolyte have been optimized to 1 mol/L TPAI and 0.1 mol/L I₂. The well known additive 4-tert-butylpyridine caused desorption of the dye D149 from ZnO films and was therefore not suitable for D149-sensitized ZnO solar cells.

The suitability of ionic liquid-based electrolytes for the development of ZnO solar cells was evaluated. The most frequently used ionic liquid PMIM I has a relatively high viscosity (1132 mPa·s at 20 °C), imposing severe mass-transfer limitations on the photocurrent in full sunlight. Mixing PMIM I with a low-viscosity and low-melting IL EMIM TCB has a positive effect on the performance of the cells. The presence of water, acetonitrile and electrolyte additives such as NBB, DMAp and CeMim in the IL mixtures had negative influences on the properties of the solar cells, probably due to the undesirable desorption of the dye D149. High temperature can reduce the viscosity of ionic liquid and affect the photovoltaic performance positively. The addition of iodine to the ionic liquids decreased its viscosity and increased the short-circuit current, which contributed to the improvement of the efficiency. In general, it is observed that the ZnO-based solar cells with ionic liquids have much lower V_{oc} , I_{sc} , FF and efficiency values than the cells with acetonitrile-based electrolyte. Since the problem seems to be that the ionic liquid cannot enter into the nanopores of the ZnO, larger pores by micelle structure directing agents during the electrochemical deposition of ZnO may lead to better results.

Because of the non-volatility of the ionic liquids, the cells with IL-based electrolytes were more stable than the cells with acetonitrile-based electrolyte under illumination and elevated temperature. It was observed that small amounts of dye D149 got detached from the ZnO surface in the presence of ionic liquid and the dye desorption was stronger under illumination. This instability in ionic liquid electrolyte prevented the fabrication of a completely solvent-free and stable ZnO solar cell based on an organic dye. Exploration of alternative ionic-liquid electrolyte compositions or modification of the ZnO surface (for example with SiO₂^[207] or TiO₂^[208]) is, therefore, required for fabricating stable devices based on ZnO films sensitized with this organic dye. Unfortunately, for the modification of the ZnO surface with SiO₂ or TiO₂ usually high temperature treatments are needed, which makes this methods only suitable for flexible

metal sheet-based ZnO solar cells.

Dyes with phosphonic acid anchoring groups were expected to bind more strongly to metal oxide surfaces, thus displaying better photovoltaic performance and long-term stability compared to carboxylic acid anchors. The comparative study has shown that the conversion efficiencies of the dyes with phosphonic acid anchoring groups were much lower than that with carboxylic acid groups due to the lower amount of the adsorbed dye and consequently the lower absorbance of the sensitized ZnO films in the visible region. Among all the dyes studied, the best performing ZnO cells were obtained with the organic dye D149. However, in the case of the dye D149, the interaction between ZnO and the dye is very weak, desorption of the dye turned out to be critical, especially in the presence of electrolyte additives, which interacted with the ZnO surface. In general, ruthenium dyes were found not to be appropriate for ZnO due to the deterioration of the semiconducting film upon sensitization and the consecutive aggregation of Zn^{2+} /dye complexes in the pores.^[206] Organic dyes with alternative anchoring groups may overcome the weak dye-oxide interaction observed. For example, an indoline dye coded D358 with two carboxylic groups in its structure (in contrast to only one carboxylic group in D149), and perylene derivatives with anhydride groups instead of carboxylic groups can be expected to form a stronger interaction with metal oxide.

In summary, the results obtained for dye-sensitized ZnO solar cells have still shown relatively low overall conversion efficiencies when compared with TiO₂-based systems. Dye desorption in the presence of electrolyte, formation of ZnO/dye aggregates and a low injection efficiency constitute problems, which still have to be solved satisfactorily. In this regard, in this thesis some strategies have been suggested, which may help in the future to further optimize the performance and the stability of ZnO based dye-sensitized solar cells.

8 References

- [1]. E., B., *Comptes Rendus* **1839**, (9), 561-567.
- [2]. Chapin, D. M.; Fuller, C. S.; Pearson, G. L., *J. Appl. Phys.* **1954**, 25, (5), 676-677.
- [3]. Ooyama, Y.; Harima, Y., *Eur. J. Org. Chem.* **2009**, (18), 2903-2934.
- [4]. Shah, A.; Torres, P.; Tscharnner, R.; Wyrsh, N.; Keppner, H., *Science* **1999**, 285, (5428), 692-698.
- [5]. Britt, J.; Ferekides, C., *Appl. Phys. Lett.* **1993**, 62, (22), 2851-2852.
- [6]. Naghavi, N.; Spiering, S.; Powalla, M.; Cavana, B.; Lincot, D., *Prog. Photovoltaics* **2003**, 11, (7), 437-443.
- [7]. Rhee, S. W.; Kwon, W., *Korean J. Chem. Eng.* **2011**, 28, (7), 1481-1494.
- [8]. Oregan, B.; Grätzel, M., *Nature* **1991**, 353, (6346), 737-740.
- [9]. Pagliaro, M.; ebrary Inc, *Nano-age : how nanotechnology changes our future*. In Wiley-VCH: Weinheim, **2010**.
- [10]. Veerappan, G.; Bojan, K.; Rhee, S. W., *ACS Appl. Mater. Interfaces* **2011**, 3, (3), 857-862.
- [11]. Hagfeldt, A.; Boschloo, G.; Sun, L. C.; Kloo, L.; Pettersson, H., *Chem. Rev.* **2010**, 110, (11), 6595-6663.
- [12]. Cahen, D.; Hodes, G.; Gratzel, M.; Guillemoles, J. F.; Riess, I., *J. Phys. Chem. B* **2000**, 104, (9), 2053-2059.
- [13]. Toivola, M. *Dye-sensitized solar cells on alternative substrates*. Dissertation, Espoo, **2010**.
- [14]. Fang, X. M.; Ma, T. L.; Akiyama, M.; Guan, G. Q.; Tsunematsu, S.; Abe, E., *Thin Solid Films* **2005**, 472, (1-2), 242-245.
- [15]. Miettunen, K.; Halme, J.; Toivola, M.; Lund, P., *J. Phys. Chem. C* **2008**, 112,

- (10), 4011-4017.
- [16]. Ma, T. L.; Fang, X. M.; Akiyama, M.; Inoue, K.; Noma, H.; Abe, E., *J. Electroanal. Chem.* **2004**, 574, (1), 77-83.
- [17]. Toivola, M.; Ahlskog, F.; Lund, P., *Sol. Energy Mater. Sol. Cells* **2006**, 90, (17), 2881-2893.
- [18]. Jun, Y.; Kim, J.; Kang, M. G., *Sol. Energy Mater. Sol. Cells* **2007**, 91, (9), 779-784.
- [19]. Ito, S.; Ha, N. L. C.; Rothenberger, G.; Liska, P.; Comte, P.; Zakeeruddin, S. M.; Pechy, P.; Nazeeruddin, M. K.; Gratzel, M., *Chem. Commun.* **2006**, (38), 4004-4006.
- [20]. Onoda, K.; Ngamsinlapasathian, S.; Fujieda, T.; Yoshikawa, S., *Sol. Energy Mater. Sol. Cells* **2007**, 91, (13), 1176-1181.
- [21]. Kang, M. G.; Park, N. G.; Ryu, K. S.; Chang, S. H.; Kim, K. J., *Chem. Lett.* **2005**, 34, (6), 804-805.
- [22]. Park, J. H.; Jun, Y.; Yun, H. G.; Lee, S. Y.; Kang, M. G., *J. Electrochem. Soc.* **2008**, 155, (7), F145-F149.
- [23]. Redmond, G.; Fitzmaurice, D.; Graetzel, M., *Chem. Mater.* **1994**, 6, (5), 686-691.
- [24]. Rensmo, H.; Keis, K.; Lindstrom, H.; Sodergren, S.; Solbrand, A.; Hagfeldt, A.; Lindquist, S. E.; Wang, L. N.; Muhammed, M., *J. Phys. Chem. B* **1997**, 101, (14), 2598-2601.
- [25]. Ferrere, S.; Zaban, A.; Gregg, B. A., *J. Phys. Chem. B* **1997**, 101, (23), 4490-4493.
- [26]. Sayama, K.; Sugihara, H.; Arakawa, H., *Chem. Mater.* **1998**, 10, (12), 3825-3832.
- [27]. Bauer, C.; Boschloo, G.; Mukhtar, E.; Hagfeldt, A., *J. Phys. Chem. B* **2001**, 105, (24), 5585-5588.

- [28]. Katoh, R.; Furube, A.; Yoshihara, T.; Hara, K.; Fujihashi, G.; Takano, S.; Murata, S.; Arakawa, H.; Tachiya, M., *J. Phys. Chem. B* **2004**, 108, (15), 4818-4822.
- [29]. Look, D. C.; Reynolds, D. C.; Szelove, J. R.; Jones, R. L.; Litton, C. W.; Cantwell, G.; Harsch, W. C., *Solid State Commun.* **1998**, 105, (6), 399-401.
- [30]. Seager, C. H.; Myers, S. M., *J. Appl. Phys.* **2003**, 94, (5), 2888-2894.
- [31]. Forro, L.; Chauvet, O.; Emin, D.; Zuppiroli, L.; Berger, H.; Levy, F., *J. Appl. Phys.* **1994**, 75, (1), 633-635.
- [32]. Boschloo, G.; Edvinsson, T.; Hagfeldt, A., *Nanostructured Materials for Solar Energy Conversion* **2006**, 227-254.
- [33]. Look, D. C.; Farlow, G. C.; Reunchan, P.; Limpijumnong, S.; Zhang, S. B.; Nordlund, K., *Phys. Rev. Lett.* **2005**, 95, (22).
- [34]. Zhang, S. B.; Wei, S. H.; Zunger, A., *Physical Review B* **2001**, 63, (7).
- [35]. Grätzel, M., *Nature* **2001**, 414, (6861), 338-344.
- [36]. Xu, C.; Wu, J.; Desai, U. V.; Gao, D., *J. Am. Chem. Soc.* **2011**, 133, (21), 8122-8125.
- [37]. Chen, C. Y.; Wang, M. K.; Li, J. Y.; Pootrakulchote, N.; Alibabaei, L.; Ngoc-le, C. H.; Decoppet, J. D.; Tsai, J. H.; Gratzel, C.; Wu, C. G.; Zakeeruddin, S. M.; Gratzel, M., *ACS Nano* **2009**, 3, (10), 3103-3109.
- [38]. Chen, W.; Zhang, H. F.; Hsing, I. M.; Yang, S. H., *Electrochem. Commun.* **2009**, 11, (5), 1057-1060.
- [39]. Xu, F.; Dai, M.; Lu, Y. N.; Sun, L. T., *J. Phys. Chem. C* **2010**, 114, (6), 2776-2782.
- [40]. Jiang, C. Y.; Sun, X. W.; Lo, G. Q.; Kwong, D. L.; Wang, J. X., *Appl. Phys. Lett.* **2007**, 90, (26).
- [41]. Chen, Z. H.; Tang, Y. B.; Liu, C. P.; Leung, Y. H.; Yuan, G. D.; Chen, L. M.; Wang, Y. Q.; Bello, I.; Zapien, J. A.; Zhang, W. J.; Lee, C. S.; Lee, S. T., *J.*

- Phys. Chem. C* **2009**, 113, (30), 13433-13437.
- [42]. Peh, C. K. N.; Ke, L.; Ho, G. W., *Mater. Lett.* **2010**, 64, (12), 1372-1375.
- [43]. Raksa, P.; Nilphai, S.; Gardchareon, A.; Choopun, S., *Thin Solid Films* **2009**, 517, (17), 4741-4744.
- [44]. Plank, N. O. V.; Snaith, H. J.; Ducati, C.; Bendall, J. S.; Schmidt-Mende, L.; Welland, M. E., *Nanotechnology* **2008**, 19, (46).
- [45]. Chen, H. H.; Du Pasquier, A.; Saraf, G.; Zhong, J.; Lu, Y., *Semicond. Sci. Technol.* **2008**, 23, (4).
- [46]. Kwak, D. J.; Kim, J. H.; Park, B. W.; Sung, Y. M.; Park, M. W.; Choo, Y. B., *Curr. Appl. Phys.* **2010**, 10, S282-S285.
- [47]. Tan, B.; Toman, E.; Li, Y. G.; Wu, Y. Y., *J. Am. Chem. Soc.* **2007**, 129, (14), 4162-4163.
- [48]. Zhang, Q. F.; Dandeneau, C. S.; Park, K.; Liu, D. W.; Zhou, X. Y.; Jeong, Y. H.; Cao, G. Z., *J. Nanophotonics* **2010**, 4.
- [49]. Zheng, Y. Z.; Tao, X.; Wang, L. X.; Xu, H.; Hou, Q.; Zhou, W. L.; Chen, J. F., *Chem. Mater.* **2010**, 22, (3), 928-934.
- [50]. Saito, M.; Fujihara, S., *Energy Environ. Sci.* **2008**, 1, (2), 280-283.
- [51]. Yoshida, T.; Zhang, J.; Komatsu, D.; Sawatani, S.; Minoura, H.; Pauporte, T.; Lincot, D.; Oekermann, T.; Schlettwein, D.; Tada, H.; Wohrle, D.; Funabiki, K.; Matsui, M.; Miura, H.; Yanagi, H., *Adv. Funct. Mater.* **2009**, 19, (1), 17-43.
- [52]. Liu, X.; Luo, Y.; Li, H.; Fan, Y.; Yu, Z.; Lin, Y.; Chen, L.; Meng, Q., *Chem. Commun.* **2007**, (27), 2847-2849.
- [53]. Grätzel, M., *C. R. Chim.* **2006**, 9, (5-6), 578-583.
- [54]. Ke, L.; Bin Dolmanan, S.; Shen, L.; Pallathadk, P. K.; Zhang, Z.; Lai, D. M. Y.; Liu, H., *Sol. Energy Mater. Sol. Cells* **2010**, 94, (2), 323-326.
- [55]. Tian, Y. S.; Hu, C. G.; Wu, X. H.; Wu, Q.; Cao, C. L., *Sol. Energy Mater. Sol.*

- Cells* **2012**, 98, 83-87.
- [56]. Horiuchi, H.; Katoh, R.; Hara, K.; Yanagida, M.; Murata, S.; Arakawa, H.; Tachiya, M., *J. Phys. Chem. B* **2003**, 107, (11), 2570-2574.
- [57]. Berginc, M.; Krasovec, U. O.; Jankovec, M.; Topic, M., *Sol. Energy Mater. Sol. Cells* **2007**, 91, (9), 821-828.
- [58]. Jerman, I.; Jovanovski, V.; Vuk, A. S.; Hocevar, S. B.; Gaberscek, M.; Jesih, A.; Orel, B., *Electrochim. Acta* **2008**, 53, (5), 2281-2288.
- [59]. Zhang, R.; Pan, J.; Briggs, E. P.; Thrash, M.; Kerr, L. L., *Sol. Energy Mater. Sol. Cells* **2008**, 92, (4), 425-431.
- [60]. Grätzel, M., *Journal of Photochemistry and Photobiology C-Photochemistry Reviews* **2003**, 4, (2), 145-153.
- [61]. Nazeeruddin, M. K.; Kay, A.; Rodicio, I.; Humphrybaker, R.; Muller, E.; Liska, P.; Vlachopoulos, N.; Grätzel, M., *J. Am. Chem. Soc.* **1993**, 115, (14), 6382-6390.
- [62]. Nazeeruddin, M. K.; De Angelis, F.; Fantacci, S.; Selloni, A.; Viscardi, G.; Liska, P.; Ito, S.; Bessho, T.; Grätzel, M., *J. Am. Chem. Soc.* **2005**, 127, (48), 16835-16847.
- [63]. Nazeeruddin, M. K.; Pechy, P.; Grätzel, M., *Chem. Commun.* **1997**, (18), 1705-1706.
- [64]. Wang, P.; Zakeeruddin, S. M.; Moser, J. E.; Nazeeruddin, M. K.; Sekiguchi, T.; Grätzel, M., *Nat. Mater.* **2003**, 2, (6), 402-407.
- [65]. Wang, P.; Klein, C.; Humphry-Baker, R.; Zakeeruddin, S. M.; Grätzel, M., *J. Am. Chem. Soc.* **2005**, 127, (3), 808-809.
- [66]. Chen, C. Y.; Wu, S. J.; Wu, C. G.; Chen, J. G.; Ho, K. C., *Angew. Chem., Int. Ed.* **2006**, 45, (35), 5822-5825.
- [67]. Chen, C. Y.; Wu, S. J.; Li, J. Y.; Wu, C. G.; Chen, J. G.; Ho, K. C., *Adv. Mater.* **2007**, 19, (22), 3888-3891.

- [68]. Nazeeruddin, M. K.; Bessho, T.; Cevey, L.; Ito, S.; Klein, C.; De Angelis, F.; Fantacci, S.; Comte, P.; Liska, P.; Imai, H.; Graetzel, M., *J. Photochem. Photobiol. A-Chem.* **2007**, 185, (2-3), 331-337.
- [69]. Gao, F.; Wang, Y.; Shi, D.; Zhang, J.; Wang, M. K.; Jing, X. Y.; Humphry-Baker, R.; Wang, P.; Zakeeruddin, S. M.; Gratzel, M., *J. Am. Chem. Soc.* **2008**, 130, (32), 10720-10728.
- [70]. Gao, F. F.; Wang, Y.; Zhang, J.; Shi, D.; Wang, M. K.; Humphry-Baker, R.; Wang, P.; Zakeeruddin, S. M.; Gratzel, M., *Chem. Commun.* **2008**, (23), 2635-2637.
- [71]. Matar, F.; Ghaddar, T. H.; Walley, K.; DosSantos, T.; Durrant, J. R.; O'Regan, B., *J. Mater. Chem.* **2008**, 18, (36), 4246-4253.
- [72]. Bessho, T.; Yoneda, E.; Yum, J. H.; Guglielmi, M.; Tavernelli, I.; Imai, H.; Rothlisberger, U.; Nazeeruddin, M. K.; Gratzel, M., *J. Am. Chem. Soc.* **2009**, 131, (16), 5930-5934.
- [73]. Wang, M. K.; Moon, S. J.; Xu, M. F.; Chittibabu, K.; Wang, P.; Cevey-Ha, N. L.; Humphry-Baker, R.; Zakeeruddin, S. M.; Grätzel, M., *Small* **2010**, 6, (2), 319-324.
- [74]. Hwang, S.; Lee, J. H.; Park, C.; Lee, H.; Kim, C.; Lee, M. H.; Lee, W.; Park, J.; Kim, K.; Park, N. G., *Chem. Commun.* **2007**, (46), 4887-4889.
- [75]. Horiuchi, T.; Miura, H.; Uchida, S., *Chem. Commun.* **2003**, (24), 3036-3037.
- [76]. Mishra, A.; Fischer, M. K. R.; Bauerle, P., *Angew. Chem., Int. Ed.* **2009**, 48, (14), 2474-2499.
- [77]. Zeng, W. D.; Cao, Y. M.; Bai, Y.; Wang, Y. H.; Shi, Y. S.; Zhang, M.; Wang, F. F.; Pan, C. Y.; Wang, P., *Chem. Mater.* **2010**, 22, (5), 1915-1925.
- [78]. Ito, S.; Zakeeruddin, S. M.; Humphry-Baker, R.; Liska, P.; Charvet, R.; Comte, P.; Nazeeruddin, M. K.; Pechy, P.; Takata, M.; Miura, H.; Uchida, S.; Grätzel, M., *Adv. Mater.* **2006**, 18, (9), 1202-1205.
- [79]. Fang, J. H.; Wu, J. W.; Lu, X. M.; Shen, Y. C.; Lu, Z. H., *Chem. Phys. Lett.*

- 1997**, 270, (1-2), 145-151.
- [80]. He, J. J.; Benko, G.; Korodi, F.; Polivka, T.; Lomoth, R.; Akermark, B.; Sun, L. C.; Hagfeldt, A.; Sundstrom, V., *J. Am. Chem. Soc.* **2002**, 124, (17), 4922-4932.
- [81]. Yum, J. H.; Jang, S. R.; Humphry-Baker, R.; Grätzel, M.; Cid, J. J.; Torres, T.; Nazeeruddin, M. K., *Langmuir* **2008**, 24, (10), 5636-5640.
- [82]. Lee, Y. G.; Park, S.; Cho, W.; Son, T.; Sudhagar, P.; Jung, J. H.; Wooh, S.; Char, K.; Kang, Y. S., *J. Phys. Chem. C* **2012**, 116, (11), 6770-6777.
- [83]. Saji, V. S.; Pyo, M., *Curr. Appl. Phys.* **2010**, 10, (3), S410-S413.
- [84]. Zhang, Z. P.; Evans, N.; Zakeeruddin, S. M.; Humphry-Baker, R.; Grätzel, M., *J. Phys. Chem. C* **2007**, 111, (1), 398-403.
- [85]. Plass, R.; Pelet, S.; Krueger, J.; Grätzel, M.; Bach, U., *J. Phys. Chem. B* **2002**, 106, (31), 7578-7580.
- [86]. Wolfbauer, G.; Bond, A. M.; Eklund, J. C.; MacFarlane, D. R., *Sol. Energy Mater. Sol. Cells* **2001**, 70, (1), 85-101.
- [87]. Hardin, B. E.; Snaith, H. J.; McGehee, M. D., *Nat. Photonics* **2012**, 6, (3), 162-169.
- [88]. Boschloo, G.; Hagfeldt, A., *Acc. Chem. Res.* **2009**, 42, (11), 1819-1826.
- [89]. Oskam, G.; Bergeron, B. V.; Meyer, G. J.; Searson, P. C., *J. Phys. Chem. B* **2001**, 105, (29), 6867-6873.
- [90]. Bergeron, B. V.; Marton, A.; Oskam, G.; Meyer, G. J., *J. Phys. Chem. B* **2005**, 109, (2), 937-943.
- [91]. Wang, Z. S.; Sayama, K.; Sugihara, H., *J. Phys. Chem. B* **2005**, 109, (47), 22449-22455.
- [92]. Nusbaumer, H.; Moser, J. E.; Zakeeruddin, S. M.; Nazeeruddin, M. K.; Grätzel, M., *J. Phys. Chem. B* **2001**, 105, (43), 10461-10464.
- [93]. Yella, A.; Lee, H. W.; Tsao, H. N.; Yi, C. Y.; Chandiran, A. K.; Nazeeruddin,

- M. K.; Diau, E. W. G.; Yeh, C. Y.; Zakeeruddin, S. M.; Grätzel, M., *Science* **2011**, 334, (6056), 629-634.
- [94]. Feldt, S. M.; Gibson, E. A.; Gabrielsson, E.; Sun, L.; Boschloo, G.; Hagfeldt, A., *J. Am. Chem. Soc.* **2010**, 132, (46), 16714-16724.
- [95]. Kumara, G. R. A.; Kaneko, S.; Okuya, M.; Tennakone, K., *Langmuir* **2002**, 18, (26), 10493-10495.
- [96]. O'Regan, B. C.; Lenzmann, F., *J. Phys. Chem. B* **2004**, 108, (14), 4342-4350.
- [97]. Smestad, G. P.; Spiekermann, S.; Kowalik, J.; Grant, C. D.; Schwartzberg, A. M.; Zhang, J.; Tolbert, L. M.; Moons, E., *Sol. Energy Mater. Sol. Cells* **2003**, 76, (1), 85-105.
- [98]. Bach, U.; Lupo, D.; Comte, P.; Moser, J. E.; Weissortel, F.; Salbeck, J.; Spreitzer, H.; Grätzel, M., *Nature* **1998**, 395, (6702), 583-585.
- [99]. Krüger, J. *Interface engineering in solid-state dye-sensitized solar cells*. Dissertation, Lausanne, **2003**.
- [100]. Welton, T., *Coord. Chem. Rev.* **2004**, 248, (21-24), 2459-2477.
- [101]. Gorlov, M.; Kloo, L., *Dalton Trans.* **2008**, (20), 2655-2666.
- [102]. Kuang, D. B.; Klein, C.; Ito, S.; Moser, J. E.; Humphry-Baker, R.; Evans, N.; Durrant, J. R.; Graetzel, C.; Zakeeruddin, S. M.; Graetzel, M., *Adv. Mater.* **2007**, 19, (8), 1133-1137.
- [103]. Fabregat-Santiago, F.; Bisquert, J.; Palomares, E.; Otero, L.; Kuang, D. B.; Zakeeruddin, S. M.; Gratzel, M., *J. Phys. Chem. C* **2007**, 111, (17), 6550-6560.
- [104]. Kuang, D. B.; Klein, C.; Zhang, Z. P.; Ito, S.; Moser, J. E.; Zakeeruddin, S. M.; Grätzel, M., *Small* **2007**, 3, (12), 2094-2102.
- [105]. Wang, P.; Wenger, B.; Humphry-Baker, R.; Moser, J. E.; Teuscher, J.; Kantele, W.; Mezger, J.; Stoyanov, E. V.; Zakeeruddin, S. M.; Grätzel, M., *J. Am. Chem. Soc.* **2005**, 127, (18), 6850-6856.
- [106]. Fredin, K.; Gorlov, M.; Pettersson, H.; Hagfeldt, A.; Kloo, L.; Boschloo, G., *J.*

- Phys. Chem. C* **2007**, 111, (35), 13261-13266.
- [107]. Cao, Y. M.; Zhang, J.; Bai, Y.; Li, R. Z.; Zakeeruddin, S. M.; Gratzel, M.; Wang, P., *J. Phys. Chem. C* **2008**, 112, (35), 13775-13781.
- [108]. Yoshida, Y.; Baba, O.; Larriba, C.; Saito, G., *J. Phys. Chem. B* **2007**, 111, (42), 12204-12210.
- [109]. Zistler, M.; Wachter, P.; Wasserscheid, P.; Gerhard, D.; Hinsch, A.; Sastrawan, R.; Gores, H. J., *Electrochim. Acta* **2006**, 52, (1), 161-169.
- [110]. Wachter, P.; Schreiner, C.; Zistler, M.; Gerhard, D.; Wasserscheid, P.; Gores, H. J., *Microchim. Acta* **2008**, 160, (1-2), 125-133.
- [111]. Papageorgiou, N.; Athanassov, Y.; Armand, M.; Bonhote, P.; Pettersson, H.; Azam, A.; Grätzel, M., *J. Electrochem. Soc.* **1996**, 143, (10), 3099-3108.
- [112]. Kawano, R.; Watanabe, M., *Chem. Commun.* **2005**, (16), 2107-2109.
- [113]. Wachter, P. *Studies of charge transport and phase transition equilibria in blends of ionic liquids for dye-sensitized solar cells*. Dissertation, Regensburg, **2008**.
- [114]. Zhao, D. B.; Liao, Y. C.; Zhang, Z. D., *Clean-Soil Air Water* **2007**, 35, (1), 42-48.
- [115]. Boschloo, G.; Haggman, L.; Hagfeldt, A., *J. Phys. Chem. B* **2006**, 110, (26), 13144-13150.
- [116]. Yu, Z.; Gorlov, M.; Boschloo, G.; Kloo, L., *J. Phys. Chem. C* **2010**, 114, (50), 22330-22337.
- [117]. Zhang, C. N.; Huang, Y.; Huo, Z. P.; Chen, S. H.; Dai, S. Y., *J. Phys. Chem. C* **2009**, 113, (52), 21779-21783.
- [118]. Grätzel, M., *J. Photochem. Photobiol. A-Chem.* **2004**, 164, (1-3), 3-14.
- [119]. Tsekouras, G.; Mozer, A. J.; Wallace, G. G., *J. Electrochem. Soc.* **2008**, 155, (7), K124-K128.
- [120]. Khelashvili, G.; Behrens, S.; Weidenthaler, C.; Vetter, C.; Hinsch, A.; Kern, R.;

- Skupien, K.; Dinjus, E.; Bonnemann, H., *Thin Solid Films* **2006**, 511, 342-348.
- [121]. Kitamura, T.; Maitani, M.; Matsuda, M.; Wada, Y.; Yanagida, S., *Chem. Lett.* **2001**, (10), 1054-1055.
- [122]. Murakami, T. N.; Ito, S.; Wang, Q.; Nazeeruddin, M. K.; Bessho, T.; Cesar, I.; Liska, P.; Humphry-Baker, R.; Comte, P.; Pechy, P.; Grätzel, M., *J. Electrochem. Soc.* **2006**, 153, (12), A2255-A2261.
- [123]. Kay, A.; Grätzel, M., *Sol. Energy Mater. Sol. Cells* **1996**, 44, (1), 99-117.
- [124]. Suzuki, K.; Yamaguchi, M.; Kumagai, M.; Yanagida, S., *Chem. Lett.* **2003**, 32, (1), 28-29.
- [125]. Saito, Y.; Kubo, W.; Kitamura, T.; Wada, Y.; Yanagida, S., *J. Photochem. Photobiol. A-Chem.* **2004**, 164, (1-3), 153-157.
- [126]. Hong, W. J.; Xu, Y. X.; Lu, G. W.; Li, C.; Shi, G. Q., *Electrochem. Commun.* **2008**, 10, (10), 1555-1558.
- [127]. Chen, P. Y.; Lee, C. P.; Vittal, R.; Ho, K. C., *J. Power Sources* **2010**, 195, (12), 3933-3938.
- [128]. Wang, M. K.; Anghel, A. M.; Marsan, B.; Ha, N. L. C.; Pootrakulchote, N.; Zakeeruddin, S. M.; Grätzel, M., *J. Am. Chem. Soc.* **2009**, 131, (44), 15976-15977.
- [129]. Hoyer, P.; Weller, H., *J. Phys. Chem.* **1995**, 99, (38), 14096-14100.
- [130]. Kar, S.; Dev, A.; Chaudhuri, S., *J. Phys. Chem. B* **2006**, 110, (36), 17848-17853.
- [131]. Wang, X. D.; Ding, Y.; Summers, C. J.; Wang, Z. L., *J. Phys. Chem. B* **2004**, 108, (26), 8773-8777.
- [132]. Yang, P. D.; Yan, H. Q.; Mao, S.; Russo, R.; Johnson, J.; Saykally, R.; Morris, N.; Pham, J.; He, R. R.; Choi, H. J., *Adv. Funct. Mater.* **2002**, 12, (5), 323-331.
- [133]. Mahmood, F. S.; Gould, R. D.; Hassan, A. K.; Salih, H. M., *Thin Solid Films* **1995**, 270, (1-2), 376-379.

- [134]. Demerchant, J.; Cocivera, M., *Chem. Mater.* **1995**, 7, (9), 1742-1749.
- [135]. Nonomura, K.; Yoshida, T.; Schlettwein, D.; Minoura, H., *Electrochim. Acta* **2003**, 48, (20-22), 3071-3078.
- [136]. Izaki, M.; Omi, T., *Appl. Phys. Lett.* **1996**, 68, (17), 2439-2440.
- [137]. Peulon, S.; Lincot, D., *Adv. Mater.* **1996**, 8, (2), 166-170.
- [138]. Pauporte, T.; Lincot, D., *J. Electroanal. Chem.* **2001**, 517, (1-2), 54-62.
- [139]. Yoshida, T.; Miyamoto, K.; Hibi, N.; Sugiura, T.; Minoura, H.; Schlettwein, D.; Oekermann, T.; Schneider, G.; Wohrle, D., *Chem. Lett.* **1998**, (7), 599-600.
- [140]. Yoshida, T.; Minoura, H., *Adv. Mater.* **2000**, 12, (16), 1219-1222.
- [141]. Yoshida, T.; Oekermann, T.; Okabe, K.; Schlettwein, D.; Funabiki, K.; Minoura, H., *Electrochemistry* **2002**, 70, (6), 470-487.
- [142]. Nonomura, K.; Komatsu, D.; Yoshida, T.; Minoura, H.; Schlettwein, D., *Phys. Chem. Chem. Phys.* **2007**, 9, (15), 1843-1849.
- [143]. Yoshida, T.; Zhang, J. B.; Komatsu, D.; Sawatani, S.; Minoura, H.; Pauporte, T.; Lincot, D.; Oekermann, T.; Schlettwein, D.; Tada, H.; Wohrle, D.; Funabiki, K.; Matsui, M.; Miura, H.; Yanagi, H., *Adv. Funct. Mater.* **2009**, 19, (1), 17-43.
- [144]. Pauporte, T.; Yoshida, T.; Cortes, R.; Froment, M.; Lincot, A., *J. Phys. Chem. B* **2003**, 107, (37), 10077-10082.
- [145]. Goux, A.; Pauporte, T.; Yoshida, T.; Lincot, D., *Langmuir* **2006**, 22, (25), 10545-10553.
- [146]. Rathousky, J.; Loewenstein, T.; Nonomura, K.; Yoshida, T.; Wark, M.; Schlettwein, D., Electrochemically self-assembled mesoporous dye-modified zinc oxide thin films. In *Nanoporous Materials Iv*, Sayari, A.; Jaroniec, M., Eds. Elsevier Science Bv: Amsterdam, **2005**; Vol. 156, p 315-320.
- [147]. Loewenstein, T.; Nonomura, K.; Yoshida, T.; Michaelis, E.; Wohrle, D.; Rathousky, J.; Wark, M.; Schlettwein, D., *J. Electrochem. Soc.* **2006**, 153, (4), A699-A704.

- [148]. Boeckler, C. *Elektrochemische Abscheidung von Zinkoxid-Schichten unter dem Einfluss von strukturdirigierenden Additiven für die Anwendung in farbstoffsensibilisierten Solarzellen*. Dissertation, Hannover, **2008**.
- [149]. Oekermann, T.; Yoshida, T.; Minoura, H.; Wijayantha, K. G. U.; Peter, L. M., *J. Phys. Chem. B* **2004**, 108, (24), 8364-8370.
- [150]. Yoshida, T.; Pauporte, T.; Lincot, D.; Oekermann, T.; Minoura, H., *J. Electrochem. Soc.* **2003**, 150, (9), C608-C615.
- [151]. Skoog, D. A.; Holler, F. J.; Crouch, S. R., *Principles of instrumental analysis*. 6 ed.; Thomson Brooks/Cole: Belmont, **2007**; p 1039
- [152]. Postek, M. T., *Scanning electron microscopy : a student's handbook*. Ladd Research Industries: **1980**; p 305
- [153]. Yacobi, B. G.; Holt, D. B., *Cathodoluminescence microscopy of inorganic solids*. Plenum Press: New York **1990**; p 292
- [154]. Prutton, M., *Scanning auger electron microscopy*. Wiley: Chichester, **2006**; p 368
- [155]. Goldstein, J. I., *Scanning electron microscopy and X-ray microanalysis*. 3. ed.; Springer: New York, **2007**; p 690
- [156]. Bard, A. J.; Faulkner, L. R., *Electrochemical methods : fundamentals and applications*. 2. ed.; Wiley: New York, **2001**; p 833
- [157]. Wang, J., *Analytical electrochemistry*. 3. ed.; Wiley-VCH: Hoboken, **2006**; p 250.
- [158]. Compton, R. G.; Banks, C. E., *Understanding voltammetry*. 2. Aufl. ed.; Imperial College Press: London, **2011**; p 429.
- [159]. Case, M. A.; Owusu, Y. A.; Chapman, H.; Dargan, T.; Ruscher, P., *Renew Energ* **2008**, 33, (12), 2645-2652.
- [160]. Ning, Z. J.; Fu, Y.; Tian, H., *Energy & Environmental Science* **2010**, 3, (9), 1170-1181.

- [161]. Grätzel, M., *Acc. Chem. Res.* **2009**, 42, (11), 1788-1798.
- [162]. Wang, Q.; Ito, S.; Grätzel, M.; Fabregat-Santiago, F.; Mora-Sero, I.; Bisquert, J.; Bessho, T.; Imai, H., *J. Phys. Chem. B* **2006**, 110, (50), 25210-25221.
- [163]. Bisquert, J.; Garcia-Belmonte, G.; Fabregat-Santiago, F.; Compte, A., *Electrochem. Commun.* **1999**, 1, (9), 429-435.
- [164]. Peter, L. M., *Chem. Rev.* **1990**, 90, (5), 753-769.
- [165]. Bisquert, J.; Vikhrenko, V. S., *J. Phys. Chem. B* **2004**, 108, (7), 2313-2322.
- [166]. Schlichthorl, G.; Park, N. G.; Frank, A. J., *J. Phys. Chem. B* **1999**, 103, (5), 782-791.
- [167]. Halme, J.; Vahermaa, P.; Miettunen, K.; Lund, P., *Adv. Mater.* **2010**, 22, (35), E210-E234.
- [168]. Schlichthorl, G.; Huang, S. Y.; Sprague, J.; Frank, A. J., *J. Phys. Chem. B* **1997**, 101, (41), 8141-8155.
- [169]. van de Lagemaat, J.; Park, N. G.; Frank, A. J., *J. Phys. Chem. B* **2000**, 104, (9), 2044-2052.
- [170]. Sommeling, P. M.; Spath, M.; Smit, H. J. P.; Bakker, N. J.; Kroon, J. M., *J. Photochem. Photobiol. A-Chem.* **2004**, 164, (1-3), 137-144.
- [171]. Hinsch, A.; Kroon, J. M.; Kern, R.; Uhlendorf, I.; Holzbock, J.; Meyer, A.; Ferber, J., *Prog. Photovoltaics* **2001**, 9, (6), 425-438.
- [172]. Lee, K. M.; Chiu, W. H.; Lu, M. D.; Hsieh, W. F., *J. Power Sources* **2011**, 196, (20), 8897-8903.
- [173]. Kang, M. G.; Ryu, K. S.; Chang, S. H.; Park, N. G.; Hong, J. S.; Kim, K. J., *Bull. Korean Chem. Soc.* **2004**, 25, (5), 742-744.
- [174]. Minami, T., *Semicond. Sci. Technol.* **2005**, 20, (4), S35-S44.
- [175]. Trottier, C. M.; Glatkowski, P.; Wallis, P.; Luo, J., *J. Soc. Inf. Display* **2005**, 13, (9), 759-763.

- [176]. Nam, J. G.; Park, Y. J.; Kim, B. S.; Lee, J. S., *Scripta Mater.* **2010**, 62, (3), 148-150.
- [177]. Wu, M. X.; Lin, X.; Wang, T. H.; Qiu, J. S.; Ma, T. L., *Energy Environ. Sci.* **2011**, 4, (6), 2308-2315.
- [178]. Hsieh, C. T.; Yang, B. H.; Lin, J. Y., *Carbon* **2011**, 49, (9), 3092-3097.
- [179]. Woan, K.; Pyrgiotakis, G.; Sigmund, W., *Adv. Mater.* **2009**, 21, (21), 2233-2239.
- [180]. Muduli, S.; Lee, W.; Dhas, V.; Mujawar, S.; Dubey, M.; Vijayamohanan, K.; Han, S. H.; Ogale, S., *ACS Appl. Mater. Interfaces* **2009**, 1, (9), 2030-2035.
- [181]. Sawatsuk, T.; Chindaduang, A.; Sae-Kung, C.; Pratontep, S.; Tumcharern, G., *Diamond Relat. Mater.* **2009**, 18, (2-3), 524-527.
- [182]. Yen, C. Y.; Lin, Y. F.; Liao, S. H.; Weng, C. C.; Huang, C. C.; Hsiao, Y. H.; Ma, C. C. M.; Chang, M. C.; Shao, H.; Tsai, M. C.; Hsieh, C. K.; Tsai, C. H.; Weng, F. B., *Nanotechnology* **2008**, 19, (37).
- [183]. Zhu, H.; Wei, J.; Wang, K.; Wu, D., *Sol. Energy Mater. Sol. Cells* **2009**, 93, (9), 1461-1470.
- [184]. Wei, D.; Unalan, H. E.; Han, D. X.; Zhang, Q. X.; Niu, L.; Amaratunga, G.; Ryhanen, T., *Nanotechnology* **2008**, 19, (42).
- [185]. Kyaw, A. K. K.; Tantang, H.; Wu, T.; Ke, L.; Peh, C.; Huang, Z. H.; Zeng, X. T.; Demir, H. V.; Zhang, Q.; Sun, X. W., *Appl. Phys. Lett.* **2011**, 99, (2).
- [186]. Wang, H. F.; Chen, L. Y.; Su, W. N.; Chung, J. C.; Hwang, B. J., *J. Phys. Chem. C* **2010**, 114, (7), 3185-3189.
- [187]. Hu, F. Y.; Xia, Y. J.; Guan, Z. S.; Yin, X.; He, T., *Electrochim. Acta* **2012**, 69, 97-101.
- [188]. Bisquert, J., *J. Phys. Chem. B* **2002**, 106, (2), 325-333.
- [189]. Wang, Q.; Moser, J. E.; Grätzel, M., *J. Phys. Chem. B* **2005**, 109, (31), 14945-14953.

- [190]. Koelsch, M.; Cassaignon, S.; Minh, C. T. T.; Guillemoles, J. F.; Jolivet, J. P., *Thin Solid Films* **2004**, 451, 86-92.
- [191]. Clare, B.; Kirchner, B.; ebrary Inc, Ionic liquids. In *Topics in current chemistry* 290, Springer: Heidelberg ;New York, **2009**.
- [192]. Zhao, J.; Yan, F.; Qiu, L. H.; Zhang, Y. G.; Chen, X. J.; Sun, B. Q., *Chem. Commun.* **2011**, 47, (41), 11516-11518.
- [193]. Quintana, M.; Marinado, T.; Nonomura, K.; Boschloo, G.; Hagfeldt, A., *J. Photochem. Photobiol. A-Chem.* **2009**, 202, (2-3), 159-163.
- [194]. Tanaka, H.; Takeichi, A.; Higuchi, K.; Motohiro, T.; Takata, M.; Hirota, N.; Nakajima, J.; Toyoda, T., *Sol. Energy Mater. Sol. Cells* **2009**, 93, (6-7), 1143-1148.
- [195]. Kubo, W.; Kambe, S.; Nakade, S.; Kitamura, T.; Hanabusa, K.; Wada, Y.; Yanagida, S., *J. Phys. Chem. B* **2003**, 107, (18), 4374-4381.
- [196]. Zhang, Z. P.; Ito, S.; Moser, J. E.; Zakeeruddin, S. M.; Grätzel, M., *ChemPhysChem* **2009**, 10, (11), 1834-1838.
- [197]. Le Bahers, T.; Labat, F.; Pauporte, T.; Ciofini, I., *Phys. Chem. Chem. Phys.* **2010**, 12, (44), 14710-14719.
- [198]. Kato, N.; Takeda, Y.; Higuchi, K.; Takeichi, A.; Sudo, E.; Tanaka, H.; Motohiro, T.; Sano, T.; Toyoda, T., *Sol. Energy Mater. Sol. Cells* **2009**, 93, (6-7), 893-897.
- [199]. Argazzi, R.; Bignozzi, C. A.; Heimer, T. A.; Castellano, F. N.; Meyer, G. J., *Inorg. Chem.* **1994**, 33, (25), 5741-5749.
- [200]. Galoppini, E., *Coord. Chem. Rev.* **2004**, 248, (13-14), 1283-1297.
- [201]. Nilsing, M.; Lunell, S.; Persson, P.; Ojamae, L., *Surf. Sci.* **2005**, 582, (1-3), 49-60.
- [202]. Nilsing, M.; Persson, P.; Ojamae, L., *Chem. Phys. Lett.* **2005**, 415, (4-6), 375-380.

- [203]. Li, B.; Wang, L. D.; Kang, B. N.; Wang, P.; Qiu, Y., *Sol. Energy Mater. Sol. Cells* **2006**, 90, (5), 549-573.
- [204]. Wang, P.; Klein, C.; Moser, J. E.; Humphry-Baker, R.; Cevey-Ha, N. L.; Charvet, R.; Comte, P.; Zakeeruddin, S. M.; Grätzel, M., *J. Phys. Chem. B* **2004**, 108, (45), 17553-17559.
- [205]. Kroeze, J. E.; Hirata, N.; Koops, S.; Nazeeruddin, M. K.; Schmidt-Mende, L.; Grätzel, M.; Durrant, J. R., *J. Am. Chem. Soc.* **2006**, 128, (50), 16376-16383.
- [206]. Zhang, Q. F.; Dandeneau, C. S.; Zhou, X. Y.; Cao, G. Z., *Adv. Mater.* **2009**, 21, (41), 4087-4108.
- [207]. Shin, Y. J.; Lee, J. H.; Park, J. H.; Park, N. G., *Chem. Lett.* **2007**, 36, (12), 1506-1507.
- [208]. Shin, Y. J.; Kim, K. S.; Park, N. G.; Ryu, K. S.; Chang, S. H., *Bull. Korean Chem. Soc.* **2005**, 26, (12), 1929-1930.

CURRICULM VITAE

Personal Information

Name: Juan Du
Date of Birth: December 07, 1981
Place of Birth: Anhui, China
Nationality: Chinese

Education

02. 2009 – 12. 2012 PhD Thesis, Leibniz University of Hannover, Germany
10. 2006 – 12. 2008 Master of Science Degree in “Material- and Nanochemistry”, Leibniz University of Hannover, Germany
09. 2002 – 06. 2006 Diploma Degree in “Construction Chemistry”, Fachhochschule Hildesheim/Holzminden/Göttingen, Germany
09. 2000 – 01. 2002 Undergraduate Bachelor study in “Biology”, Hefei University, China
09. 1997 – 09. 2000 High school, China
09. 1994 – 09. 1997 Middle school, China
09. 1988 – 09. 1994 Primary school, China

CONTRIBUTING WORK AND PUBLICATIONS

Publications

- J. Du, F. Bittner, D. S. Hecht, C. Ladous, J. Ellinger, T. Oekermann, M. Wark, “A carbon nanotubes-based transparent conductive substrate for flexible ZnO dye-sensitized solar cells”, Thin Solid Films, 23 December 2012, accepted.
- F. Bittner, J. Du, J. Ellinger, J. Rathousky, T. Oekermann, M. Wark, J. Caro, „Scale-up of the electrodeposition of ZnO/Eosin Y hybrid thin films for the fabrication of flexible dye-sensitized solar cell modules“, in preparation.
- K. Oum, P. W. Lohse, O. Flender, J. R. Klein, M. Scholz, T. Lenzer, J. Du, T. Oekermann, “Ultrafast dynamics of the indoline dye D149 on electrodeposited ZnO and sintered TiO₂ and ZrO₂ thin films”, Physical Chemistry Chemical Physics, 2012, 14, 15429-15437.

Poster

- J. Du, T. Oekermann, J. Caro, „Electrochemical deposition of porous ZnO films for flexible Dye-sensitized Solar Cells“, Niedersächsisches Photovoltaic Symposium, 19. 06. 2009, Hameln, Germany.
- J. Du, F. Bittner, T. Oekermann, M. Wark, „Electrodeposition of ZnO/Dye hybrid thin films for flexible Dye-sensitized Solar Cells“, Nanoday 2010, 30.09.2010, Hannover, Germany.
- F. Bittner, J. Du, T. Oekermann, M. Wark, „Electrochemical Fabrication of Photoanodes and Counter Electrodes for Flexible Dye-sensitized Solar Cell Modules“, Energy Research Fair, 08.02.2012, Hannover, Germany.
- F. Bittner, J. Du, T. Oekermann, M. Wark, „Electrochemical Fabrication of Photoanodes and Counter Electrodes for Flexible Dye-sensitized Solar Cell Modules ” , 3rd German-French Summer School on Electrochemistry & Nanotechnologies, 18.-23.09.2011, Porquerolles, France.
- F. Bittner, J. Du, T. Oekermann, M. Wark, „Electrochemical Fabrication of Photoanodes and Counter Electrodes for flexible DSCs ” , 5th Gerischer Symposium, 22.-24.06.2011, Berlin, Germany.

- F. Bittner, J. Du, T. Oekermann, M. Wark, „*Electrochemical Fabrication of Photoanodes and Counter Electrodes for flexible DSCs*” , 3rd International Conference on Hybrid and Organic Photovoltaics, 15.-18.05.2011, Valencia, Spain.

Presentation

- F. Bittner, J. Du, T. Oekermann, M. Wark, „*Electrochemical Fabrication of Photoanodes and Counter Electrodes for Flexible Dye-sensitized Solar Cell Modules*” , 3rd German-French Summer School on Electrochemistry & Nanotechnologies, 18.-23.09.2011, Porquerolles, France.

ERKLÄRUNG ZUR DISSERTATION

Hierdurch erkläre ich, dass ich meine Dissertation mit dem Titel

„Electrochemical deposition of dye-modified ZnO hybrid thin films and their application to flexible dye-sensitized solar cells“

selbständig verfasst und die benutzten Hilfsmittel und Quellen sowie gegebenenfalls die zu Hilfeleistungen herangezogenen Institutionen vollständig angegeben habe.

Die Dissertation wurde nicht schon als Masterarbeit, Diplomarbeit oder andere Prüfungsarbeit verwendet.

Hannover, den 15.10.2012

M. Sc. Juan Du